# CHANNELING EFFECT ANALYSIS OF LATTICE DISORDER IN BORON IMPLANTED SILICON

Thesis by

James Edward Westmoreland, III

In Partial Fulfillment of the Requirements for

the Degree of

Doctor of Philosophy

California Institute of Technology

Pasadena, California

1971

Submitted April 23, 1971

To my loving wife Joyce
and to my mother and my
father.

Acknowledgments

I am indebted to Dr. J.W. Mayer for his patience, assistance and guidance during the course of this work.

For helpful and enlightening discussions special thanks go to Dr. F.H. Eisen, Dr. J.A. Davies, and Dr. I.V. Mitchell. The assistance of Mr. B. Welch in performing the boron implantations is appreciated. For pleasant and fruitful collaboration I am grateful to Mr. O.J. Marsh, Dr. R.P. Hunsperger, and Dr. R.R. Hart. For invaluable help and guidance in the understanding and use of the Caltech 3 MeV accelerator I heartily thank especially Dr. C.A. Barnes and also the rest of the "Kellogites" who made it possible. Thanks go to Dr. T. Smith for performing the ellipsometry measurements.

Financial assistance from the National Aeronautics and Space Administration (NASA Traineeship) and also partial support during the course of this work by Air Force Cambridge Research Laboratories, the National Science Foundation, and the Office of Naval Research are gratefully acknowledged.

For her great patience and encouragement, I thank my wife Joyce. Finally, for their assistance in typing the manuscript Mrs. Ruth Stratton, Mrs. Carol Norris, and especially for long hours in that last week Mrs. Karen Current.

## ABSTRACT

The channeling effect technique employing both 1.8 MeV helium and 450 keV proton analyzing beams was used to extract disorder distributions for 200 keV and 300 keV boron implanted silicon crystals. The behavior of the analyzing beam was first investigated by studies of the minimum yield from single crystal substrates underlying surface amorphous layers. A simple description of the interactions of the analyzing beam in partially disordered samples was acceptable for obtaining the disorder peak depth and shape when applied to both helium and proton backscattering spectra. For samples held at temperatures below -45°C during implantation of between ~2 x $10^{14}$ and ~8 x $10^{14}$ boron ions/$cm^2$, plural scattering gave self consistent results for the dechanneling mechanism. An essentially phenomenological multiple scattering treatment of dechanneling was also given for the analysis of room temperature implants. The mechanism governing the dechanneling was shown to depend on the detailed structure of the disordered layer, so an all-inclusive treatment of backscattering spectra to extract arbitrary disorder distributions was not feasible at the present time.

The measured results for the disorder peak depths agreed well with the values for these depths calculated by D.K. Brice, but were 80-85% less than the boron projected range. The measured disorder peak widths were 60-70% less than the calculated values.

The amount of disorder in samples held at room temperature during implantation was about a factor of twenty less than that in samples

implanted at -150°C with the same dose of boron ions. Comparison of the disorder production data with the anneal of a -150°C implant showed the nonequivalence of dynamic anneal processes at a given temperature and thermal instabilities of disorder produced at lower temperatures and then warmed to the given temperature.

It was shown that analyzing beam bombardment could effect the amount of disorder measured.

The depth scale of the backscattering spectra was determined directly by layer removal. The composition of the anodic oxide layers employed in the layer removals was measured by a backscattering analysis. Stopping power measurements were given showing that the aligned beam stopping power as measured by backscattering was ~80% of the random value at 1.0 MeV, an energy near the maximum of the random stopping power curve for helium in silicon.

TABLE OF CONTENTS

## I. Introduction

In recent years, much effort has been spent in studying the motion of energetic charged particles in single crystals. Whenever a low index crystal axis or plane is aligned with a beam of positively charged particles, one observes a significant reduction in energy loss and an even larger reduction in the yield of processes requiring a close encounter with the lattice atoms (such as elastic backscattering, nuclear reactions, and inner shell X-ray production). The interest in this "channeling" effect lies both in the further understanding of the channeling mechanism itself and in its application to the study of the solid state.

Among the various applications of channeling as an analytical tool have been foreign atom location,[1,2] lattice disorder,[3] surface effects,[4] and nuclear lifetimes.[5] One recent application has been the study of ion implantation in semiconductors[6] to determine atom location and lattice disorder. The amount and depth distribution of, the temperature dependence of, and the annealing of lattice disorder produced by energetic ions are important considerations in the evaluation of ion implantation doping. These characteristics for the disorder produced in silicon and germanium during implantation with various high mass ions have been studied previously using the orientation dependence of the yield of backscattered helium ions or protons[2,3,7] (channeling effect measurements). A review of the subject of ion implantation in silicon and germanium through December, 1969, is the work of Mayer,

Eriksson, and Davies[8].

The depth resolution (~300Å) of the channeling technique in the usual experimental arrangement with semiconductor nuclear particle detectors is not sufficient to determine the depth distribution of the disorder produced by heavy ions at the implantation energies ordinarily used (40-60 keV). E. Bøgh[9] has shown how depth resolution can be improved by the use of a magnetic spectrometer. However, implantation of low Z ions of moderate energy should produce disorder distributions quite amenable to measurement by the channeling technique with semiconductor detectors. Measurements of this type have been reported by Gibson et al.[10], showing the disorder due to 400 keV lithium ions implanted in silicon. A similar effect has been observed for 1.0 MeV carbon ions implanted in germanium[11]. These preliminary qualitative results gave the impetus for a major part of this thesis, namely, the development of a quantitative analysis of channeling effect data in the form of disorder distributions versus depth in the sample.

Additional motivation came from the following earlier investigations of temperature effects. The first such study was a previous measurement[7] which showed that for implantations of 40 keV antimony ions at substrate temperatures less than 50°C the disorder created per incident ion was only mildly temperature dependent. However, later sheet conductance measurements[12] on silicon implanted with 200 keV boron ions indicated that the anneal behavior was dependent on the implantation temperature for temperatures below room temperature.

Then Hart and Marsh observed[13] in silicon a large increase in the amount of disorder produced per incident 40 keV boron ion when the sample temperature was reduced from room temperature to -120°C. These experimental results strongly indicated that there were new phenomena in the area of light ion implantations demanding explanation. Finally, if any further incentive were needed, the boron implanted silicon system had obvious relevance to device applications. Thus the present study was undertaken with the dual purposes of first obtaining disorder distributions versus depth by channeling effect measurements for the disorder created by boron ion implantation and second investigating the temperature dependence of the amount of disorder produced during implantation and of the subsequent annealing of the residual disorder present after such an implantation.

This thesis will be written almost entirely in the light of present knowledge. When the work was begun, it was not evident, for example, that disorder distributions could be obtained in a self-consistent fashion from channeling effect measurements, and calculated disorder distributions were available for only restricted ranges of implantation parameters. Further, the changes below room temperature in the amount of disorder produced during boron ion implantation and the anneal behavior of the disorder produced by this implantation were not anticipated.

Various facets of the work contained in this thesis have been published previously, and are listed below:

"Temperature Dependence of Lattice Disorder Created in Si by 40 keV Sb Ions", S.T. Picraux, J.E. Westmoreland, J.W. Mayer, R.R. Hart, and O.J. Marsh, Applied Physics Letters 14, 7 (1969).

"Production and Annealing of Lattice Disorder in Silicon by 200 keV Boron Ions", J.E. Westmoreland, J.W. Mayer, F.H. Eisen, and B. Welch, Applied Physics Letters 15, 308 (1969).

"Lattice Disorder Produced in Silicon by Boron Ion Implantation", F.H. Eisen, B. Welch, J.E. Westmoreland, and J.W. Mayer, Proceedings of International Conference on Atomic Collision Phenomena in Solids, University of Sussex, Brighton, England, 1969 (North-Holland Publishing Company, 1970, p. 111).

"Lattice Disorder Produced in GaAs by 60 keV Cd Ions and 70 keV Zn Ions", J.E. Westmoreland, O.J. Marsh, and R.G. Hunsperger, Radiation Effects 5, 245 (1970).

"Analysis of Disorder Distributions in Boron Implanted Silicon", J.E. Westmoreland, J.W. Mayer, F.H. Eisen, and B. Welch, Proceedings of International Conference on Ion Implantation in Semiconductors, Thousand Oaks, California, 1970, Radiation Effects 6, 161 (1970).

"Correlation Functions in the Theory of Atomic Collision Cascades, Ion Location and the Distribution in Depth and Size of Damage Clusters",

J.E. Westmoreland and P. Sigmund, Proceedings of International Conference on Ion Implantation in Semiconductors, Thousand Oaks, California, 1970, Radiation Effects 6, 187 (1970).

The disorder distribution calculation will be presented by first introducing the typical experimental geometry, then describing the theory of channeling and the parameters that govern its application to disorder distributions. A simple case of amorphous layers of silicon on silicon single crystal substrates will be described as an intermediate case to test some of the principles involved in the disorder calculation for more complicated distributions. The results for this simple case will be shown to be consistent with the calculation procedures used and, in fact, to suggest how such procedures can be applied logically to the more complicated cases. Finally the actual calculation and results for the real cases of interest, namely, the disorder peaks produced in samples by boron ion implantation, will be presented. Some of the limits of the simple theory are pointed out, and other theories of the mechanisms of dechanneling in disordered regions are discussed.

The ion implantation oriented portion of the thesis considers the manner in which an ion stopping in a solid creates disorder. Theoretically calculated disorder distributions are described with particular emphasis given to the theory applicable to the experimental conditions. Measured disorder distributions are compared directly with the theoretically calculated quantities for different implantation conditions. The temperature dependence of the amount of lattice disorder produced

during boron implantation at substrate temperatures between -115°C and 23°C and the subsequent anneal of the residual disorder are presented. The method of determining a depth scale, that is, the conversion of the energy of backscattered analyzing beam particles to depth information about the sample, and values of this depth scale are next given. The method involved a layer removal technique by growth of anodic oxide layers. The analysis of these layers by an application of backscattering techniques was necessary to complete the depth scale determination. An extension of the depth scale treatment for disorder is shown to have a novel application to the measurement of certain stopping powers, and an example is given in closing the thesis.

## II. Disorder Distributions from Backscattering Spectra.

### II.A Experimental Techniques

Investigations employing the channeling effect technique will have a key role in the following work. These analyses were made with the samples at room temperature using momentum analyzed beams of 1.0 - 2.5 MeV $^4He^+$. Results are included of 450 keV proton measurements carried out at the North American Rockwell Science Center. Figure 1 shows a schematic of the geometry of the backscattering analysis for single alignment. The sample is mounted on a goniometer with two degrees of rotational freedom, tilt ($\phi_1$) and rotation ($\phi_2$). The center of rotation is in the surface plane of the sample. Thus any crystal axis or plane of the sample can be aligned with the direction of the incident analyzing beam. The accuracy of the goniometer is $\pm$ 0.05°. In single alignment the analyzing beam incident on the boron implanted silicon sample is aligned parallel to a low-index axis, typically the <110> crystal axis. Some of the incident particles are backscattered through angles $\theta_L$ = 164°, exit far from any high symmetry direction, and enter the solid state silicon surface barrier detector. The energy spectrum of these particles was obtained by standard electronics shown in the block diagram in Fig. 2. The full width half maximum (FWHM) resolution of the particle detecting system was about 15 keV. The type of energy spectra that are observed are shown in Fig. 4a and will be discussed in (II.B).

The uniaxial alignment geometry is shown in Fig. 3 with the single alignment geometry included for comparison. Uniaxial alignment

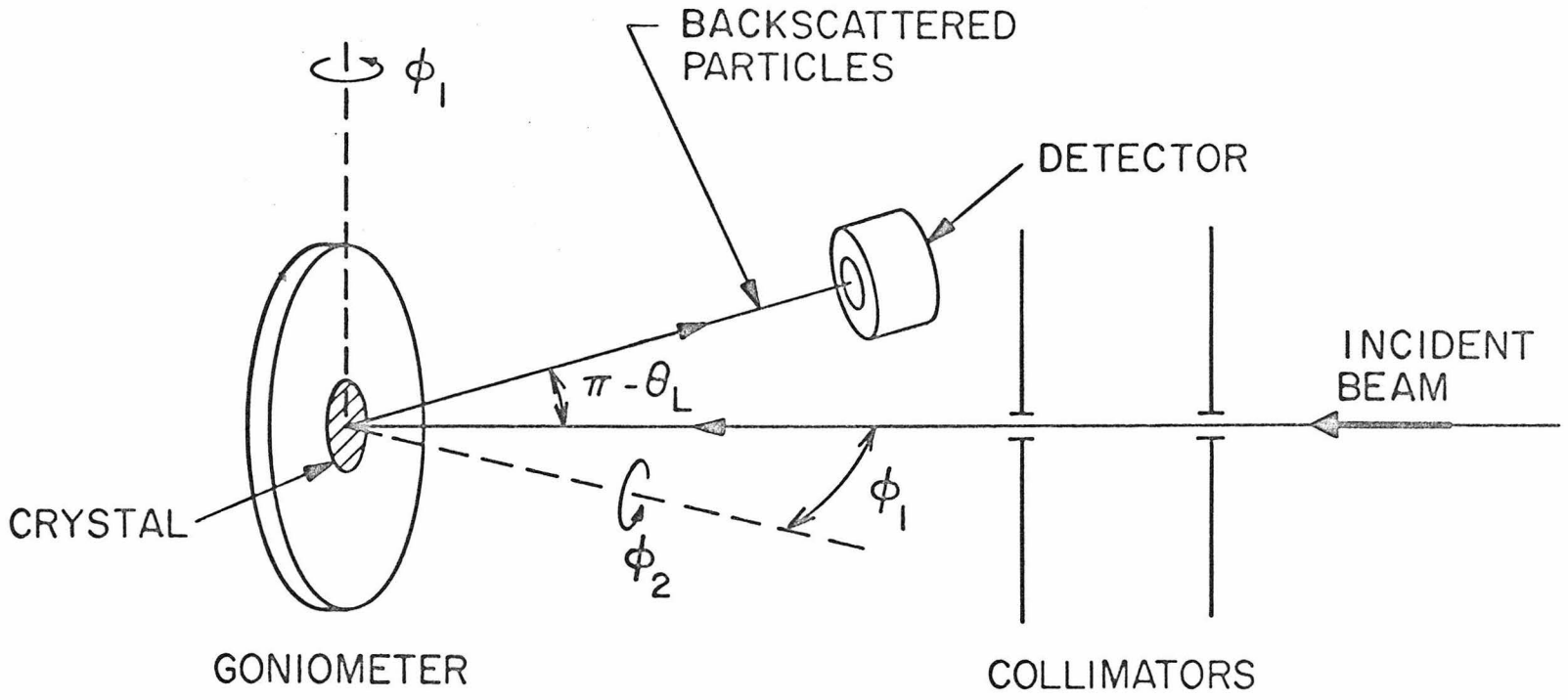


Fig. 1. Schematic Diagram of the experimental geometry for single alignment backscattering analyses.

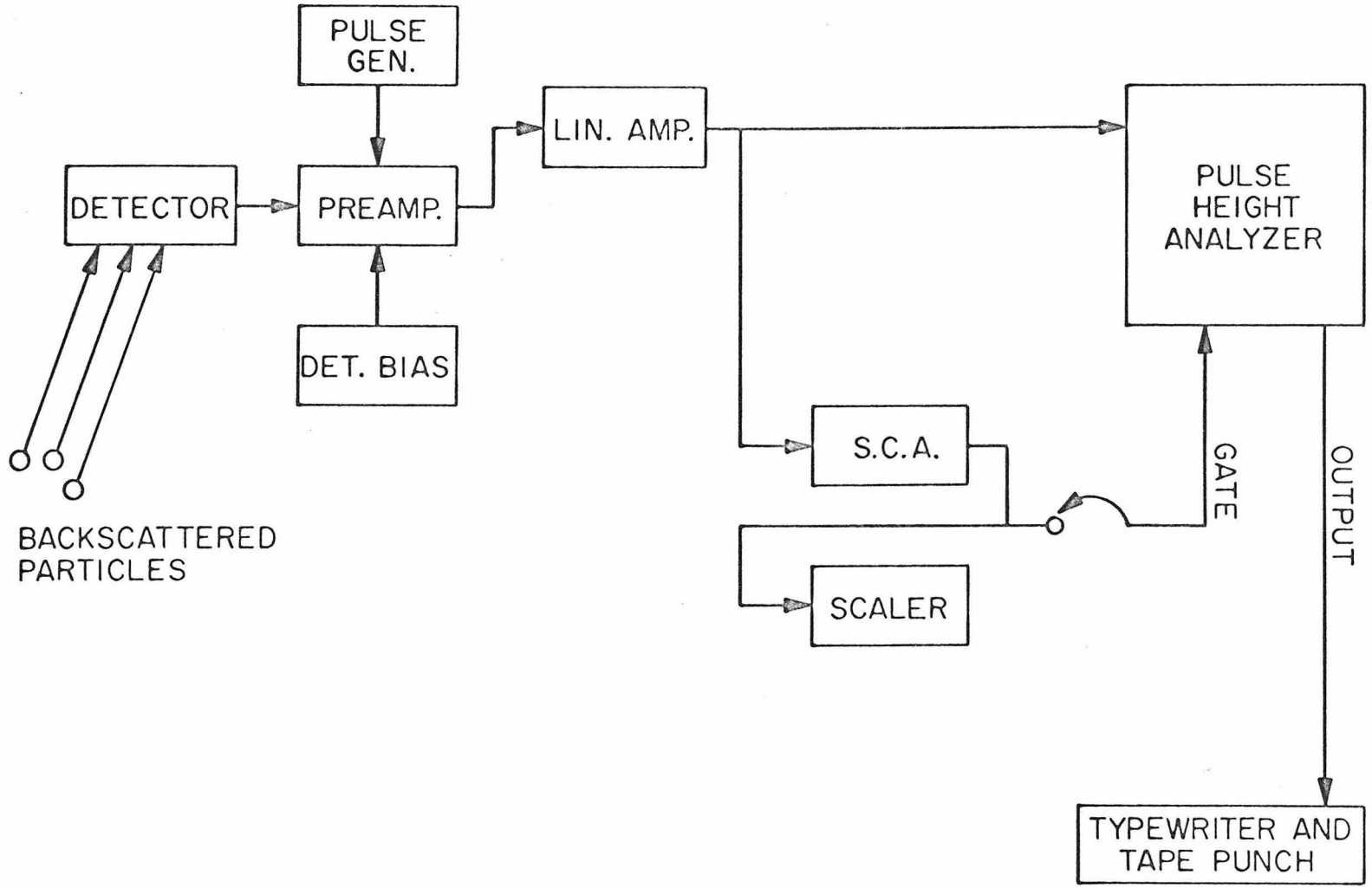


Fig. 2. Schematic diagram of the electronic instrumentation for energy analysis of backscattered particles.

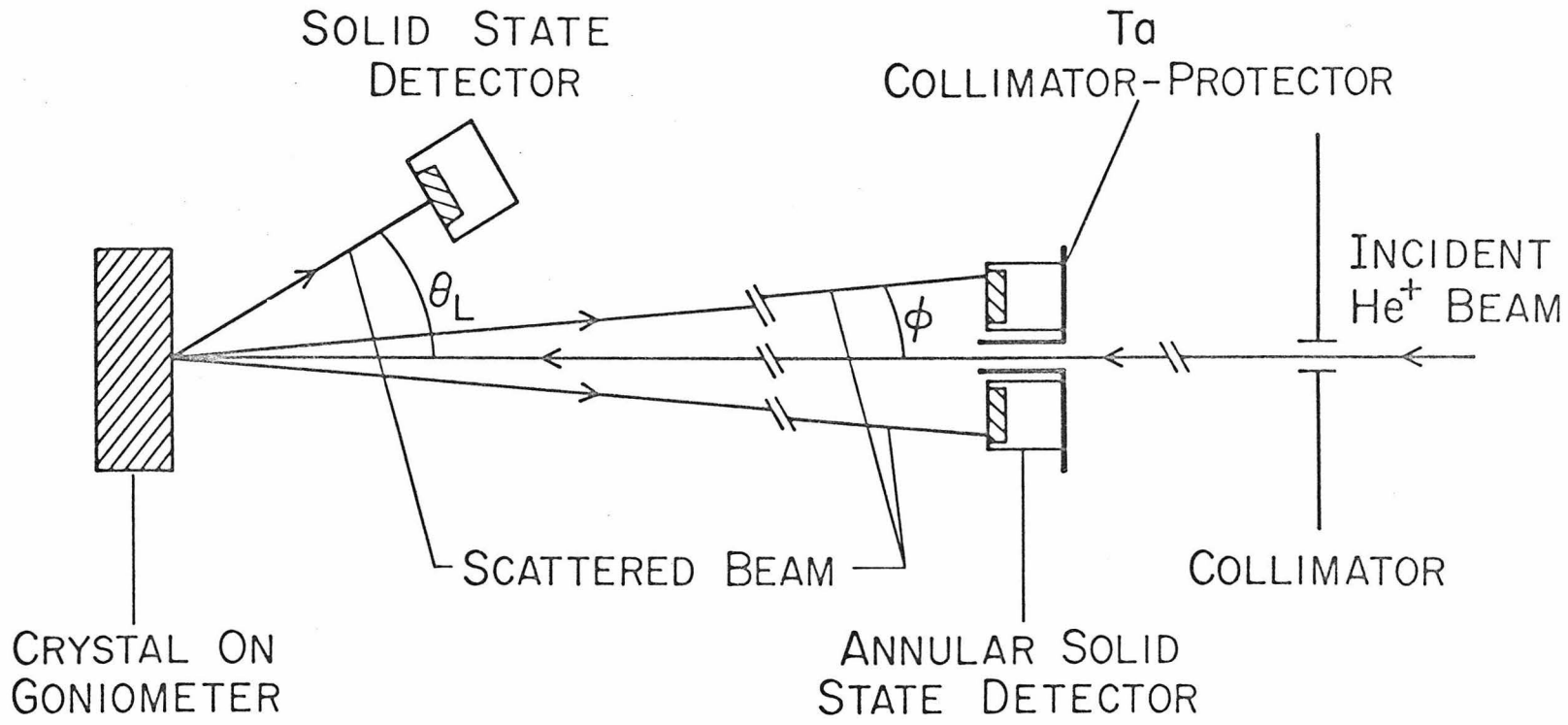


Fig. 3. Schematic diagram of the experimental geometry for single and uniaxial alignment back-scattering analysis.

employs an annular surface barrier detector positioned far enough from the silicon target along the beam axis so that the half angle subtended ($\phi$) was $\simeq 0.2°$. Since the angle subtended was less than the critical angle for channeling, the backscattered particles detected by the annular detector were essentially channeled along the <110> crystal axis.

For the 1.8 MeV $^4He^+$ analyses, the gain of the system was equivalent to better than 1% to an energy per channel in the backscattered spectra of 6.3 keV. This quantity could always be measured for calibration in the single alignment configuration by moving the analyzing beam aligned with the <110> axis to an unimplanted region of the silicon sample and recording a spectrum. After sufficient bombardment with the beam a surface contaimination of carbon would appear. Quantities of $2 \times 10^{16}$ carbon atoms/cm$^2$ producing negligible energy loss (~1 keV[14]) could be easily detected. The yield from the silicon atoms at the surface and the yield from the carbon thin target gave two easily located points in the spectrum with well known energies ($E_{obs} = k^2 E_{In}$, see Eq. (10), II.D, and V.A for more details) from which the energy per channel was then immediately available.

The silicon samples, 10-20 Ω-cm, n-type, phosphorus doped, were cut to within ~1° of the <110> axis. The ion implantations were made at energies of 200 or 300 keV with a magnetically mass separated boron ($^{11}B$) ion beam at the North American Rockwell Science Center. The silicon sample was tilted 10° off the <110> axis* and was held at

*In some cases, the implantations were made with the boron beam aligned parallel to the <110> axis. Analyses of the disorder distribution for these cases have been given in the proceedings of the Sussex Conference, Ref. 38.

the indicated temperature during the boron ion implantation. The implantation geometry is similar to the analyzing beam geometry shown in Fig. 1 except that the detector is removed and the incident beam, now boron, is swept across the sample by horizontal and vertical deflection plates to produce a uniformly implanted region of the order of 1 $cm^2$.

For below room temperature implantations the sample was mounted on a copper block which was mounted on sapphire rods. The stage to which the sapphire rods were attached was cooled by conduction with copper braid attached to an external dewar containing liquid nitrogen. This system allowed the analysis to be performed at temperatures below that of the boron ion implantation. It also permitted annealing to temperatures of 90°C. The sample for analysis on the Caltech 3 MV accelerator could be mounted on a copper block mounted on a lava insulator. Heaters in the copper block allowed annealing treatments to be performed up to 250°C. For temperatures higher than 250°C the sample was removed from the goniometer to an annealing furnace.

II.B Backscattering Spectra and Schematic Disorder Distribution

Typical energy spectra of the backscattered particles will be presented and common features will be discussed. All analyses of this thesis were performed in the single alignment geometry except for one detailed in (V.D).

Figure 4a shows, as an example, backscattering spectra obtained from a 1.8 MeV $^4He^+$ analysis of an unimplanted silicon sample and of one containing some disorder (created by implantation of $5 \times 10^{14}$ 200 keV boron ions/cm$^2$). Aligned spectra or aligned yield refers to those backscattering spectra in which the incident analyzing beam is aligned parallel to a low index crystal axis (for the data reported in this thesis always <110>). Random spectra or random yield refers to those in which the incident beam is far from any high order symmetry direction of the crystal.* The random spectra are equivalent to the yield from an amorphous target of the same composition. One of the principal purposes of this thesis is to extract from these spectra a disorder distribution as shown schematically in Fig. 4b.

The disordered layer, region D of Fig. 4a, probably consists of clusters of displaced atoms or vacancies as well as strained regions around these damaged clusters. The presence of these atoms which are located off the crystal lattice sites results in scattering of the aligned beam. These scattering effects may be classified as follows: 1) large angle scattering events which deflect particles in the analyzing beam through large angles so that some are scattered into the solid state detector (recall Fig. 1), resulting in the disorder peak shown in region

*Because of the small acceptance half angle (1.47°) of the detector, considerable effort is necessary to locate a representative random direction.

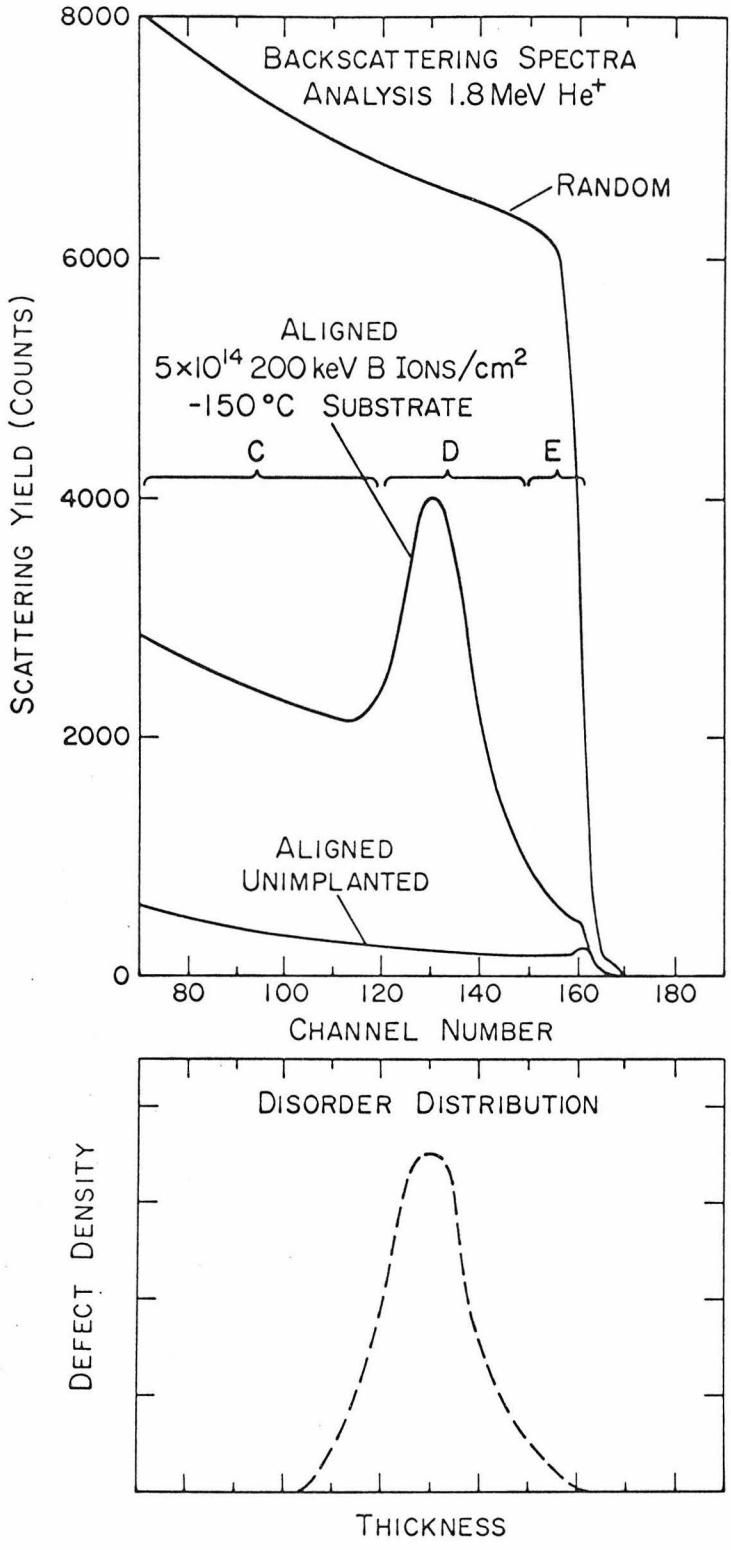


Fig. 4a. Energy spectra (6.3 keV/channel) for 1.8 MeV $^{4}He^{+}$ backscattered from silicon samples.

Fig. 4b. Schematic distribution for disorder versus depth corresponding to aligned spectrum from implanted sample in Fig. 4a.

D of Fig. 4a; 2) small angle forward scattering events which spread the angular distribution of the aligned beam and ultimately result in the dechanneling of those particles in the beam which have been scattered beyond the critical angle for channeling. These dechanneled particles can then scatter both from the silicon atoms off lattice sites and from those on lattice sites as well. This increase in the number of dechanneled particles begins in the lightly damaged portion of the sample near the surface, region E of Fig. 4a. The major portion of the increase occurs in the more heavily disordered region D. It is the increase in the number of dechanneled particles that accounts for the fact that the yield in region C of Fig. 4a behind the disorder peak does not return to the value observed in the unimplanted sample. Layer removal studies of implanted samples have shown that there is no disorder in depths of the sample behind the peak. To extract the disorder distribution from the observed backscattering spectrum, it is necessary to estimate the effect of this dechanneling on the total backscattered yield as a function of depth in the disordered layer. The development of a conversion of the energy of the backscattered particles to a measure of depth in the sample is undertaken in detail in (V). For now, one can regard the channel number as a linear depth scale. This will be shown to be a good approximation in (V).

For the large angle backscattering technique to be useful as a probe, one must be able to extract distributions such as Fig. 4b from spectra such as Fig. 4a. The manner in which the effects of dechanneling and large angle backscattering are combined to produce

aligned spectra is presented schematically in Fig. 5. For simplicity it has been assumed that the random spectrum and the aligned yield from the unimplanted sample are independent of depth. (This, of course, cannot be assumed in the actual calculation.) Then all spectra are divided point by point by the level of the random spectrum to give the normalized ordinate shown in Fig. 5. The normalized aligned spectrum from the unimplanted sample is $\chi_1$ where $\chi_1$ is determined by the fraction of the aligned beam that is scattered outside the critical angle for channeling as the beam penetrates into the sample. This component of the beam is called the random component as it is assumed that dechanneled particles can interact with all the lattice atoms. In an implanted sample the presence of scattering centers in disordered regions causes an increase in the amount of dechanneling, and the random fraction $\chi_R$ of the aligned analyzing beam is increased above its value $\chi_1$ for an unimplanted sample. At a given depth $\chi_R$ is composed of both $\chi_1$ and a contribution proportional to P, the total probability that aligned particles have been dechanneled by this depth. At any given depth (channel) the observed normalized yield $\chi_2$ in an aligned spectrum is composed of $\chi_R$ and the desired normalized component of yield proportional to the number of scattering centers N' in that thickness increment. To obtain N', one must then calculate $\chi_R$ and in turn to obtain $\chi_R$ one must evaluate P.

Although expressions for scattering by thin layers have been studied in detail both theoretically and experimentally in the regions of single, plural, and multiple scattering, it was not known how to

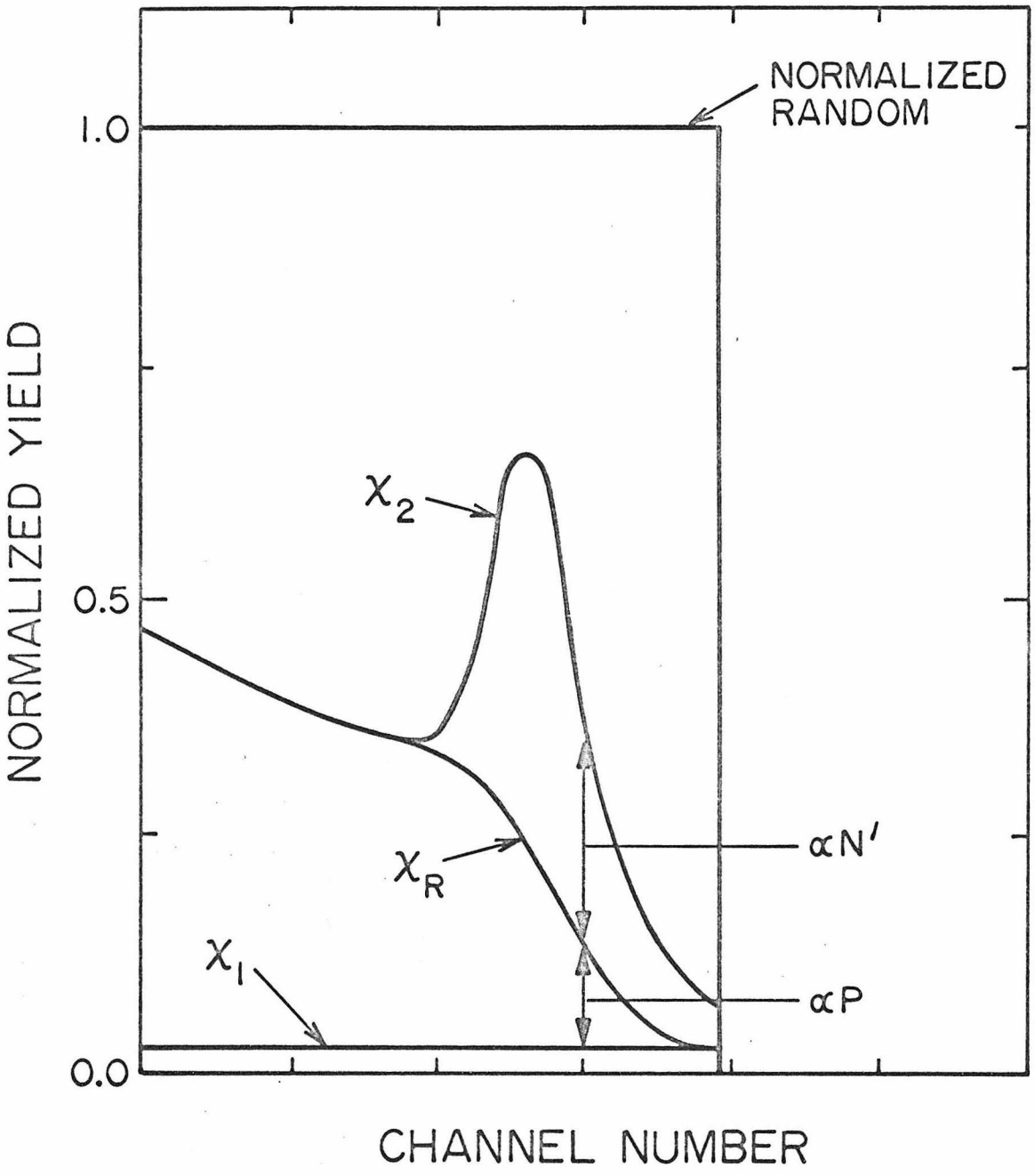


Fig. 5. Schematic spectra showing method of treating contributions to normalized aligned spectrum from a disordered sample.

apply those results to the case of interest here where the scattering centers are distributed in some fashion in a more or less single crystal medium. To decide what expression or expressions to use for P and how to apply such expressions to the dechanneling of particles into the random component of the analyzing beam, a simpler case was first considered. The case chosen was that of amorphous layers of silicon formed on silicon single crystal substrates by ion implantation. This allowed one to investigate the magnitude of the random fraction $\chi_R$ in a single crystal overlaid by a known number of scattering centers. These scattering centers spread the beam angular distribution so that some of the particles enter the substrate with angles of incidence greater than the channeling angle. These studies suggested a form for P for the disordered regions of most interest.

The linear depth scale was measured directly by a successive layer removal technique because of various inadequacies in the available stopping power data. One of the implantation produced disorder peaks was used as a marker and traced as more and more of the silicon surface was anodically oxidized and stripped off. In addition to allowing a description of the dechanneling this depth scale gave the shape of the desired disorder distributions.

So using the information about P gained from study of amorphous layers, this thesis will describe the method of calculating P and $\chi_R$ in order to obtain N'.

II.C Critical Angles and Minimum Yields.

To understand the channeling effect technique analyses and the procedure to be taken to extract disorder distributions from the backscattering spectra, one needs a description of some of the parameters governing channeling. This discussion will summarize just those basic quantities needed to understand channeling as it will be applied in this thesis.

The channeling of an energetic beam of particles in a single crystal occurs whenever the crystal axis or plane is aligned with the beam direction. During channeling the incident particles are steered by a series of gentle correlated collisions with the lattice atoms of the rows or planes. In order for an energetic beam of particles to be steered by the lattice, the beam direction must be oriented within a certain critical angle ($\psi_c$) of the crystal axis or plane.

The critical angle is a particularly useful parameter for characterizing the channeling process. A theoretical framework has been developed by Lindhard[15] for quantitatively interpreting the channeling angular distributions and, in particular, the critical angle. In Lindhard's treatment, the steering of the particle is described by its interaction with the average potential of the row or plane. The discrete atomic potentials are replaced by a continuum

model* giving an average potential $\overline{V}(r)$ depending only on the perpendicular distance r from the row or plane. Lindhard has shown that a good approximation is to treat the transverse energy of the channeled particle as conserved. If the energy in the transverse motion of the particle is insufficient to overcome the potential barrier presented by the lattice row (plane) then one may write

$$\overline{V}(r) = \frac{1}{2} M_1 (v\sin\psi)^2 \approx E\,\psi^2 \qquad (1)$$

where $\frac{1}{2} M_1 v^2 = E$ the energy of the particle, $\psi$ is the angle of incidence of the particle with respect to the row and $\overline{V}(r)$ is the average potential at an impact parameter r with the row corresponding to incident angle $\psi$. The minimum impact parameter ($r_{min}$) corresponds to the maximum or "critical" angle ($\psi = \psi_c$) for which the particle can be steered by the crystal row. For larger angles of incidence the particle penetrates the row and is able to undergo large angle scattering. Thus

$$\psi_c = \sqrt{\frac{\overline{V}(r_{min})}{E}} \qquad (2)$$

For axial channeling,

$$\psi_c = \alpha\,\psi_1, \text{ for } \psi_1 < a/d \quad \text{and} \quad \psi_1 < \rho_r/d \qquad (3)$$

---

*Detailed angular distribution calculations for axial channeling have been performed by Feldman[16,17] without the use of the average potential approximation by following the individual collisions in a Monte Carlo type calculation. Comparison of these results[18] to average potential calculations by Andersen[19] has shown good agreement over the range of validity of the average potential model.

where

$$\psi_1 = \left[\frac{2Z_1Z_2e^2}{Ed}\right]^{\frac{1}{2}} , \qquad (4)$$

and

$$\alpha = \left[\tfrac{1}{2}\log\left(\frac{3a^2}{\rho_r^2 \log 2} + 1\right)\right]^{\frac{1}{2}} , \qquad (5)$$

$Z_1$ and $Z_2$ are projectile and lattice atomic numbers, d is the spacing along the row, a the Thomas-Fermi screening distance associated with the potential ($a = 0.885\, a_o(Z_1^{2/3} + Z_2^{2/3})^{-1/2} \approx 0.1$ to $0.2\text{Å}$ where $a_o = 0.529\text{Å}$, the Bohr radius), and $\rho_r^2$ is the mean square vibrational amplitude of the lattice atoms in the plane perpendicular to the row. The main functional dependence of the critical angle is contained in $\psi_1$ which involves energy, atomic number, and lattice spacing. Note that $Z_2e/d$ is simply the nuclear charge per unit distance along the row. The constant $\alpha$ depends only on the vibrational amplitude and the screening distance a. The value of $\alpha$ is of the order of unity. Detailed numerical calculations by Andersen[19] have shown that Eq. (5) is accurate in the region $\psi_1 < \rho_r/d$.

For low Z particles at MeV energies, the conditions $\psi_1 < a/d$, and $\psi_1 < \rho_r/d$ are usually fulfilled. However, for $\psi_1 > a/d$, a less accurate expression must be used.[15] This is the region of heavy ions at keV energies, and the channeling criterion for a particle of energy E and angle of incidence relative to a row is now given by the following:

$$\psi \lesssim \psi_2 = \left[\frac{a\alpha\psi_1}{d\sqrt{2}}\right]^{\frac{1}{2}} \qquad (6)$$

For energies less than a few hundred keV, $\psi_2$ is between 3° and 5° for ions heavier than boron incident along either the <110> or the <111> axis in silicon. Equation (6) indicates that $\psi_2$ depends only weakly on energy or atomic number.

The planar case is treated in a similar manner.[15] Since only axial critical angles are directly connected with the analyses to be presented in this thesis, it will be simply noted that detailed formulas are available, for example, in Lindhard,[15] and have been studied in detail by experiment.[20,21]

Table I includes for ready reference a summary of typical values of channeling parameters for helium, hydrogen, and boron in silicon.

The discussion of channeling has so far been independent of the role of the channeled particles in a particular experiment. Now one specializes to the case of charged particles used as an analyzing beam to probe a single crystal solid. The motion of particles with angles of incidence with crystal lattice rows $\psi < \psi_c$ determines the particular effects that make channeling both a useful probe and an interesting mechanism to investigate. In this case the particles are steered so that they never come closer than $r_{min}$ to lattice sites. Since $r_{min}$ is of the order of 0.1 - 0.2Å [15] all close encounter processes such as large angle backscattering (impact parameter ~$10^{-3}$Å

Typical Values of Channeling Parameters

Helium (He), Hydrogen (H), and Boron (B) in Silicon

| Lattice Constant $d_o = 5.43\text{Å}$ | | |
|---|---|---|
| $a_{He} = 0.172\text{Å}$ | $a_H = 0.180\text{Å}$ | $a_B = 0.158\text{Å}$ |
| $d_{<110>} = \frac{d_o}{\sqrt{2}} = 3.84\text{Å}$ | | |
| $\rho_r = 0.106\text{Å}$ | $\rho_r/d = 1.6°$ | |
| $\alpha_{He \text{ and } H,EXP.} = 0.90 \pm 0.06$ | $\alpha_{B,THEO.} = 1.09$ | |
| $a_{He}/d = 2.6°$ | $a_H/d = 2.7°$ | $a_B/d = 2.4°$ |

| | $\psi_1$ (°) |
|---|---|
| 1.8 MeV He | 0.62 |
| 1.0 MeV He | 0.83 |
| 0.450 MeV H | 0.87 |

| | $\psi_1$ (°) | $\psi_2$ (°) |
|---|---|---|
| 200 keV B | 2.9 | 2.3 |

TABLE I

for 150° backscattering) will experience a drastic reduction in yield. As an example, for the <110> axis in undamaged silicon at an angle $\theta_L$ = 164°, one sees a 35-fold decrease below the amorphous target yield in the number of backscattered particles for a 1.8 MeV $^4He^+$ incident beam. This was just what was seen for the aligned unimplanted spectrum in Fig. 4a. In contrast to this reduction in the yield from the ordinary "on-lattice site" atoms the yield from "off-lattice-site" atoms* has no orientational dependence. For this reason the large angle backscattering can be used as a probe of the amount of lattice disorder present.

As previously mentioned the yield of close-encounter processes has a marked dependence on the orientation of the incident beam with respect to the crystal lattice. The lattice will also determine the externally observed intensity as a function of angle between the observed emission direction and a crystal-axis or plane for charged particles emitted or scattered from crystal atomic nuclei. This latter effect is usually referred to as "blocking."[15,22,23] According to Lindhard[15] reversibility arguments require that the angular dependences are not only governed by the same parameters but are in fact the same in cases

*"Off-lattice site" here means displacement of the order of the Thomas Fermi screening radius a perpendicular to the direction of the aligned beam. This is the approximate minimum separation of a lattice atom from a lattice site required for this atom to backscatter the aligned analyzing beam. The yield from atoms displaced parallel to this direction will still experience an orientational dependence for analyzing beams aligned with this direction. There are some regular interstitial sites such as the tetrahedral interstitial sites[8] which are along the <111> but not along the <110> lattice rows. The yield from atoms displaced to these sites would experience an orientational dependence for the analyzing beam incident along the <111> but not the <110>.

where the slowing down of the particles is small enough to be neglected. Physically, the emitted particle emerging from a lattice atom in a crystal row or plane at an angle less than the critical angle would have to pass so close to the nearest neighboring atoms of the row or plane that there would be a very large probability for it to undergo a larger angle of scattering than the critical angle. So, for example, in large angle backscattering experiments, one could align crystal axes with the incident beam direction (single alignment), with the detector (blocking), or simultaneously with both (double alignment,[24,25] uniaxial alignment[26]). In this thesis the single and uniaxial alignment techniques will be employed.

The discussion of channeling of the analyzing beam so far has emphasized the behavior of particles inside the target sample. It is useful to think of an external beam of particles impinging on the sample as one now discusses what happens as the beam passes a surface. The same effects exist for the exiting beam in blocking experiments with the wording changed appropriately. The incident beam is well collimated with the angular spread of the beam less than 0.1°. Some fraction of the incident beam will enter the crystal with an impact parameter with a row or plane of atoms so small that after the first scattering it has too much transverse energy to be steered or channeled by the concerted action of the crystal atoms. This portion of the beam will have an angle of incidence with the crystal symmetry direction greater than $\psi_c$, hence will interact with the crystal as though it were an amorphous stopping medium. Thus, it is referred to as the random

component. The approximation commonly used[15] is to treat the beam as being composed of two components, a channeled component which is well aligned and a random component which experiences no effect due to the crystallinity of the sample.

Another characterization of the channeling process is the measurement of the yield of backscattered particles when the analyzing beam is perfectly aligned with a crystal axis or plane. The minimum yield $\chi_{min}$ is defined as the ratio of the minimum value of the yield when the incident beam is aligned with the crystal symmetry direction of interest (aligned yield), to the value of the yield with the beam far from any high symmetry direction of the crystal (random yield), the yields being compared at the same energy.* For illustration one may refer to Fig. 4a. For an undamaged silicon sample, the minimum yield is then by definition the ratio of the value of the aligned unimplanted spectrum in channel number 158 to the value of the random spectrum in the same channel after compensating for detector resolution effects.** A similar quantity can be defined for the spectrum from the implanted sample of Fig. 4a.

The minimum yield is another useful experimental parameter for characterizing the channeling behavior since it is a measure of that

---

*The difference in aligned and random depth scales will be discussed in V.C.

**The front edge of the random is sensitive to minor planar channeling or to the presence of a thin oxide layer. To obtain a representative random value, the approximation used near the front edge is to project the curve of the relatively slowly varying random spectrum behind the front edge (e.g. channels 120-145 in Fig. 4a) to the channel of interest.

fraction of the beam which is not channeled. Its value for particles scattered near the surface of an undamaged sample is essentially just the fraction of the beam penetrating the crystal sufficiently near a crystal row (or plane) so that this fraction of the particles are deflected by more than the critical angle and are no longer channeled. An estimate of the minimum yield for axial channeling can be made from the ratio of the areas around the row ($\pi r_{min}^2$) to the total crystal area per row (1/Nd),

$$\chi_{min} = \pi N d r_{min}^2 \tag{7}$$

where N is the atomic density, d the lattice spacing along the row and $r_{min}$ is the minimum impact parameter for a channeled particle with the row. Using Picraux's result[27] of $r_{min}^2 \cong \rho_r^2$, one obtains a rough estimate of $\chi_{min} \approx \pi N d \rho_r^2$ or for small vibrations $r_{min} \approx a$ giving $\chi_{min} \approx \pi N d a^2$ where $\rho_r^2$ is the mean square vibrational amplitude perpendicular to the row and a is the Thomas-Fermi screening distance.

As for the case of planar critical angles, the case of minimum yields for planar channeling has been treated elsewhere[15,27] but it will not be used and so is not described in this thesis.

The major advantage of the critical angle treatment given above is the simplicity of the resulting formulas and the insight they give into the channeling process. The major effects which have not been included in this discussion of axial critical angles are surface transmission and the depth dependence. Detailed numerical calculations[19] have shown that surface transmission has a negligible effect on axial

critical angles. Depth dependences have not been treated analytically except in a few special cases.[28,29] In fact, experimentally measured values are reported as near the surface as possible or extrapolated to zero depth.[27] However, for 1.8 MeV helium in silicon the critical angle $\psi_c$ changes by less than 10%[20] from the surface to a depth of 1μ, so this is a small effect in the regions of interest of this thesis.

In conclusion the analyzing beam is often treated as an aligned component interacting only with off-lattice-site atoms and a random component interacting with all target atoms. These quantities are initially defined by the entrance of the beam into the sample. The aligned component decreases as the beam penetrates the sample, more strongly in the case of a disordered sample. Governing the overall motion of particles is their angle of incidence with the crystal lattice rows. If this angle is less than some critical angle $\psi_c$, the particles may be regarded as in the channeled or aligned component.

II.D Minimum Yields for Amorphous Layers on Single Crystal Substrates

Before treating the discrete disorder peak case illustrated in Fig. 4a, the influence of amorphous layers* on the minimum yield of backscattered particles from the underlying, undamaged material will be discussed. The aim of the disorder analysis is to try to handle the small angle forward scattering processes taking place in the disordered layers. With amorphous layers one chooses a simple case with a layer of scattering centers followed by a single crystal substrate. By varying both the energy of the analyzing beam and the thickness of the amorphous layers, one can determine whether the energy and thickness dependences of the minimum yield from the crystalline region is consistent with the treatment of the forward scattering in the amorphous layer. The angular distribution of the analyzing beam is calculated from the number of scattering centers/$cm^2$ in the amorphous layers. By comparison of the measured values of the minimum yield and values calculated from the beam angular distribution (employing the value of the critical angle in the crystalline region) one determines if a direct relationship exists between the number of scattering centers and the measured values of the minimum yield. Such a relationship is vital to extending the disorder analysis to more complicated disorder distributions, where the random fraction of the aligned beam corresponds to the minimum yield in the present case. Finally, the absolute values of the results allow a prediction of the error to be expected when such a treatment is applied

*Different thicknesses of such layers are made by different energy implantations of $1 \times 10^{16}$ boron ions/$cm^2$ with the samples held at -150°C during the boron implantation.

to more complicated disorder distributions.

There is no channeled component of the analyzing beam in the heavily disordered layer to be discussed because of the amorphous nature of the layer. The angular distribution of the analyzing beam is spread by small angle scattering as it passes through the amorphous layer. The layer will be treated as a scattering foil with a known number of scattering centers. This change in the angular distribution causes an increased backscattering yield from the underlying crystal directly related to the number of particles of the analyzing beam which have angles of incidence with the rows of atoms greater than the critical angle for channeling.

Sixteen aligned and random spectra were obtained from four different thickness amorphous layers in the single alignment configuration of Fig. 1 by employing 1.0, 1.5, 2.0, and 2.5 MeV $^4He^+$ analyzing beams. Also for the thickest layer spectra were obtained employing a 450 keV proton analyzing beam and a 1.8 MeV $^4He^+$ analyzing beam. The spectra all contain the same general features. Consider, for example, the aligned and random spectra obtained at 1.8 MeV and shown in Fig. 6. The aligned yield follows the random yield at the surface and then drops below the random yield deeper within the sample. The experimental values of the minimum yield $\chi_R$ are obtained from the spectra of Fig. 6 as follows:

$$\chi_R = A/B \tag{8}$$

where A is the minimum value of the aligned spectrum behind the layer

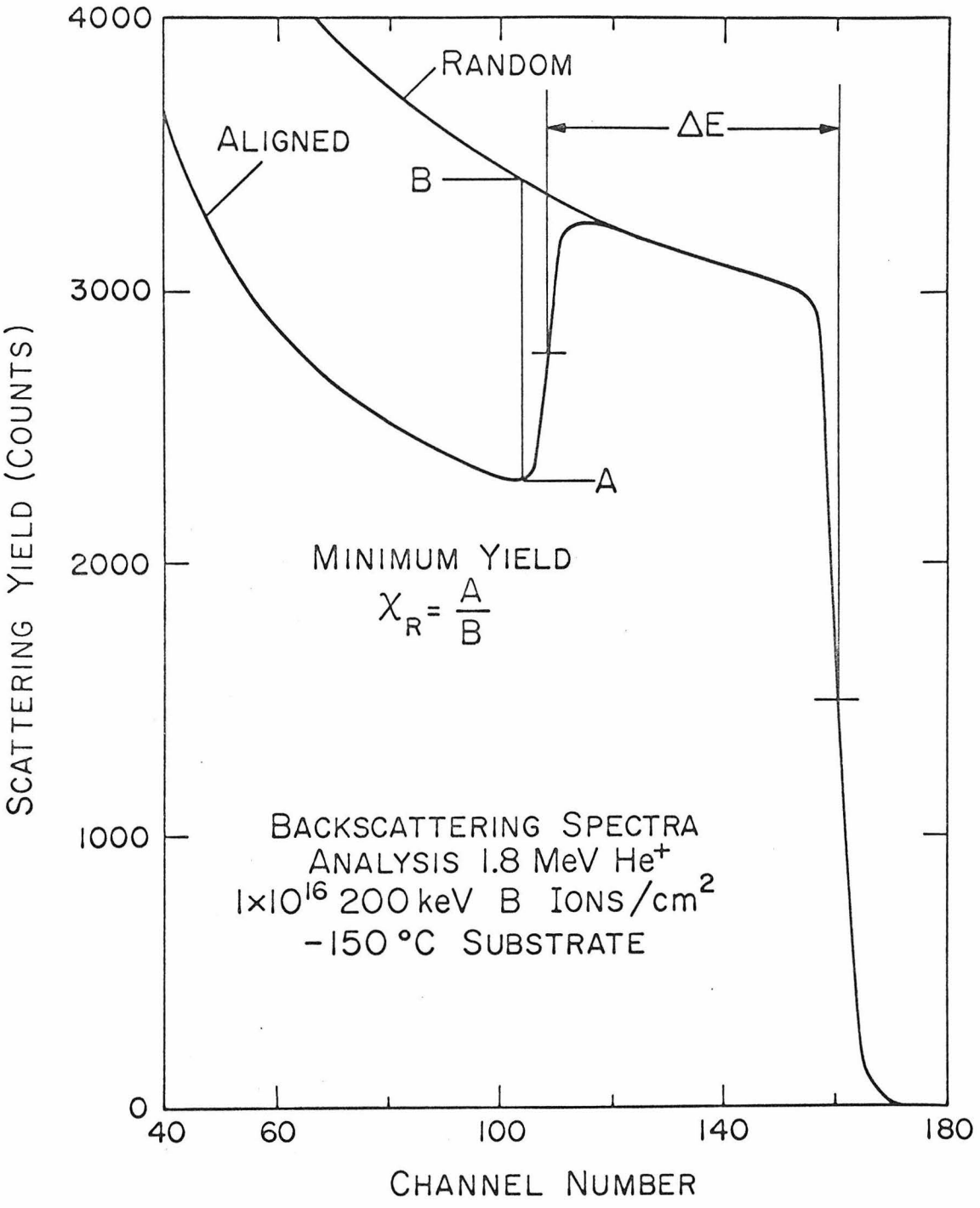


Fig. 6. Spectra from 1.8 MeV $^4He^+$ analysis of an amorphous layer.

and B is the value of the random spectrum at the same energy (see Fig. 6). The value of $\chi_R$ depends on analyzing beam energy and layer thickness

For the calculation of $\chi_R$, the heavily disordered layer is approximated by a layer of thickness $\Delta t$ of scattering centers of the number density of silicon ($5.00 \times 10^{22}$ atoms/cm$^3$). All thicknesses and depths in this thesis will be reported in units of length. What is actually measured is the number of scattering centers/cm$^2$ in all cases. Then the number density of silicon is used to convert to the length unit. This length may not be the actual linear depth in the sample because the implanted layer may have a different density from crystalline silicon. In fact, for the amorphous layers to be considered in more detail in this section, there is evidence[30] that the density may be less than that of single crystal silicon by as much as 10%. This in no way affects the comparisons made with theory, for example in (III), because all theoretical calculations of disorder distributions, measurements of stopping power, or the like assume that the density of the medium is just that of single crystal silicon (2.33g/cm$^3$).

The first step in measuring $\Delta t$ is to obtain $\Delta E$ the width in energy for all sixteen cases as illustrated in Fig. 6. The high energy leading edges of both random and aligned spectra coincide and are determined by the system energy resolution. The energy corresponding to silicon surface atoms is the midpoint of the rise to the random level. The drop of the aligned spectrum (in approximately channel 115) below the random spectrum has the same width as the front edge, that is, is again determined by the system energy resolution. This suggests the

presence of a sharp interface between the amorphous layer and the underlying undamaged substrate. For such a sharp interface the rear edge of the amorphous layer corresponds to the midpoint of the drop in the aligned spectrum from the random spectrum to the minimum of the aligned spectrum (see Fig. 6). This assumes that the aligned spectrum near channel 115 in Fig. 6 is just a superposition of the yields from the rear edge of the amorphous layer and the front edge of the underlying crystalline substrate and that the midpoints of these two yields occur in the same channel. A more detailed description of this type of analysis has been given recently by Mitchell et al.[31] as is discussed briefly in (V.B).

The values of $\Delta E$ in keV and normalized values at each energy are given in Table II. The error in one $\Delta E$ determination is composed of the error in determining the energy per channel (<1%) and the errors in choosing each midpoint ($\pm$0.5 channel). The widths in number of channels vary, so the estimated absolute error varies from $\pm$2.5% for the thickest layer (sample NX-2-38-1) in the 1.0 MeV measurement to $\pm$7.5% for the thinnest layer (sample 66C) in the 2.5 MeV measurement. All normalized values for a given sample are within $\pm$4% of the average for all four energies.

The thicknesses $\Delta t$ were calculated from the $\Delta E$ values using the following depth scale for heavily disordered layers:

$$(\Delta E/\Delta t) = k_{Si}^{2} \; S_R(E_1) - \sec \theta_L \; S_R(E_2) \qquad (9)$$

TABLE II

Values of $\Delta E$ for Different Thickness Amorphous Layers

| Analyzing Beam Energy | 1.0 MeV | | 1.5 MeV | | 2.0 MeV | | 2.5 MeV | |
|---|---|---|---|---|---|---|---|---|
| Sample | keV | Normalized | keV | Normalized | keV | Normalized | keV | Normalized |
| NX-2-38-1 | 355 | 1.000 | 337 | 1.000 | 299 | 1.000 | 281 | 1.000 |
| 66A | 298 | 0.839 | 277 | 0.823 | 249 | 0.833 | 225 | 0.801 |
| 66B | 237 | 0.668 | 216 | 0.641 | 190.3 | 0.638 | 173.0 | 0.616 |
| 66C | 163.8 | 0.462 | 147.7 | 0.438 | 132.6 | 0.443 | 129.6 | 0.461 |

where $\theta_L$ is the backscattering angle in the laboratory system of coordinates, $E_1$ the incident energy, $E_2 = k^2 E_1$, $S_R(E)$ the random stopping power of the analyzing beam in silicon at Energy E, and $k^2$ as follows:

$$k^2 = \left[ \frac{M_1 \cos \theta_L}{M_1 + M_2} + \left[ \left[ \frac{M_1 \cos \theta_L}{M_1 + M_2} \right]^2 + \frac{M_2 - M_1}{M_1 + M_2} \right]^{1/2} \right]^2 \qquad (10)$$

$M_1$ is the projectile atom and $M_2$ the target atom from which $M_1$ is scattered. The depth scale expression, of which Eq. (9) is a special case, is discussed in (V.C).

To apply Eq. (9) one needs the stopping powers for helium in silicon. These are not available below 1 MeV and for 1 to 2.5 MeV are only known to an estimated error of $\pm 10\%$[14]. However, independent values[32] of the stopping power for protons in silicon in the energy range 350 to 480 keV are available. For this reason the 450 keV proton measurement of the thickest layer was performed. Since the $\Delta E$ values for the four different measurements scale well, a single depth scale determination would allow calculation of the thicknesses $\Delta t$ for all four layers from the average of the ratios in Table II. The results obtained by F.H. Eisen[32] for $S_R(E)$ were used for the proton measurement giving a value of $\Delta t$ of 6500Å for sample NX-2-38-1. The purpose of the 1.8 MeV helium measurement was to estimate the error in this proton thickness measurement. Values of $S_R(E)$ for the 1.8 MeV helium analysis were estimated using the value[14] of 25.7 eV/Å computed from the measurements of Gobeli.[33] (The other value available for this number was 24.1 eV/Å from the proton value of Janni[34] for $S_R$(450 keV) scaled by 4.0, a

factor given by Whaling[14]. This is a difference of only 6% well within the ±10% error estimated by Whaling.) For $S_R$(1.0 MeV) the value of 33.1 eV/Å obtained in this thesis (V.D) was used. This value has been recently confirmed by other measurements.[35] These results give a value of 6230Å for Δt for sample NX-2-38-1, a difference of only 4.3% from the proton measurement result. This is taken as a measure of the stopping power errors.

The Δt values were scaled to the 6500Å by the ratios of 1.000:0.832:0.649:0.448 giving thicknesses of 6500Å, 5400Å, 4200Å, and 2900Å. The values of the 2.5 MeV measurements were omitted in the average ratio calculation since they seem to be consistently further away from the other values. Based on the sharp interface approximation the thickness of these layers seems known to within the variation of the values from the average, a maximum of ±3% for the thinnest layer, plus the absolute error due to stopping power errors estimated at ±5%, or about ±8% error in a given value of Δt.

The small angle scattering in the amorphous layer is treated in the plural scattering regime in the manner of Keil et al.[36] or in the multiple scattering regime in the manner of Moliere[37]. The Gaussian approximation to Moliere's angular distribution will be used. Another Gaussian approximation due to Lindhard[15] is compared to the Moliere one since it was used[38] in some of the earlier disorder calculations to be described in (II.E).

The plural and multiple scattering in the small angle approximation the differential cross section may be represented[39] as follows:

$$d\sigma = \left[\frac{2Z_1Z_2e^2}{pv}\right]^2 \frac{2\pi\theta d\theta}{(\theta^2 + \theta_a^2)^2} \tag{11}$$

where $Z_2$ is the atomic number of the scattering centers, $Z_1$,p, and v the atomic number, momentum, and velocity respectively of the scattered particle in the center of mass system of coordinates. The screening angle $\theta_a$ describes the screening of the nuclear charge by the atomic electrons and is defined[39] as follows:

$$\theta_a = \frac{\hbar}{pa}\left(1.13 + 3.76\left(\frac{Z_1Z_2}{137\beta}\right)^2\right)^{\frac{1}{2}} \tag{12}$$

where a is the Thomas-Fermi screening radius, and $\beta = v/C$. Since the data given by Keil et al. are in terms of reduced angles, the following reduced critical angle was defined:

$$\theta_k = \frac{\psi_c}{\theta_a} \tag{13}$$

Experimentally measured values[20] of $\psi_c$ are about 25% less than values calculated from Eqs. (3), (4), and (5). The experimental data were fitted by the least squares approach to Eq. (3) to obtain a value of $\alpha = 0.90$ for the <110> axis in silicon with which to calculate $\psi_c$.

The mean number m of single scattering processes which a particle experiences traversing an amorphous layer of thickness t is the following:

$$m = Nt\sigma \tag{14}$$

where N is the atomic density and, letting $\theta$ be the scattering angle,

$$\sigma = \int_{\theta=0}^{\theta=\pi} \left(\frac{d\sigma}{d\Omega}\right) d\Omega \tag{15}$$

The quantity $d\sigma/d\Omega$ is the probability that a particle will be scattered through an angle whose magnitude lies between $\theta$ and $\theta + d\theta$ independently of whether or not other deflections occur at the same time into other angular regions. The quantity m depends on the exact behavior of $d\sigma/d\Omega$ for small values of the argument $\theta$. For theoretical treatments of plural and multiple scattering more complicated quantities than m are defined to characterize the detailed angular distribution. When $d\sigma$ is represented by Eq. (11), m in Eq. (14) has the same value as the other more complicated quantities. The approach taken in this thesis is to use Eq. (11) for $d\sigma$ obtaining m as follows:

$$m = 4\pi Nt\left(\frac{Z_1 Z_2 e^2}{pv\theta_a}\right)^2 \tag{16}$$

(The contribution at $\theta = \pi$ is negligible and has been dropped from Eq. (16)).

Under the approximation that all particles scattered outside the critical angle $\psi_c$ (reduced critical angle $\theta_k$) in passage through an amorphous layer are in the random component of the beam in the underlying undamaged regions of the sample, the minimum yield $\chi_R$ defined in Eq. (8) is the following:

$$\chi_R = \hat{G}^* (m, \theta_k) \tag{17}$$

where m is from Eq. (16) and $\hat{G}^*$ is the value of the normalized angular distribution $\hat{G}^*$ integrated over angles greater than $\theta_k$. Thus $\hat{G}^*$ is the fraction of particles scattered through angles greater than $\theta_k$. $\hat{G}^*$ is obtained from Table 2 of Keil et al.[36]

For multiple scattering, following Lindhard,[15] one has that, as a result of many small scattering processes, the beam distribution for small values of $\psi$ may be approximated by a Gaussian as follows:

$$f(\psi)\ 2\pi \sin\psi\ d\psi = \exp\left(-\frac{\psi^2}{\Omega^2}\right) 2\psi\ d\psi/\Omega^2 \tag{18}$$

where $\Omega^2$ is the mean square scattering angle and $\psi$ is the polar angle with respect to the axial channeling direction. Again $\chi_R$ as defined in Eq. (8) is just the fraction of particles with angles $\psi$ greater than $\psi_c$, so $\chi_R$ is Eq. (18) integrated over angles greater than $\psi_c$. The contribution at the endpoint of integration is negligible so $\chi_R$ is the following:

$$\chi_R = \exp\left(-\frac{\psi_c^2}{\Omega^2}\right) \tag{19}$$

Two formulations of the mean square scattering angle $\Omega^2$ will be compared. The Gaussian approximation to the Moliere distribution is characterized by $\Omega^2 = \Omega_M^2$ defined as follows:

$$\Omega_M^2 = \frac{Z_1^2 Z_2^2 e^4 \pi N t B}{E_L^2} \tag{20}$$

where $E_L$ is the energy of the scattered particle in the laboratory system of coordinates. The quantity B in Eq. (20) is related to m as follows:

$$m = \left(\frac{\gamma^2}{e}\right) \frac{e^B}{B} \tag{21}$$

and

$$\frac{\gamma^2}{e} = 1.167 \tag{22}$$

The Lindhard treatment of multiple scattering uses $\Omega^2 = \Omega_L^2$ where

$$\Omega_L^2 = \frac{2\pi Z_1^2 Z_2^2 e^4}{E_L^2} Nt \ \ell n(1.29\varepsilon) \tag{23}$$

and

$$\varepsilon = \frac{a M_2 E_L}{Z_1 Z_2 e^2 (M_1 + M_2)} \tag{24}$$

This gives an alternate expression for the mean square scattering angle within the Gaussian approximation to the beam angular distribution.

Figure 7 shows experimental values of $\chi_R$ versus the reduced critical angle $\theta_k$ defined in Eq. (13). The experimental values of $\chi_R$ are the results for spectra from the different energy helium analyzing beams on the different thickness amorphous layers. The two lower solid lines in Fig. 7 are the values of $\chi_R$ as a function of $\theta_k$ calculated from the plural scattering expression, Eq. (17), for values of m

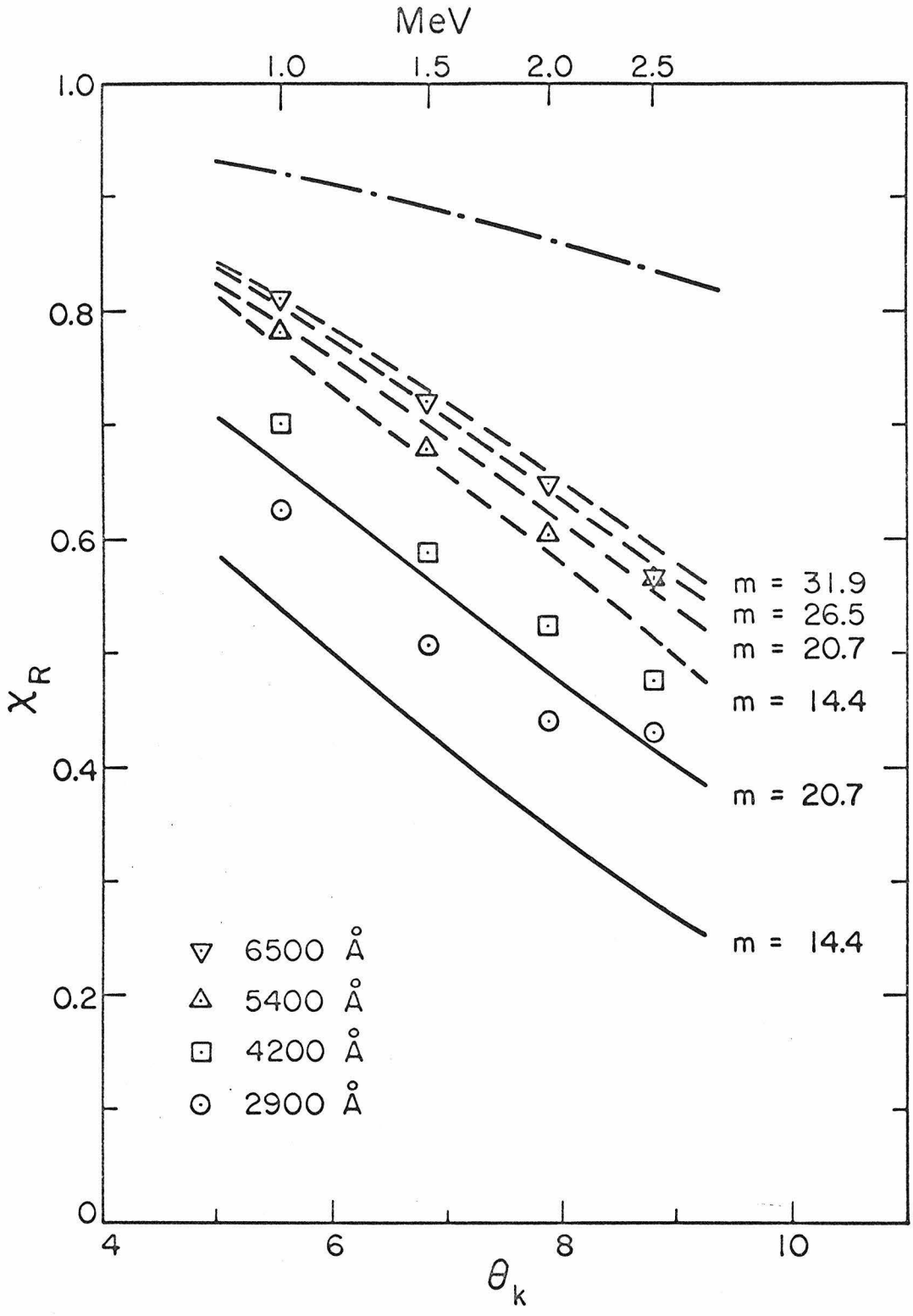


Fig. 7. Experimental values of $\chi_R$ from different energy $^4He^+$ analyses of different thickness amorphous layers. Calculated values of $\chi_R$ based on (1) solid lines - plural scattering, (2) dashed lines - Moliere multiple scattering, (3) dash-dot line - Lindhard multiple scattering.

(14.4 and 20.7) determined from Eq. (16) for the two thinner layers. The plural scattering results of Keil et al. are valid for $0.6 \lesssim m \lesssim 20$ and according to Keil et al.[36] join in the region $m \approx 20$ with the results of Moliere's theory of multiple scattering[37]. So, similarly, the four upper dashed lines in Fig. 5 are the values of $\chi_R$ calculated from the Moliere multiple scattering expression, Eqs. (19) and (20), for the beam angular distribution for m = 14.4, 20.7, 26.5, and 31.9. Values of $\chi_R$ calculated by the Moliere approach are relatively slowly varying functions of m in this region.

The uppermost dash-dot line in Fig. 7 is the result of calculating $\chi_R$ for the 6500Å layer using the Lindhard expression $\Omega_L^2$ from Eqs. (23) and (24) in Eq. (19). This treatment does not appear satisfactory for these amorphous layers. In fact, the ratio $\Omega_M^2/\Omega_L^2$ is readily available from Eqs. (20) and (23), and is $B/(2\ell n(1.29\varepsilon))$. This quantity has a value of about 0.4 for the multiple scattering region, but it is a slowly varying function of energy and m. For example, it varies for 1.0 MeV helium in silicon from 0.37 for m = 25 to 0.42 for m = 40. For helium in silicon and m = 32 it varies from 0.40 for 1.0 MeV to 0.35 for 2.5 MeV.

Increasing values of $\theta_k$ in Fig. 7 correspond to increasing energy of the $^4He^+$ analyzing beam. The slope of the solid lines with increasing $\theta_k$ agrees with the slope of the data points, so the calculated energy dependence of $\chi_R$ agrees with the experimental one. For the two thicker layers the Moliere calculated value of $\chi_R$ agrees to within 5% with the measured value. For the two thinner layers, the plural scattering values lie 14% to 35% below the measured values of $\chi_R$ for the

2900Å layer and 6% to 13% below the measured values for the 4200Å layer. However, the Moliere multiple scattering values of $\chi_R$ lie 22% to 16% above the measured values for the 2900Å layer and 1% to 16% above for the 4200Å. There appears to be a rather broad transition region between plural and multiple scattering where neither calculation works very satisfactorily in terms of the absolute value of $\chi_R$ calculated.

The results of this work with amorphous layers indicate that Eqs. (12) and (16) for $\theta_a$ and m respectively give qualitatively correct descriptions for forward scattering in the regions of interest in this thesis. This determination was necessary because the experiments of Leisegang[40] for the scattering of electrons in thin gold foils showed that in the region of plural scattering, values of m calculated from these equations differed from experimental values by nearly an order of magnitude. Although in the region of multiple scattering these expressions for m and $\theta_a$ had been confirmed by experiment for electrons,[41,42] there were some errors in Moliere's work (see Scott[43] for details). Bichsel's measurements[44] of the multiple scattering of protons at 2.2 MeV agree to within 10% to 20% with the Gaussian approximation to Moliere's distribution for reduced angles less than 0.80 but indicate large differences in the single scattering tail. These varied results then indicated that the expressions for m and $\theta_a$ should be experimentally verified in each case to which they were to be applied.

Finally the amorphous layer results indicate that the choice of the critical angle as the dividing point between aligned and random

components of the analyzing beam leads to consistent results. In retrospect a better way to study the forward scattering and back-scattering processes might be to evaporate thin metal films on single crystals and then employ the same line of investigation carried out with amorphous layers created by ion implantation.

II.E Disorder Distributions for Discrete Disorder Peaks

The principal problem to be attacked is that of extracting disorder distributions from the discrete disorder peak type of spectrum of Fig. 4a. For an increment of thickness one would like to evaluate the probability that a particle has been dechanneled, that is, that a particle in the aligned component of the analyzing beam has been scattered into the random component by the scattering centers in that given increment of thickness. From this one could then obtain the desired disorder distribution from aligned spectra. Unfortunately accurate analytical expressions for this probability are available only for two limiting cases: (a) when the dechanneling is due entirely to single deflections greater than $\psi_c$, and (b) when it is due to multiple scattering in which a total deflection greater than $\psi_c$ is the result of many (i.e. more than ~20) deflections each of which is much smaller than $\psi_c$. These limiting expressions will be presented, and a method of treating dechanneling in the region between these limits will be described. Whatever the treatment of the scattering process, it will be necessary to obtain the angular distribution of the analyzing beam as a function of depth in the sample and to formulate criteria for deciding when particles have been dechanneled. The procedure used is an extension of the method employed in the investigation of the minimum yields behind amorphous layers.

Specifically the approach taken is to calculate a distribution of scattering centers based on the following assumptions:

1. In an aligned orientation the analyzing beam is composed of an aligned or channeled component and a random component.

2. All particles scattered outside the critical angle are dechanneled from the aligned component of the beam into the random component.

3. The normalized random component (random fraction) of the analyzing beam is composed of two parts: the fraction that would have been dechanneled by a perfect crystal represented by the normalized aligned yield of an unimplanted sample and the fraction dechanneled by forward scattering from the same scattering centers which produce the backscattering yield.

4. All scattering centers give the same amount of dechanneling independent of their location within the crystal channel or of their association in the form of complex defect clusters.

5. A particle in the random component of the beam never becomes a part of the aligned component of the beam.

Assumption one is the common one[15] taken in describing the analyzing beam, as it moves through the sample. In fact, it is an approximation because the portion of the beam in the region of angular incidence $\psi_c \lesssim \psi \lesssim 2\psi_c$ is in some sort of transition region between being a part of the well-aligned component and the random component.

Assumption two implements assumption one by specifying the point of division of the beam into aligned and random components. It is the same as used in the determination of the $\chi_R$ values of the

amorphous layers.

Assumption three contains the important points relating to the sources of the random fraction of the analyzing beam $\chi_R$. First it treats as independent the different contributions to the spreading of the angular distribution of the analyzing beam. It represents these different contributions by letting $\chi_R$ be a simple sum. The contribution to this sum from the undamaged lattice is then available empirically from the measured aligned yield from an undamaged sample, shown in Fig. 4a, normalized by the random spectrum. An even more important point is that the only other contribution to $\chi_R$ is from dechanneling of the aligned beam by forward scattering from the scattering centers composing the disorder. This contribution to $\chi_R$ is usually the dominant one for the cases of interest in this thesis. For example, for 1.8 MeV helium analyses, $\chi_1$ is $\lesssim 0.05$ at 7,000Å where $\chi_R$ may be $\gtrsim 0.3$. Assumption three further requires that particles scattered to angles less than the critical angle do not experience a faster dechanneling rate than the initially well aligned beam.

Assumption four is one of the most limiting assumptions when one tries to apply this treatment to a general backscattering spectrum from an arbitrary distribution of disorder. The distribution of atoms in the disordered layer as a function of distance from the lattice row is not known. Neither is the backscattering or forward scattering probability of atoms for the aligned component of the analyzing beam known as a function of the distance of these atoms from the lattice rows especially in the crucial region near the row. So, as a first

approximation, the scattering probabilities are taken as arising from the presence of a number of individual scattering centers/$cm^2$. That is, the centers producing the backscattering are the same centers that produce the dechanneling contribution $\chi_R - \chi_1$. One case where this assumption clearly breaks down will be discussed in the analysis of room temperature implants.

Assumption five requires that the probability of particles in the random component of the beam being scattered into the aligned component of the beam is small. For an undamaged crystal the situation is the same as the emission of charged particles from lattice site, that is, the blocking effect occurs so the probability of "rechanneling" by single collisions is accordingly small. For a damaged crystal there may be a significant probability of scattering back into a channel by the disordered regions, but this probability is assumed to be negligible for the present investigations.

These assumptions form the basis of a simple model of the dechanneling process. The intent of this work is to see whether this approximate treatment yields self consistent, physically meaningful results.

As Bøgh has shown,[4] the density N' of centers producing the backscattering is given as a function of the depth t by:

$$N'(t) = N \frac{\chi_2(t) - \chi_R(t)}{1 - \chi_R(t)} \qquad (25)$$

where N is the atomic density of the crystal, $\chi_R$ is the random fraction of the analyzing beam, and $\chi_2$ is the normalized yield in the aligned spectrum, i.e., the aligned yield divided by the random yield (random

spectrum, Fig. 4a). The quantities $\chi_2$ and $\chi_R$ have been identified in the schematic Fig. 5. Equation (25) may be derived by observing that the random fraction of the beam $\chi_R$ interacts with all the lattice atoms whereas the aligned fraction of the beam $1 - \chi_R$ interacts only with the "off-lattice site" atoms N'. Then $\chi_2 = \chi_R + (1 - \chi_R)N'/N$ from which Eq. (25) follows directly. The disorder calculation should use values of the aligned yield at depth t normalized to the random yield at that depth. For convenience the value of the random spectrum at the same energy was used. The difference of the random spectrum depth scale from the aligned spectrum depth scale as discussed in (V.C) introduces only a negligible error because the height of the random spectrum varies only slowly with energy behind the front edge. The value of N used in the calculation is the total number of lattice atoms equivalent to the thickness of the sample corresponding to one channel. The measurement of a depth scale for the sample will be discussed in (V.C). The result of that measurement will simply be employed here. For 1.8 MeV helium spectra under this experimental geometry the depth scale is $(45 \pm 2)$ eV/Å. Since the electronics are set to give 6.3 keV per channel (see (II.A)), this gives 140Å per channel or finally $N = 7.0 \times 10^{16}$ atoms/cm$^2$ per channel.

The problem of determining the disorder distribution from measurements of the aligned and random backscattered energy spectra then becomes one of estimating or calculating $\chi_R(t)$. An approximation to the yield from the random component which has been used in earlier work[2,3] is represented by the straight line labeled R' in Fig. 8.

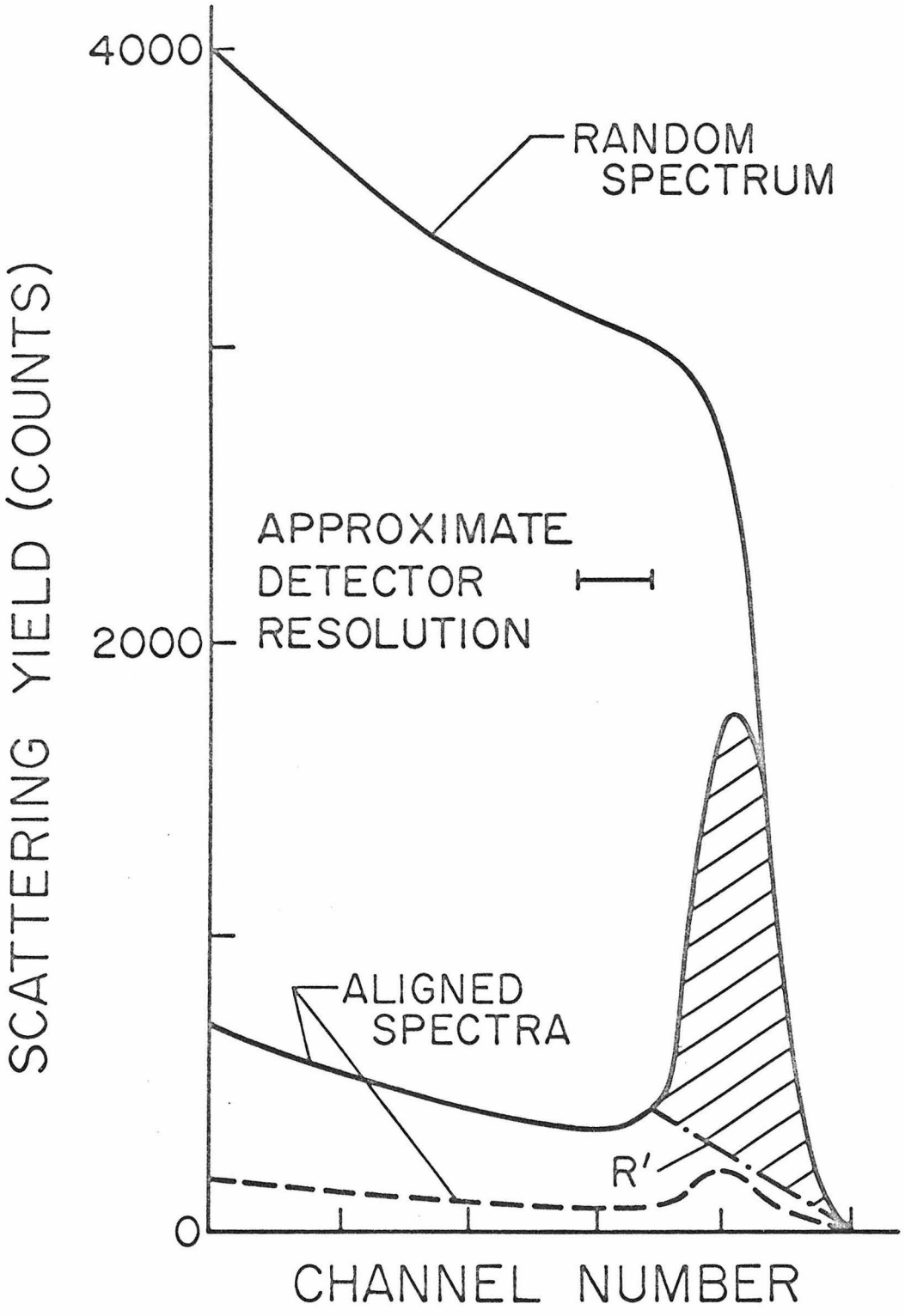


Fig. 8. Schematic spectra showing disorder analysis technique before this thesis.

This shows schematically a typical case in which the straight line approximation was applied. The disorder peak was at the surface of the sample and had a half width comparable to or slightly larger than the detector resolution. While the straight line approximation facilitates making rough estimates of the relative amounts of disorder represented by the disorder peak in cases of wider disorder distributions, it is an oversimplification to assume that $\chi_R$ varies with t in this manner. To extract disorder distributions from the backscattering data, the following expression, originally suggested by Feldman,[45] was used for $\chi_R$:

$$\chi_R(t) = \chi_1(t) + [1 - \chi_1(t)]\, P(t) \qquad (26)$$

where $\chi_1(t)$ is the normalized aligned yield from an unimplanted sample and P(t) is the probability that a particle in the aligned beam has been scattered through an angle greater than the critical angle. The choice of the forward scattering mechanism governing the dechanneling for the sample being analyzed determines the choice of P(t) in Eq. (26).

For single scattering, the following Rutherford scattering cross section[46] is employed to obtain a value for P(t):

$$\frac{d\sigma}{d\Omega_{cm}} = \frac{Z_1^2 Z_2^2 e^4}{16 E_L^2} \left(\frac{M_1 + M_2}{M_2}\right)^2 \csc^4\left(\frac{\theta_{cm}}{2}\right) \qquad (27)$$

where $E_L$ is the initial energy of the projectile in the lab and $\theta_{cm}$ the scattering angle in the center-of-mass system. Then, the probability P(t) for Eq. (26) is just Eq. (27) integrated from $\psi_c$ to $\pi$ and

multiplied by the total number of scattering centers traversed as follows:

$$P(t) = \int_{\psi_{c,cm}}^{\pi} \frac{d\sigma}{d\Omega_{cm}} \, d\Omega_{cm} \int_{0}^{t} N'(T)dT \tag{28}$$

or,

$$P(t) = \frac{\pi Z_1^2 Z_2^2 e^4}{4E_L^2} \left(\frac{M_1 + M_2}{M_2}\right)^2 \left(\csc^2\left(\frac{\psi_{c,cm}}{2}\right) - 1\right) \int_{0}^{t} N'(T)dT \tag{29}$$

Since $\psi_c \lesssim 1°$ for the cases of interest[20], the following relation[46] between laboratory angle ($\theta_L$) and center of mass angle ($\theta_{cm}$):

$$\cot\theta_L = \cot\theta_{cm} + \left(\frac{M_1}{M_2}\right) \csc\theta_{cm} \tag{30}$$

gives in the limit of small angles,

$$\psi_{c,cm} = \left(\frac{M_1 + M_2}{M_2}\right) \psi_{c,L} \tag{31}$$

Neglecting the one with respect to the $\csc^2$ term in Eq. (29), using $\csc\phi \simeq \phi^{-1}$, inserting Eq. (31), and finally substituting for $\psi_{c,L}$ from Eqs. (3) and (4) yields the following expression for P(t) for the case of single scattering:

$$P(t) = \frac{\pi Z_1 Z_2 e^2 d}{2E_L \alpha^2} \int_{0}^{t} N'(T)dT \tag{32}$$

To describe the dechanneling by plural scattering the expression for P(t) is obtained from Eq. (17) as follows:

$$P(t) = \hat{G}^*(m, \theta_k) \tag{33}$$

where m is obtained from Eq. (16) by replacing N as follows:

$$N = \int_0^t N'(T)dT \tag{34}$$

and N'(t) is the density of scattering centers producing the backscattering yield as a function of depth.

To use Lindhard's expression for multiple scattering one again replaces N in Eq. (23) as was shown in Eq. (34). This is essentially a phenomenological approach because the amorphous layer work indicated that some discrepancy existed in the Lindhard expression, but the results are sufficiently interesting to be worth observing in this restricted sense. So with this understanding, the expression for P(t) for the Lindhard version of multiple scattering is, in analogy to Eq. (19), the following:

$$P(t) = \exp\left(-\frac{\psi_{c,L}^2}{\Omega^2}\right) \tag{35}$$

or

$$P(t) = \exp\left(-\lambda\left[\int_0^t N'(T)dT\right]^{-1}\right) \tag{36}$$

where

$$\lambda = \frac{\alpha^2 E_L}{4\pi Z_1 Z_2 e^2 d \ \ell n(1.29\varepsilon)} \tag{37}$$

The disorder distribution calculation begins by evaluating N' for the first point in the aligned energy spectrum behind the surface peak assuming P(t=0)=0. From Eq. (26) this gives $\chi_R(t=0)=\chi_1(t=0)$ and from Eq. (25), N'(t=0).* This value of N' is used to evaluate the scattering in this layer of the sample from Eq. (16) and then to obtain the value of P(t) from Eq. (33) to be used with the next data point.** The results will be presented versus channel number, hence, really as functions of energy. The energy can be converted to depth with the depth scale. The yield $Y_R(E)$ from the random fraction of the beam $\chi_R(E)$ will be given where

$$Y_R(E) = \chi_R(E) \cdot R(E) \tag{38}$$

and R(E) is again just the random spectrum from Fig. 4a.

Figure 9 shows the aligned spectrum of Fig. 4a (solid squares and dashed line) and the results for $Y_R(E)$ calculated with three of the different expressions for P(t) corresponding to three of the different treatments of the dechanneling. In each case one expression was used for P(t) for the entire calculation. Figure 10 shows the results for the number of scattering centers as a function of channel number for the aligned spectrum of Fig. 4a for each treatment. The ordinate is given as the concentration of silicon atoms required to produce an

---

*Here t=0 is chosen behind the surface peak. Actually $t \approx 330\text{Å}$, as the surface peak is approximately the system energy resolution which in turn is about 15 keV. The depth scale to connect keV to Å will be discussed in (V.C). This 330Å has been added to the disorder peak depths in Table III.

**Again for plural scattering each value of $\hat{G}^*$ must be obtained from Table 2 of Reference 36. For single or multiple scattering one employs Eqs. (32) or (36) respectively instead of Eqs. (16) and (33).

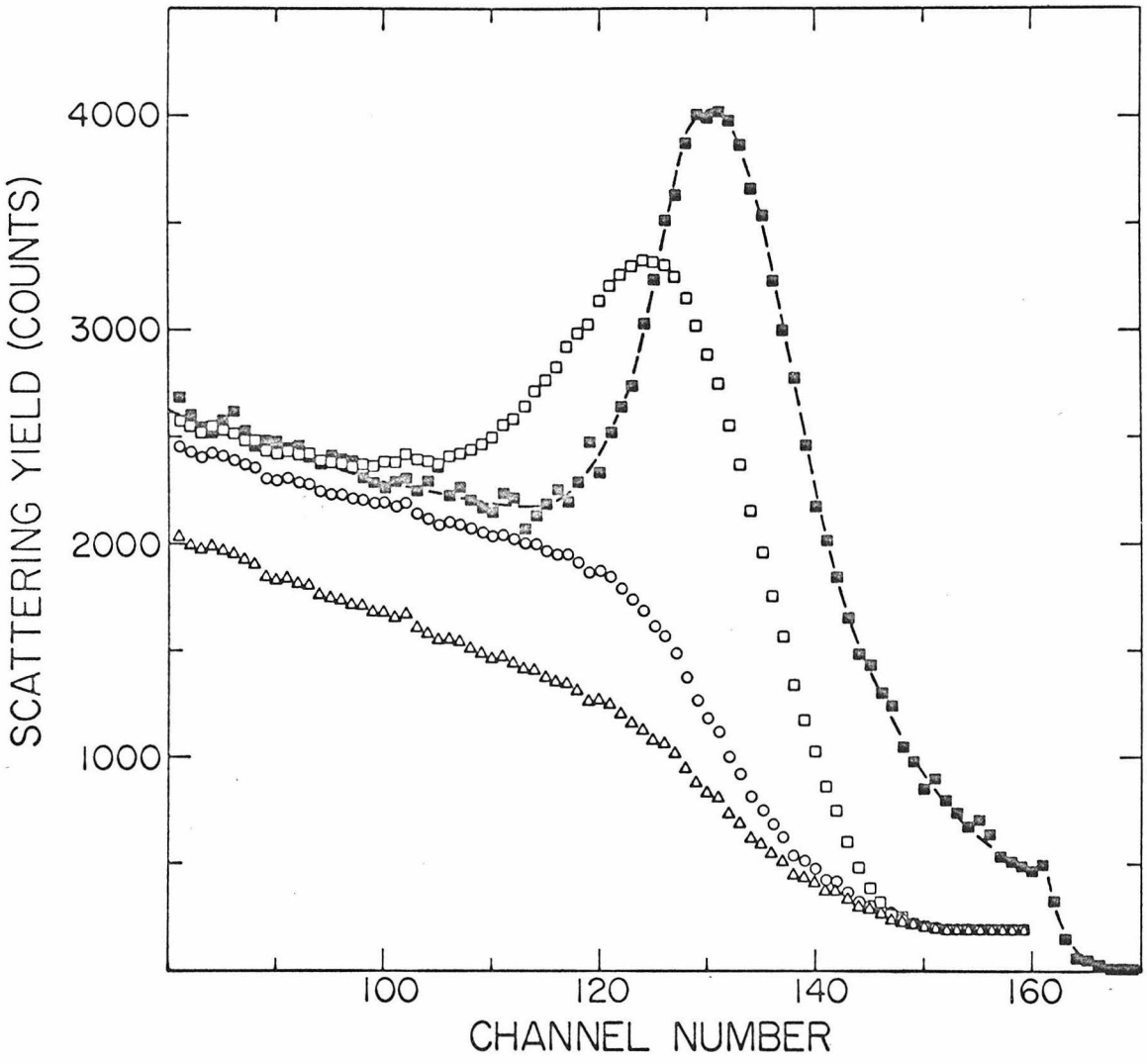


Fig. 9. Aligned spectrum (▩ and dashed line) from a 1.8 MeV $^4He^+$ analysis of a sample implanted at -150°C with 5 x $10^{14}$ 200 keV boron ions/$cm^2$. Other date are yields from random fraction of analyzing beam calculated by treatments of dechanneling based on plural scattering (o), single scattering (Δ), and Lindhard multiple scattering (□).

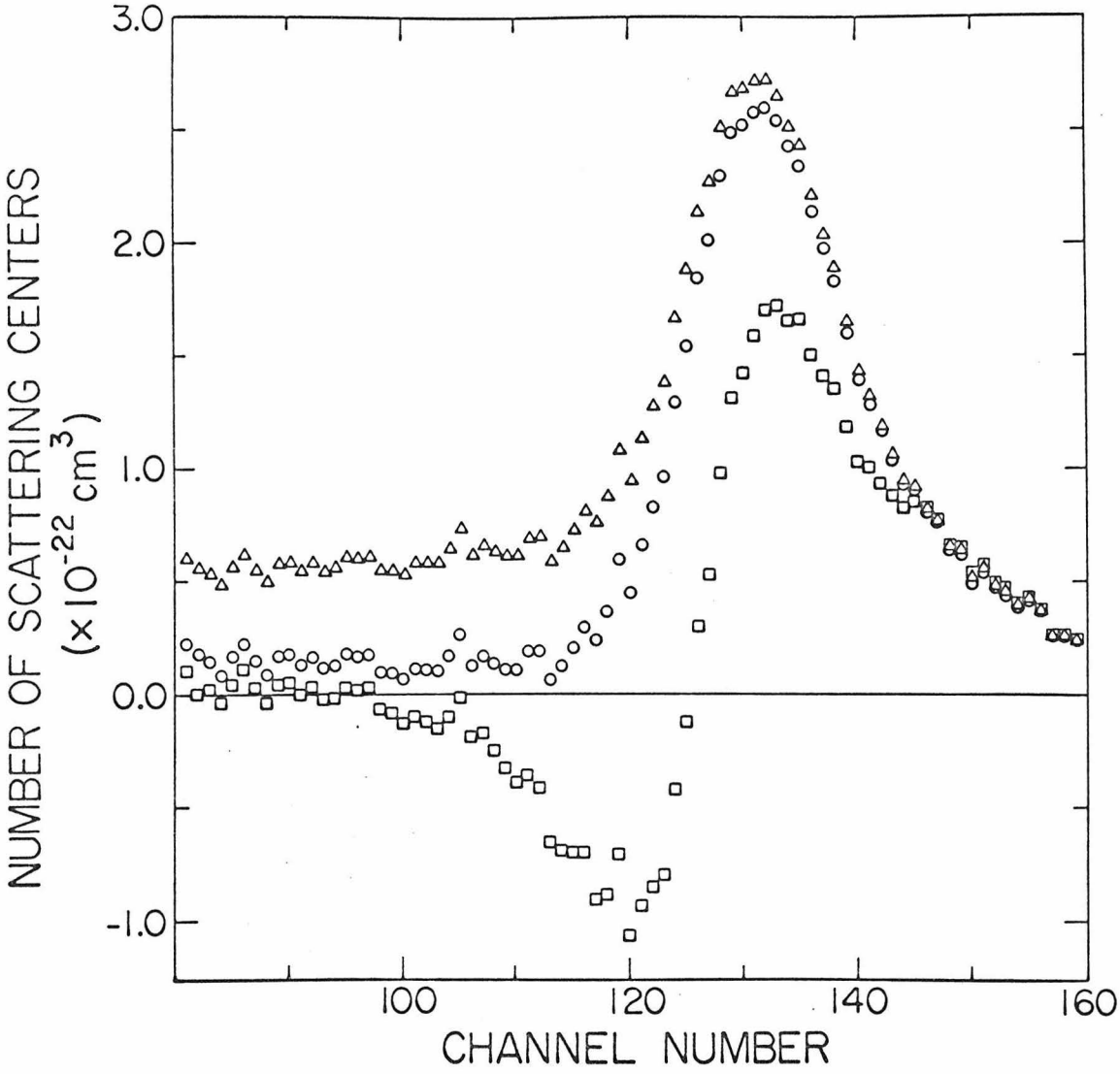


Fig. 10. Scattering center densities for aligned spectrum of Fig. 9 calculated from treatments of dechanneling based on plural scattering (o), single scattering (Δ), and Lindhard multiple scattering (□).

amount of scattering equivalent to that calculated which is N'(t) from Eq. (25) multiplied by $7.14 \times 10^5$ $cm^{-1}$. Thus, the atomic density of single crystal silicon, $5 \times 10^{22}$ atoms/$cm^3$, is equivalent to a random yield. The test of the self-consistency of the results for the disorder distribution calculation is based upon layer removal studies of the kind to be discussed in (V.B) and (V.C) which established the absence of disorder in depths of the sample behind the disorder peak. The value of $Y_R(E)$ is fixed only at the surface of the sample by the minimum yield of the undamaged sample. Yet it should approach the value of the aligned spectrum immediately behind the disorder peak due to the absence of disorder there. Equivalently this portion of the aligned spectrum behind the peak is due to dechanneled analyzing beam, not to disorder. The results of each treatment of the dechanneling in Figs. 9 and 10 will be presented in turn and discussed with respect to this self-consistency criterion.

Estimating that the region of validity of plural scattering according to Keil et al. might encompass nearly the whole of the disorder distribution of Fig. 4a, the plural scattering expression for P(t) was applied for the entire calculation. The resulting values of $Y_R$ the yield from the random component of the analyzing beam are the open circles in Fig. 9. This curve begins low and increases as more of the disordered region is sampled. It approaches to within 6-7% of the aligned spectrum. This error is less than those found in the plural scattering calculation of the minimum yields behind amorphous layers (II.D). The distribution of scattering centers N' calculated

at the same time as $Y_R$ and shown as the open circles in Fig. 10 reflects the behavior of $Y_R$ starting at a low value, rising to a peak, and returning close to zero deep in the sample. A fit of this nature is satisfactory to determine the position and shape of the disorder distribution. The total number of scattering centers/cm$^2$ represented by the disordered layer can be defined as the sum of channels 114 - 160 in Fig. 10, which gives a value of $7.4 \times 10^{17}$ scattering centers/cm$^2$.

The $Y_R$ values as calculated by the plural scattering treatment of dechanneling never quite reach the aligned yield. The aligned spectrum below about channel 110 (Fig. 9) increases faster than the aligned spectrum for an undamaged sample (Fig. 4a), indicating a breakdown in assumption three. Although the errors in the plural scattering $Y_R$ values are relatively small, they may reflect the faster dechanneling rate behind the disorder peak than that predicted by assumption three. However, with the number of approximations involved in the treatment of dechanneling other sources of error cannot be excluded.

The single scattering expression should be applicable[36] for values of m (Eq. (16)) less than about 0.5. This corresponds to only a thickness of $5.1 \times 10^{16}$ silicon atoms/cm$^2$ and is equivalent to a thickness of amorphous silicon of only 102Å. Principally, disorder distributions versus depth in the samples were desired for samples similar to those represented by the spectra of Fig. 4a where the plural scattering treatment has already worked well enough to indicate that there is at least a factor of ten more scattering centers present than in the region of

applicability of single scattering. Summing channel by channel the plural scattering results over the first ten channels (151 - 160) in Fig. 10 gives $5.2 \times 10^{16}$ scattering centers/cm$^2$ so the dechanneling in the principal portion of the disordered layer would appear to be governed by the plural scattering regime. Still, for comparison, the scattering center distribution shown as the open triangles in Fig. 10 was calculated for this sample using the single scattering expression of Eq. (32) throughout the entire aligned spectrum. The single scattering distribution in Fig. 10 rises above the plural scattering result and then remains a large distance above zero for all depths of the sample. This indicates that single scattering underestimates the dechanneling for the bulk of the disordered layer. The single scattering $Y_R(E)$ values shown in Fig. 9 as open triangles indicate that only in the region of small amounts of dechanneling near the surface, do the single and plural scattering results agree well.

For comparison, because it will be used later in a phenomenological analysis of room temperature implants, the Lindhard multiple scattering expression* of Eq. (36) was also applied to the aligned spectrum of Fig. 4a. A negative scattering center density appears in the results for the scattering center distribution shown as open squares in Fig. 10. This negative value means that the dechanneling has been over-estimated as can be seen more clearly from the $Y_R(E)$ values shown as open squares

*The Moliere distribution was not employed because values of B (Eq. (21)) do not exist for m (Eq. (16)) less than 3.18.

in Fig. 9. The eventual return of the multiple scattering distribution to zero after such an "undershoot" has no physical meaning and is only an artifact of the calculation.

Regardless of the detailed treatment of the mechanism of dechanneling, it should be noted that one can minimize the effect of dechanneling on his experimental investigation by proper choice of analyzing beam particle and energy. Figures 11, 12, and 13 illustrate the type of spectra obtainable for the same samples, using different analyzing beams.* Because the scattering cross section is greater at lower energies the effects of dechanneling are greater for $^4He^+$ at 1.0 MeV (Fig. 11) than at 1.8 MeV (Fig. 12) as can be seen by comparing the spectra for the same sample. The effect of using protons instead of $^4He^+$ at the same energy would be to reduce the amount of dechanneling. However, at the energy of 450 keV at which protons were used in Fig. 13, the increase in the scattering cross section with decreased energy cancels out this effect and results in greater dechanneling than with 1.8 MeV $^4He^+$.

To ascertain whether the plural scattering treatment of dechanneling was a fortuitous choice for the particular disorder distribution (Fig. 9) as represented by this particular analyzing beam particle and energy (1.8 MeV $^4He^+$), the same approach was applied to a wider range of amounts of disorder, using now for analysis a 450 keV proton beam. Figure 14 shows the calculated scattering center distributions. The measurements were performed at room temperature on samples that were held at -50°C during the boron ion implantation. For the $1 \times 10^{14}$

*Structure is sometimes seen behind the disorder peaks in room temperature implants. Compare the data points presented in Fig. 15. The surface peak in the aligned spectra (e.g., about channel number 160 in Fig. 11) appears to be enhanced in room temperature implants.

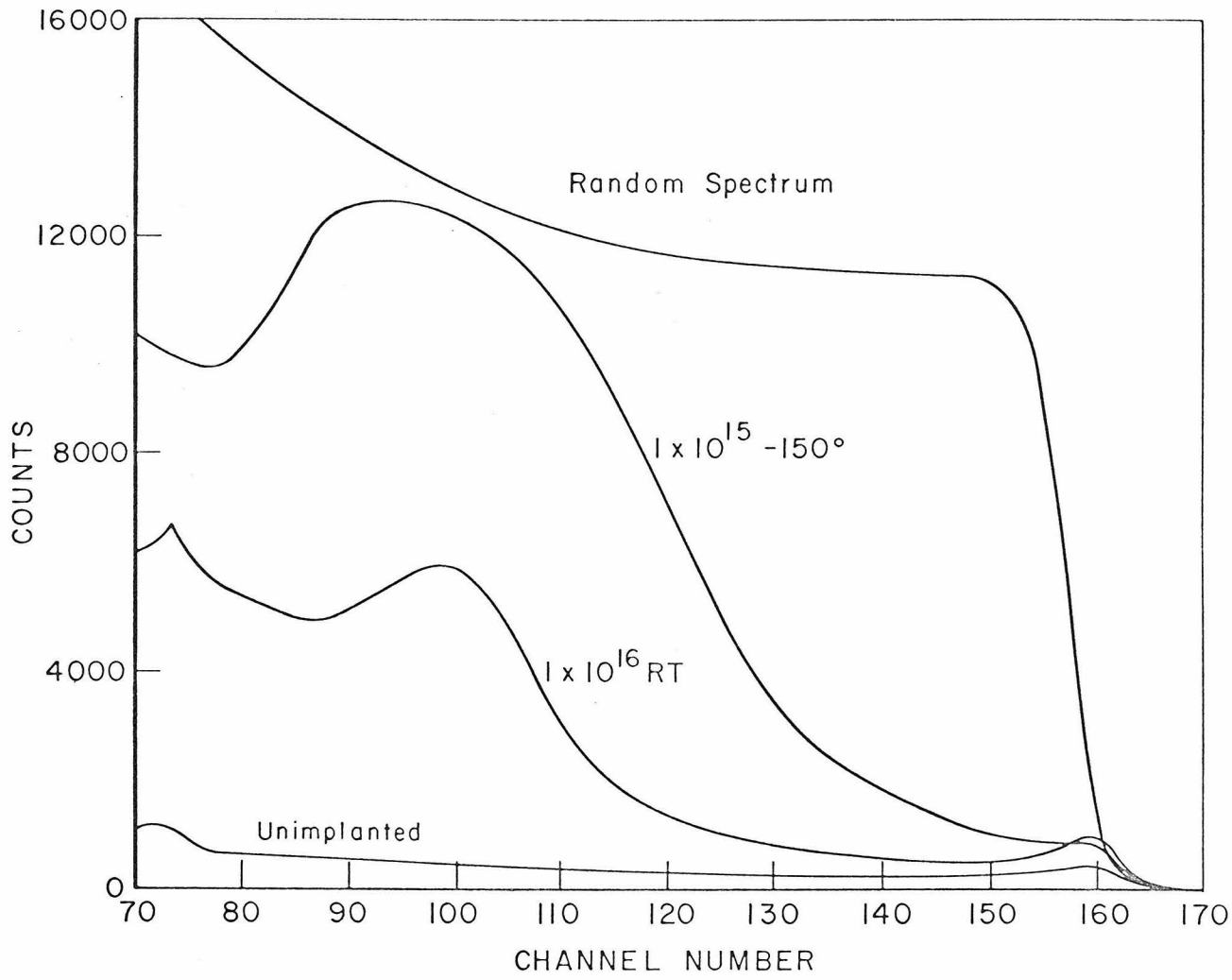


Fig. 11. Aligned and random spectra from 1.0 MeV $^4He^+$ analyses of various boron implanted samples.

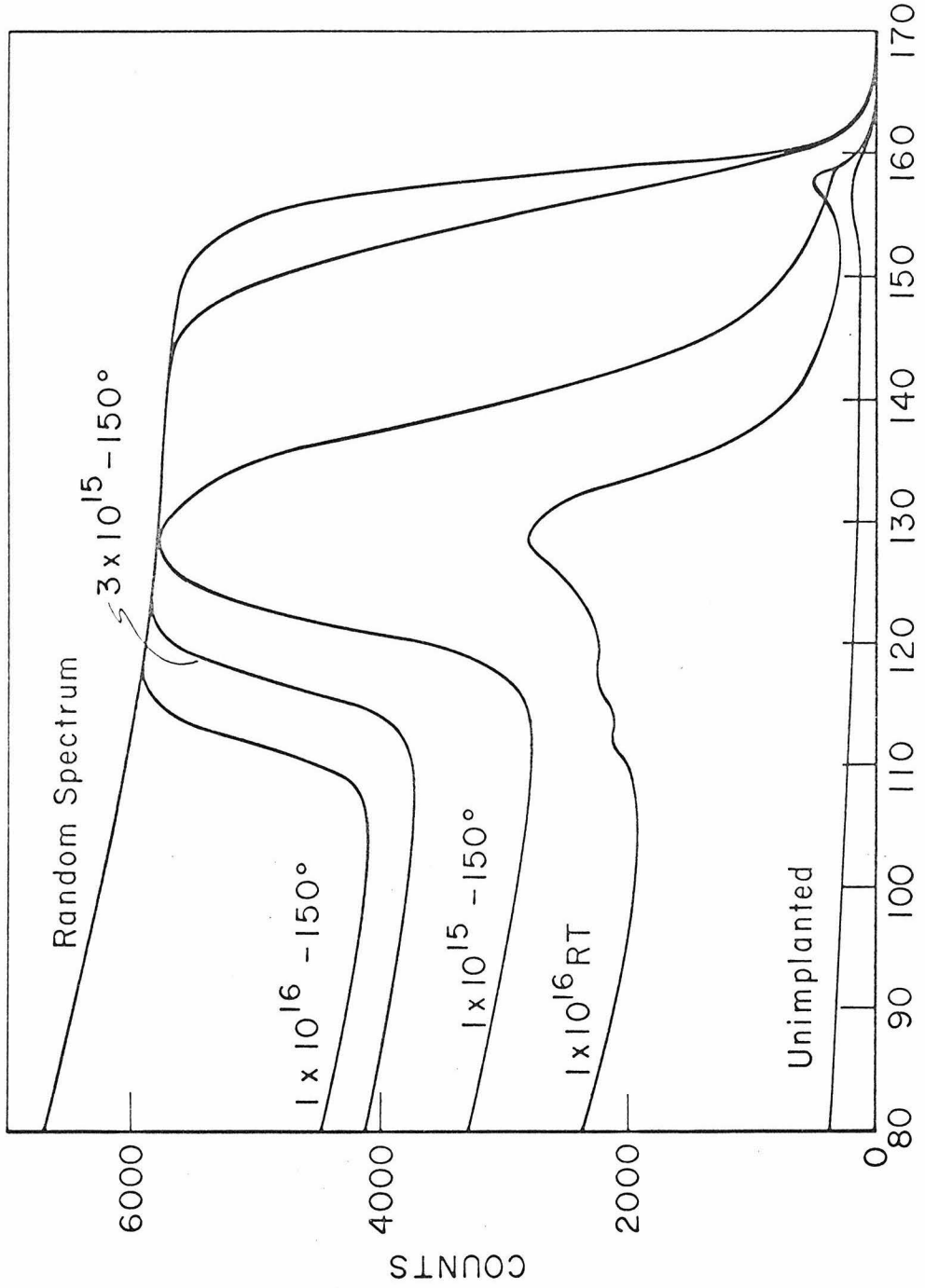


Fig. 12. Aligned and random spectra from 1.8 MeV $^4He^+$ analyses of various boron implanted samples.

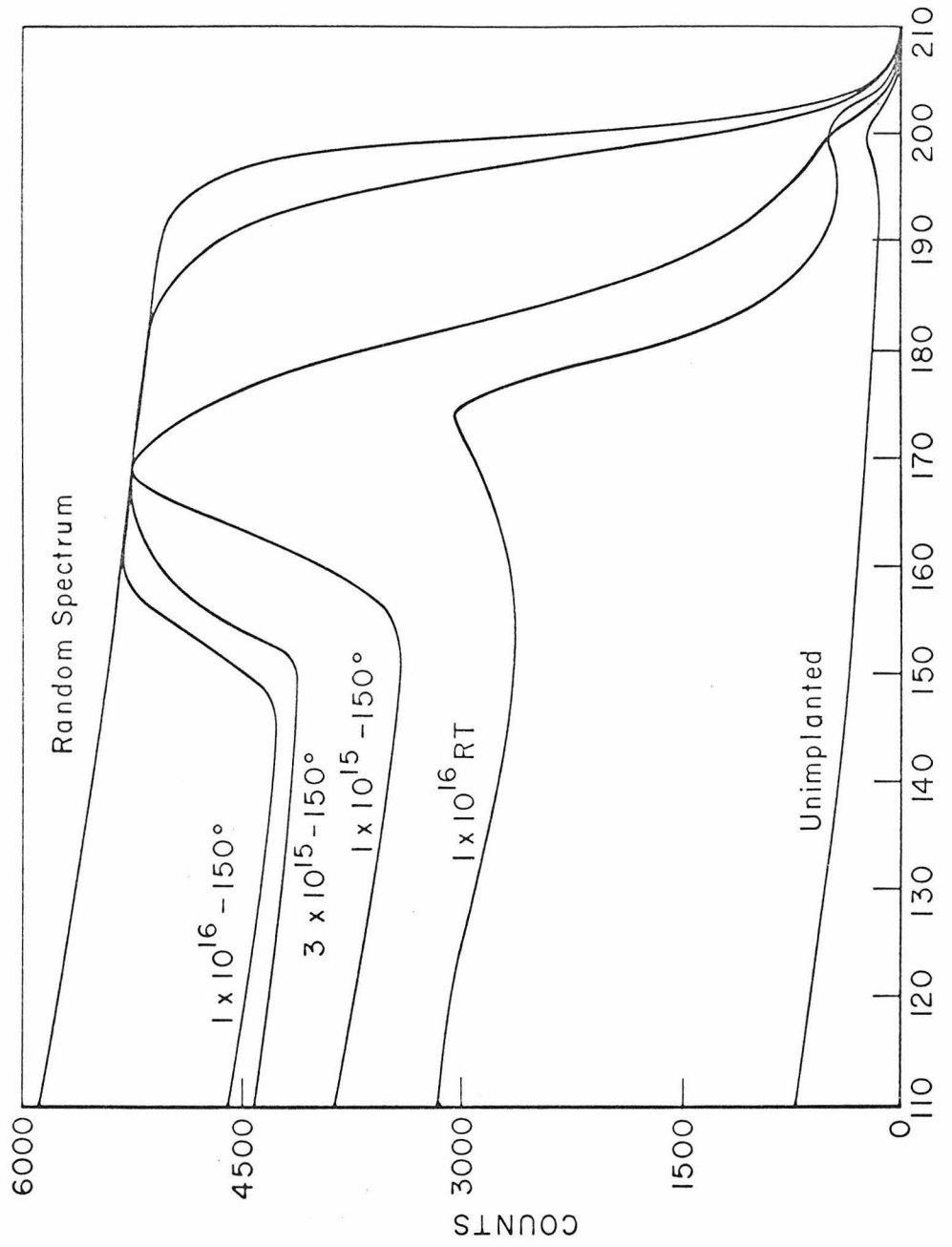


Fig. 13. Aligned and random spectra from 450 keV proton analyses of various boron implanted samples.

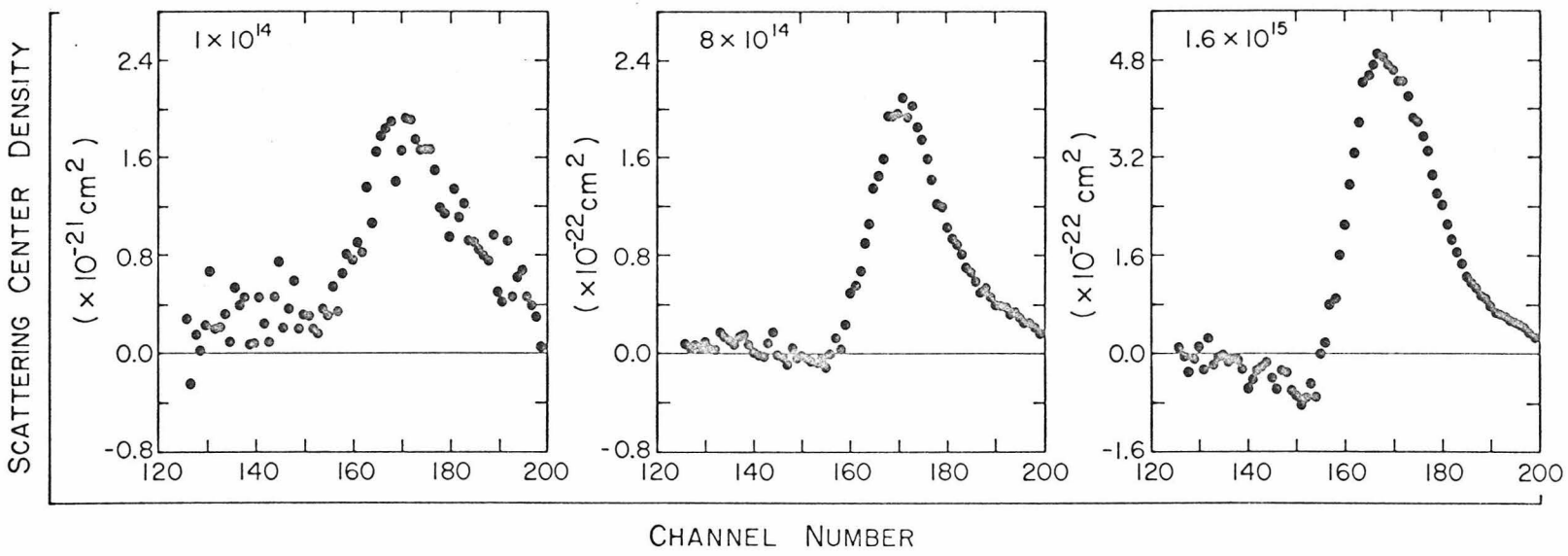


Fig. 14. Scattering center densities calculated from plural scattering treatment of dechanneling for for 450 keV proton analyses of samples at -50°C during implantations of 1 x $10^{14}$, 8 x $10^{14}$ and 1.6 x $10^{15}$ 200 keV boron ions/$cm^2$.

ions/cm$^2$ sample of Fig. 14, the plural scattering slightly underestimates the dechanneling. For intermediate amounts of disorder, $\lesssim 2 \times 10^{22}$ scattering centers/cm$^3$, the scattering center distributions return to zero behind the disorder peak. However, when the number of scattering centers becomes greater than $2 \times 10^{22}$/cm$^3$, the plural scattering treatment begins to overestimate the dechanneling as is again indicated by the appearance of a negative scattering center density in the $1.6 \times 10^{15}$ ions/cm$^2$ sample of Fig. 14. So, for moderate amounts of disorder in low temperature implants the results obtained using the plural scattering approach satisfy fairly well the requirements of a self consistent disorder distribution calculation.

While the plural scattering approach just described appears to work fairly well in some cases, there is some experimental evidence which indicates that the situation is not so simple as has been assumed in this treatment. Digressing a moment, one recalls that these spectra are studies of actual boron implanted silicon samples, hence represent actual distributions of disorder, whatever their form or composition. Figure 15 shows the 1.8 MeV helium backscattering spectra from two samples, one of which is different from those presented so far. The dashed line is the analysis of a $1 \times 10^{15}$ 200 keV boron ions/cm$^2$ implant with the silicon substrate held at -150°C during the boron implantation. The solid line is from the analysis of a $2 \times 10^{16}$ 200 keV boron ions/cm$^2$ implant with the silicon substrate held at room temperature during the boron implantation. The relations of the amount of disorder, the substrate temperature, and the dose are discussed in

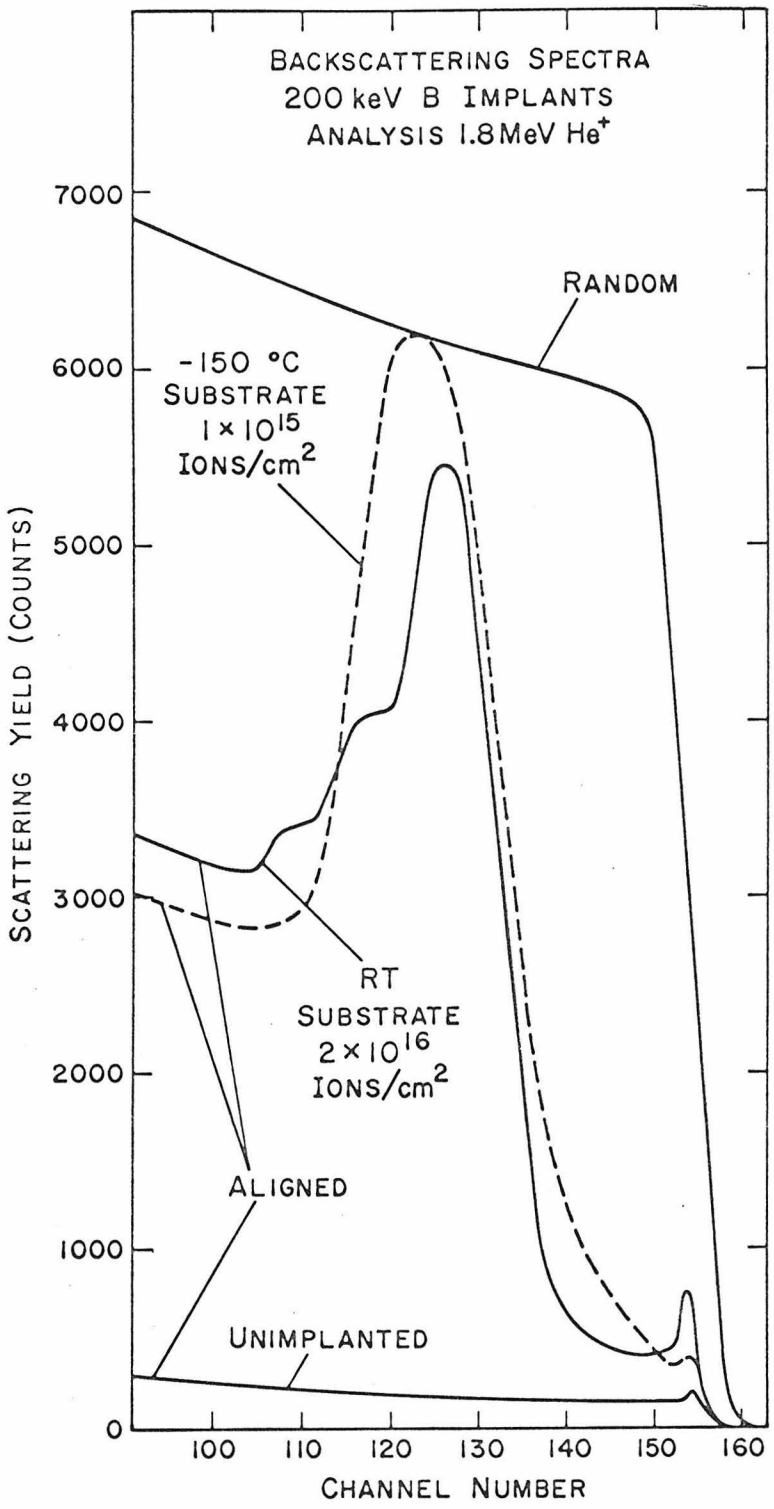


Fig. 15. Spectra from 1.8 MeV $^{4}He^{+}$ (room temperature) analyses of samples at -150°C (dashed line) and room temperature (solid line) during boron implantation.

(IV.B). The important aspect to notice at this point is that even though the amount of disorder in the sample implanted at -150°C is greater than that in the sample implanted at room temperature, the level behind the disorder peak for the sample implanted at -150°C is lower than that for the sample implanted at room temperature. This indicates that the dechanneling is affected by the detailed nature of the defects in the disordered layer and is clear evidence of the restrictiveness of assumption 4. There is at present no way to take this into account in general as has already been discussed. However, it is clear that since the plural scattering works reasonably well for the low temperature implant type of disorder as indicated in Figs. 9 and 10 it cannot work for the room temperature samples where it will underestimate the dechanneling.

One approach to the distributions of disorder present in room temperature implants is to assume that there is some difference in the nature of the disordered regions from those created by low temperature implantations due perhaps to annealing effects or lattice strain due to the high boron concentrations. Then it is reasonable to assume that a different mechanism might now be responsible for dechanneling of the analyzing beam. Historically[38] the multiple scattering treatment suggested by Lindhard[15] was tried. Realizing the problems with this approach now, it is still useful to reproduce the results to see what can be said.

Some typical results of this multiple scattering dechanneling calculation are presented in Fig. 16 for samples implanted with boron

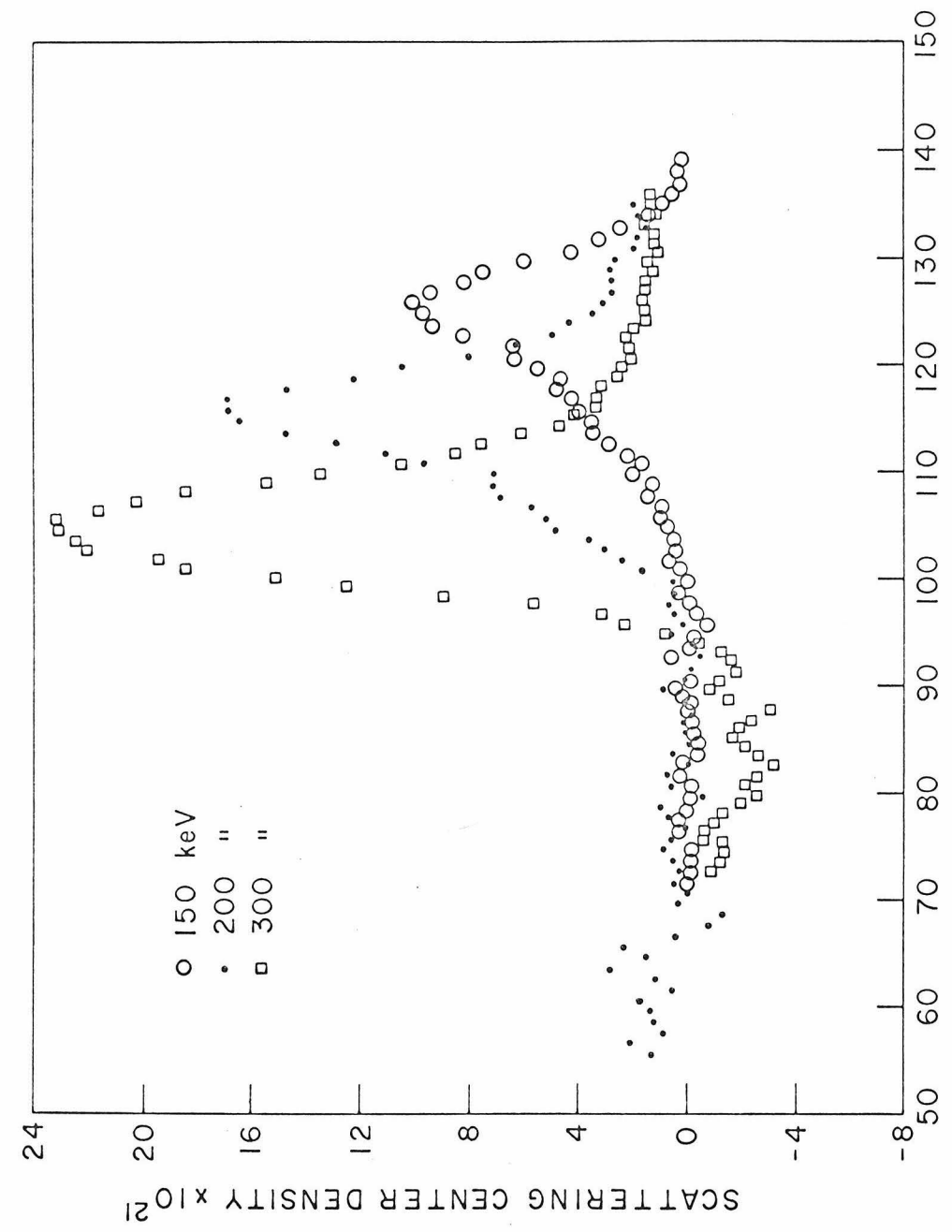


Fig. 16. Scattering center densities calculated from Lindhard multiple scattering treatment of dechanneling for 1.8 MeV $^4He^+$ analyses of samples at room temperature during implantation of 1 x $10^{16}$ boron ions/$cm^2$ at energies of 150 keV (o), 200 keV (•), and 300 keV (□).

at room temperature at different energies to produce different disorder distributions. The analyzing beam giving the spectra is again 1.8 MeV helium. In each case the density of scattering centers shows a well defined peak returning to zero on the back side of the peak with some dip below zero exhibited for the deepest peak. The return to zero of the density of the scattering centers is as always a necessary condition for the validity of this kind of disorder distribution calculation where measurements after layer removal have indicated no disorder beyond the peak. So the multiple scattering treatment does treat dechanneling in room temperature implants in a consistent manner. This agreement of the multiple scattering expression is rather fortuitous, however. Physically it means that for each back-scattering center in the disordered layers of the room temperature implants, the multiple scattering expression by chance assigns the appropriate amount of additional dechanneling to the analyzing beam to account for its final distribution on emerging from the disordered layer. One can argue that this is due to a subtle change such as strain in the lattice giving more forward scattering per unit back-scattering than one would calculate based on a model of individual centers responsible for both types of scattering.

To illustrate that Eq. (36) was only a fortuitous choice for the room temperature implants the calculated scattering center density for the multiple scattering treatment applied to the low temperature disorder was made to return to zero without becoming negative by adjusting the value of $\lambda$ in Eq. (37). The result of a calculation

in which $\lambda$ was increased by 75% over the value calculated from Eq. (37), is shown in Fig. 17 for a low temperature implant. Also shown in Fig. 17 is the scattering center distribution obtained from the sample* after approximately 3500Å of silicon had been removed from the surface by the layer removal technique to be described in (V.B). Again the higher value of $\lambda$ was used and the agreement with the distribution for the original sample is good. Although this is only phenomenology, it is interesting to realize that increasing $\lambda$ physically amounts to increasing $\alpha$, that is, increasing the angle at which a particle is described as having been dechanneled into the random component of the beam by a constant factor times the critical angle. If this is an indication that the choice of the critical angle for the changeover from aligned to random beam was incorrect but that a value larger than $\psi_c$ is better, this particular line of reasoning can be closed by saying that smaller critical angles for analyzing beam particles moving through the disordered layers in the room temperature implants are a reasonable description of the overall "rougher" lattice due to strain and distortion.

The plural scattering treatment of the dechanneling mechanism is clearly the more physical approach to disorder distribution calculations since this method employs a one-to-one relationship between backscattering centers and forward scattering (dechanneling) centers. The multiple scattering approach can at best be regarded as looking at the dechanneling mechanism as an unknown function. The corrected difference between the aligned and random yields is the input to generate as

*The disorder peak after layer removal (□) was shifted down 19 channels for direct comparison of the two shapes.

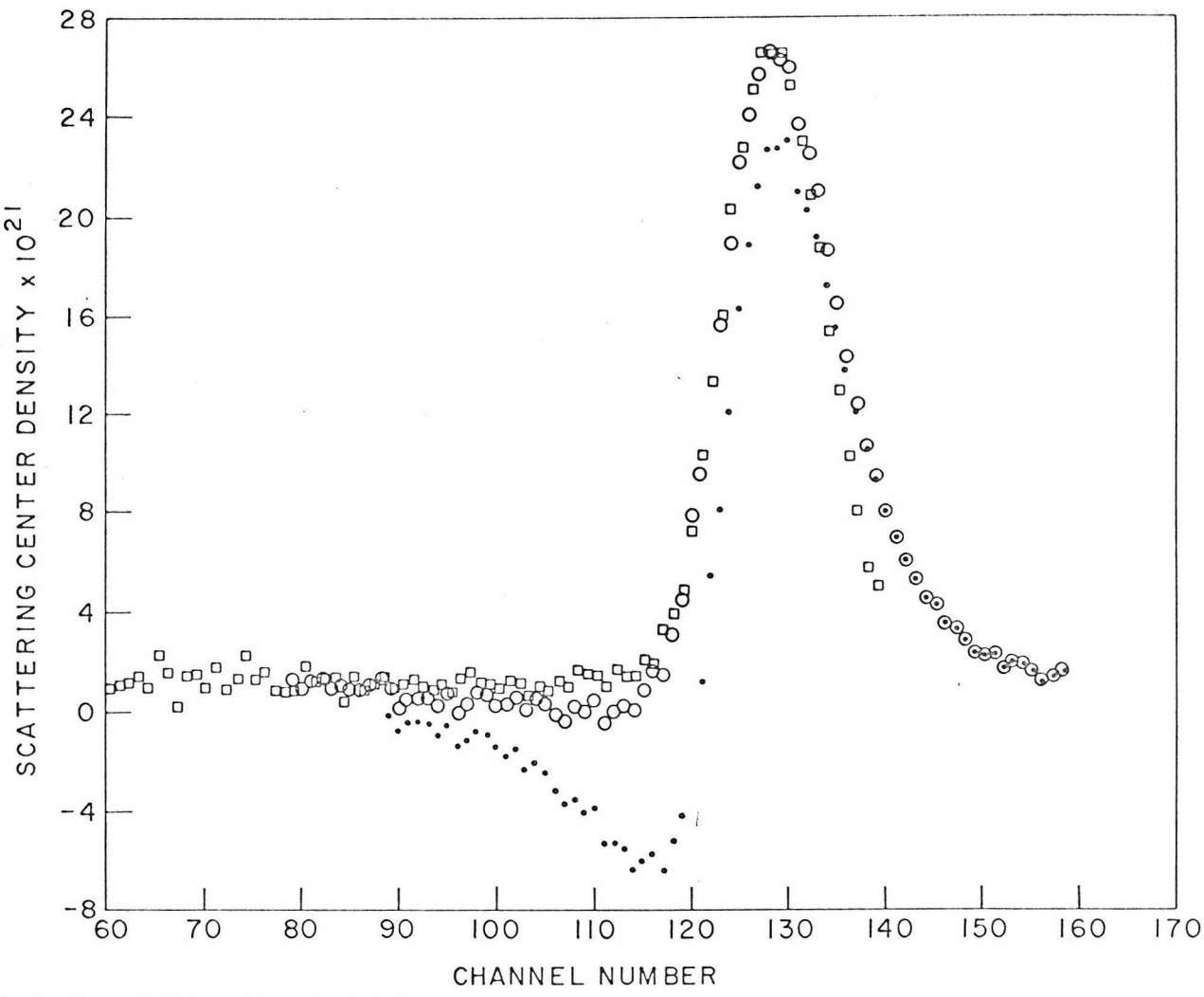


Fig. 17 Scattering center densities calculated from Lindhard multiple scattering treatment of dechanneling from 1.8 MeV $^4He^+$ analyses of a sample at -150°C during implantation of 5 x $10^{14}$ 200 keV boron ions/cm$^2$. The value of $\lambda$ is from Eq. (37)(•), increased by 75% above value from Eq. (37)(o), and after 3500Å of silicon removed from surface of sample using increased value of $\lambda$(□).

output some new value of the random fraction of the beam. The results of the Lindhard multiple scattering expression in calculating $\chi_R$ as discussed in (II.D) not only varied from 14% to 47% from the measured values of $\chi_R$ but even more important seemed to have the wrong energy dependence. It was certainly a more unsatisfactory treatment than the Moliere approach which again has been more or less empirically verified by other experiments. Thus the multiple scattering treatment lacks the justification of the plural scattering treatment. In fact, the only justification for this treatment of dechanneling is that for certain disorder regions it fulfills the self consistent criterion of the disorder distribution calculation.

The attempts to allow for the effects of dechanneling have thus been only partially successful. This is not surprising in view of the complexity of the problem and the necessary approximate nature of the calculation. Within the limits of the theory and the assumption of the disorder calculation, the plural scattering seems to be the most valid dechanneling mechanism described, and it is moderately satisfactory for the kind of disorder found in the low temperature implants. For the simple purpose of reducing the dechanneling and accentuating the disorder peak for a given analyzing beam one should use higher energies. This must be balanced against the requirement of maintaining adequate stopping power to give the desired depth resolution (see V.C.).

# III. Implantation Caused Disorder Distributions.

## III. A General Description

Spectra have been presented from analyses of disorder distributions in silicon. It has simply been stated that these disordered samples were produced by implanting boron ions into silicon single crystals. The process by which an ion coming to rest in a solid produces disorder will be discussed and the important quantities characterizing the stopping process outlined. The theoretical calculations of disorder distributions that are available will be described, emphasizing the one relevant to the work of this thesis. Then the measured values for the disorder peak depths and widths will be presented and compared with the theoretically calculated quantities.

III.B Theoretical Considerations.

It has been known for many years that bombardment of a crystal with energetic (keV to MeV) heavy ions produces regions of lattice disorder. An extensive review of work in this field up to 1966 has been given by Carter and Colligan[47]. More recently ion implantation in semiconductors has received increased attention and has been reviewed by Mayer, Eriksson, and Davies[8]. The disorder produced by ion bombardment can be observed by techniques sensitive to lattice structure, such as electron-transmission microscopy, electron diffraction, and, as used in the present study, MeV-particle channeling.

As an ion slows down and comes to rest in a crystal, it makes a number of collisions with the lattice atoms. In these collisions, sufficient energy may be transferred from the ion to displace an atom from its lattice site. The displaced atom can in turn displace other atoms, and so on - thus creating a cascade of atomic collisions. This leads to a distribution of vacancies, interstitial atoms, and other types of lattice disorder in the region around the ion track. The precise nature of these disordered regions is not known at present. As the number of ions incident on the crystal increases, the individual disordered regions begin to overlap. At some point an amorphous layer is formed. The total amount of disorder and the distribution in depth of the disorder depend on ion species, ion energy, total ion dose, ion dose rate, channeling effects on the bombarding ion, and the temperature of the substrate during the implantation. In general, one deals with <u>average</u> quantities resulting from implantation by many atoms, i.e., the average number of displaced lattice atoms, their spatial distribution, etc.

In considering the disorder created by an incident ion, one must first determine the partition of energy between electronic and nuclear processes. A similar procedure is used in determining the range distribution of implanted atoms. The difference between range and disorder calculations is that in the latter case, the energy partition of the displaced atoms must be considered also. In either case the crystal structure can influence the amount of energy lost in nuclear collisions. For example, a well-channeled particle loses most of its energy in electronic processes, and so creates less disorder than a particle whose initial direction of motion is not aligned with any low-order lattice axis or plane. In this work, the concern is with nonchanneled implants.

Lindhard et al.[48] have derived a theoretical treatment for the distribution of energy between electronic and nuclear processes for both the primary (incident) particle and the secondary (knocked-on) particles, assuming that no particles are channeled. To a first approximation the electronic stopping is separable from the nuclear stopping and constitutes a viscous damping. It contributes part of the energy loss but essentially no angular scattering. The elastic collisions with the host nuclei contribute the remainder of the energy loss and essentially all of the angular scattering. The electronic stopping initially increases linearly with the velocity of the incident ion for boron in silicon, up to energies of the order of two MeV. The nuclear stopping is calculated by employing a differential cross section for nuclear collisions. At low enough energies the nuclear

stopping dominates for any ion target combination. For boron in silicon the nuclear stopping reaches a maximum at 3 keV, then falls off with energy. At 17 keV the electronic and nuclear stopping are equal.

Distributions of disorder created in silicon by boron ions with energies above a few tens of keV reflect the fact that the major part of the energy loss occurs in the electronic stopping mode. There is a relatively low disorder production rate near the surface with a buried layer of somewhat higher disorder density corresponding to the nuclear processes which dominate the stopping near the end of the boron ion track. Any attempts to calculate such disorder distributions must properly account for electronic stopping to give reasonable results.

There are in addition to Monte Carlo treatments other theoretical calculations of disorder distributions. Sigmund and Sanders[49] have presented an integro-differential equation which governs the spatial distribution of energy deposited into atomic processes by energetic ions moving through an amorphous solid. Because of the large number of variables involved it is not practical to obtain solutions to the equation by the usual numerical techniques. Sigmund and Sanders have reduced the number of variables by introducing the moments of the damage distribution. Even then it is prohibitive to include the electronic stopping in the solutions for $M_1 \neq M_2$ or for more than the first few moments for $M_1 = M_2$. ($M_1$ is the projectile; $M_2$, the target atom). An extension of the work of Sigmund and Sanders was performed in collaboration with Sigmund.[50] A correlation function approach was employed

to investigate details of disorder distributions not available from the simple disorder distribution functions. Again solutions to the resulting moment equations could only be obtained for the first few moments for a power law atomic interaction potential in the elastic scattering limit. Neither this work nor the work of Sigmund and Sanders will be further included in this thesis because for boron in silicon the role of electronic stopping cannot be neglected.

The method of disorder distribution calculation due to Brice[51,52] includes electronic stopping but then must neglect the effect of recoiling secondaries from collisions with the primary projectile. Brice's method breaks the analysis of the damage process into two steps. First, he determines the spatial distribution of the ions at intermediate energies E' below their initial energy E. Then from these distributions, a knowledge of the interaction cross section, and the experimentally measured values of the partition of the transferred energy into electronic and atomic processes[53,54,55], he determines the initial spatial distribution of the energy deposited into atomic processes. This resultant spatial distribution is taken to represent the final distribution of damage in the solid.

Brice points out that the principal approximation in his determination of the spatial distribution of energy deposited into atomic processes is the neglect of energy transport through the recoil of struck target atoms. In particular, the quantity which is assumed small is the range of the average recoil atom relative to the range of

the incident ions. Brice notes that it is difficult to estimate the region of validity of this approximation from first principles. At least at not too low energies and for a fixed incident energy the approximation should be more valid for the lighter incident ions on a given substrate than for the heavier ones since the range of the recoils will be smaller. Also, as Brice indicates, diffusion, saturation, and annealing effects must be negligible for his results to correlate with experimental observations.

For a more quantitative estimate of the validity of the principal approximation, Brice compares his average damage depths for $M_1 = M_2$ with those calculated exactly by Sigmund et al.[56]. For example for silicon bombarding silicon at 40 keV, he finds that his two step method underestimates the average damage depth by 17%, consistent with the fact that the neglected recoils would actually tend to carry energy deeper into the solid. He concludes that for boron bombarding silicon, his calculations should be applicable for boron energies greater than 9 keV.

In addition to the specific problems of a given calculation any theoretical analysis of structural damage produced in a solid by bombardment with atomic projectiles requires the choice of some measure by which the damage can be quantified. The structural damage should depend on the energy which ultimately resides in atomic processes. For example, the theoretical depth distribution of vacancy production[57] as calculated by a Monte Carlo technique, has been shown to be proportional to Brice's calculated depth distribution of energy deposited

into atomic processes for 60 keV boron incident on silicon[51]. The total neutron damage in silicon,[58,59,60] as measured by carrier removal has been shown experimentally to be proportional to the total energy deposited into atomic processes. In addition, the depth distribution of more complex forms of damage has been shown to be roughly proportional to calculated depth distribution of energy deposited into atomic processes for 400 keV oxygen ions incident on silicon[51,61,62]. The energy deposited into atomic processes is thus a basic quantity which is accessible to precise quantification and which seems to correlate well with experimental measures of damage in a solid.

The major consideration then in using Brice's calculation is deciding on the validity of the neglect of the effects of recoils. To give a feeling for the numbers involved, one may comment that for a bombarding boron ion energy of 100 keV, the range of an initial recoiling silicon atom with an energy equal to the maximum classical energy transfer is $\sim$0.3 of the boron range. Since such a collision is so unlikely, the limit it sets is pessimistic. However, for such a factor the recoiling silicon atoms will surely do little to change the shape of the disorder distribution. In the final analysis, it is this result which justifies the application of Brice's calculation to the cases of experimental interest in this thesis.

III.C Disorder Peak Depths and Widths

Disorder peak depths and disorder peak widths for the disorder distributions obtained from 1.8 MeV $^4He^+$ analyses performed at room temperature on boron implanted silicon samples are presented in Table III. The boron dose for the samples held at -150°C during implantation was $5 \times 10^{14}$ ions/cm$^2$ (see Fig. 9), and the plural scattering mechanism was used for the dechanneling calculation. The boron dose for the samples held at room temperature during implantation was $1 \times 10^{16}$ ions/cm$^2$, and the Lindhard multiple scattering expression was used for the dechanneling calculation. The doses are chosen to give comparable disorder densities at the peak of the disorder for the two implantation temperatures. The factor of twenty difference in dose required will be discussed in (IV.B). It will be pointed out there that a significant amount of annealing takes place in the room temperature implants during the implantation itself, and the disorder distributions may no longer represent primary distributions of energy into atomic processes. The boron range and range straggling are the values calculated by F.H. Eisen with a computer program written by W.S. Johnson. The program numerically evaluates the integral equations for the projected range distribution derived by Lindhard, Scharff, and Schiott[63]. It employs an experimentally measured value[32] of the electronic stopping power for boron in silicon of

$$\frac{1}{N}\frac{dE}{dx} = 2.06 \times 10^{-16} \frac{(eV)^{\frac{1}{2}}cm^2}{atom} \; E^{\frac{1}{2}}$$

TABLE III.

Disorder Peak Depths and Widths
1.8 MeV $^4He^+$ Analyzing Beam
Samples at Room Temperature for Analysis

| Implant Energy (keV)* | Calc. B Range (Å) | Peak Depth (Å) | Calculated Peak Depth** (Å) | Peak Width† (Å) | $2.35\Delta R_p$ (Å) | Calculated Peak Width** (Å) |
|---|---|---|---|---|---|---|
| 200(-150°C) | 5000 | 4200 | 4200 | 2200 | 1800 | 2800 |
| 200(RT) | 5000 | 3950 | 4200 | 1600 | 1800 | 2800 |
| 300(-150°C) | 7000 | 5900 | 5900 | 2150 | 2000 | 3100 |
| 300(RT) | 7000 | 5650 | 5900 | 2100 | 2000 | 3100 |

*The temperatures following the implant energy are those of the substrate during the boron implantation.

†The term width always means full width at half maximum (FWHM) of the relevant distribution.

**Values from D.K. Brice (52). See also (†).

or

$$\frac{dE}{dx} = 0.103 \frac{(eV)^{\frac{1}{2}}}{\mathring{A}} \times E^{\frac{1}{2}} \quad \text{for crystalline silicon.}$$

Assuming that the boron projected range distribution is Gaussian with a standard deviation $\Delta R_p$, the FWHM of the distribution is $2\sqrt{2\ell n 2}\Delta R_p = 2.35\ \Delta R_p$*.

The originally measured peak depths and widths in keV were converted to Å with the 45 eV/Å depth scale from (V.C) for presentation in Table III. The values given are averages over three samples in each case, and the scatter for a given case is ±8% about the presented average for the damage depths and ±15% about the presented average for the damage widths. Within these errors the room temperature implants have slightly shallower peak depths than the cold implants. This difference suggests that the annealing that takes place during the room temperature boron implantation causes a slight shift of the disorder peak. For comparison with the calculated boron range one must recall the estimated ±5% error in the depth scale which is now a relevant source of error in the conversion to Å. In both 200 and 300 keV implants the disorder peak depth is for the cold implants ~85% of the calculated boron range and for the room temperature implants ~80% of the calculated boron range. For comparison the calculated FWHM of the boron projected range distribution was included in Table III and is in all cases comparable to the FWHM of the disorder distribution.

---

*Values of $R_p$ have recently been measured by A. Moline (Bell Telephone Laboratories) and agree with Eisen's calculated values.

The values for the depths and widths of the damage peaks as calculated by Brice[52] are included in Table III. The agreement between the experimental and calculated results for the disorder peak depth is good. However, the measured values of the FWHM of the disorder distributions are for the room temperature implants 60% to 70% of the calculated values, for the cold implants 70% to 80% of the calculated values. The experimental results suggest that the residual disorder distributions at the time of measurement have been affected by the annealing taking place especially during implantation at room temperature and even possibly during implantation at -150°C. Also, the data presented in Table III for the cold implants were obtained after the samples had warmed to room temperature. As will be discussed in (IV.B) approximately a 30% reduction in the disorder observed takes place during this warm up. To effect the measured widths, these annealing processes must be more effective in the more lightly disordered wings of the disorder distribution. Such an effect would immediately explain the narrower measured distributions. It is also possible that the measured disorder for these boron ion implantations is a nonlinear function of the amount of energy deposited into atomic processes, a result that has been shown to be the case experimentally by Picraux et al.[64] for 200 keV antimony ion implantations into silicon.

The major conclusion is that the measured disorder peak depth is shallower than the peak in the boron range distribution. The calculated values of Brice for the disorder peaks are in close agreement with the measured values.

# IV. Annealing Effects on Disorder.

## IV. A General Description.

The preceding sections of this thesis have treated the disorder produced by boron ion implantation into silicon first as a relatively abstract structure, that is, the emphasis was on the extraction of the disorder distribution versus depth in the sample and comparison of the experimentally measured parameters of the distributions with those that could be calculated theoretically. Various annealing effects have been alluded to where necessary to make plausible some of the approaches taken in the investigation and some of the conclusions drawn. Now one considers how the disorder is effected by different treatments. Two different kinds of effects will be described. The dependence of the amount of lattice disorder produced on substrate temperature during ion implantation and the effect on the lattice disorder by subsequent anneal treatments will be discussed. Then the effect of the analyzing beam itself on the lattice disorder will be described.

IV.B Temperature and Dose Dependence of Disorder Production and of Anneal of Disorder

The lattice disorder created in silicon by 200 keV boron ions has been investigated both as a function of substrate temperature during implantation and by measurements of the residual lattice disorder present after subsequent anneals of these implants. Previous measurements[7] showed that for implantations of 40 keV antimony ions at substrate temperatures less than 50°C, the disorder created per incident ion was only mildly temperature dependent. Recent channeling effect measurements[13] on silicon implanted at -120°C and 23°C with 40 keV boron ions demonstrated that the amount of disorder was markedly greater in the lower temperature implants. The temperature dependence of the lattice disorder produced during boron implantation at substrate temperatures between -115°C and 23°C has been measured here.

Figure 12 showed 1.8 MeV $He^+$ aligned backscattering spectra from silicon implanted with boron ions at substrate temperatures of -150°C and room temperature where the random spectrum was included for comparison. The aligned spectrum for a dose of $10^{15}$ ions/cm$^2$ at -150°C reaches the random level. Higher doses of $3 \times 10^{15}$ ions/cm$^2$ and $1 \times 10^{16}$ ions/cm$^2$ at -150°C cause the region of contact of the aligned yield with the random yield to spread progressively to the surface and deeper into the silicon sample. (Other spectra from the $1 \times 10^{16}$ ions/cm$^2$ cold implant have already been presented in Fig. 6 in the different context of (II.D).) Part of the apparent motion of the disorder deeper into the crystal with increasing boron dose is due to the increase in

the depth scale with increasing amounts of disorder in the crystal. This is only a change of ~9% as will be discussed in (V.C). However, the rear edge of the disorder peak in the 1 x $10^{15}$ ions/cm$^2$ sample is 37 channels deep ($\Delta t \approx 5400$Å) while the rear edge of the disorder peak in the 1 x $10^{16}$ ions/cm$^2$ is 46 channels ( t = 6500Å), a change of ~24%. So the disorder builds up deeper in the crystal than the original peak with increasing boron dose.

The increase in depth of the rear edge of the heavily disordered region is consistent with range and disorder calculations. One can approximate the boron range distribution by a Gaussian as follows:

$$N(x) = \left( \frac{N_T}{\Delta R_p \sqrt{2\pi}} \right) \exp \left( - \frac{(x - R_p)^2}{2(\Delta R_p)^2} \right) \qquad (39)$$

where $R_p$ and $\Delta R_p$ are the average projected boron range and range straggling respectively and $N_T$ is the total boron dose in ions/cm$^2$. From Table IV for a 200 keV boron ion in silicon $R_p$ = 5000Å and $\Delta R_p$ = 780Å. The aligned yield just reaches the random yield in the -150°C, 1 x $10^{15}$ ions/cm$^2$ implant at the peak of the disorder where the boron concentration is approximately $N_1(R_p)$ (Eq. (39) with $N_T = 10^{15}$ ions/cm$^2$). The rear edge of the region where the aligned yield reaches the random yield for the $10^{16}$ ions/cm$^2$ implant should occur at a value $x_D$ where $N_2(x_D)$ (Eq. (39) with $N_T = 10^{16}$ ions/cm$^2$) has the same value for the boron concentration as $N_1(R_p)$. The value of $x_D$ can be determined from solving these two cases of Eq. (39) simultaneously as follows:

$$N_2(x_D) = \left(\frac{10^{16}}{\Delta R_p\sqrt{2\pi}}\right) \exp\left(-\frac{(x_D - R_p)^2}{2(\Delta R_p)^2}\right)$$

$$= N_1(R_p) = \frac{10^{15}}{\Delta R_p\sqrt{2\pi}} \qquad (40)$$

or

$$x_D = R_p \pm \Delta R_p \sqrt{2\ell n 10} \qquad (41)$$

The positive sign is to be chosen giving $x_D = 6700\text{Å}$. The result of this very approximate plausibility argument agrees with the calculated value of 6500Å.

In contrast with the low temperature implants, a room temperature implant requires a dose of $>2 \times 10^{16}$ ions/cm$^2$ to form an amorphous region. A more exact comparison of the disorder produced by a given dose is not in order at present, since recent experiments have shown a substantial difference in the amount of disorder produced at room temperature when the dose rate is changed from 0.2 μA/cm$^2$ to 2.0 μA/cm$^2$.

The amount of disorder is reduced by post-implantation thermal anneal treatments. Figure 18 shows a sequence of 1.8 MeV $He^+$ aligned backscattering spectra recorded at room temperature in the single alignment geometry after successive ten minute isochronal anneals of a silicon sample implanted with $2 \times 10^{14}$ boron ions/cm$^2$ at -150°C. The disorder represented by the peak in the backscattering spectra anneals significantly by 210°C and has all but disappeared by 325°C. However, there is

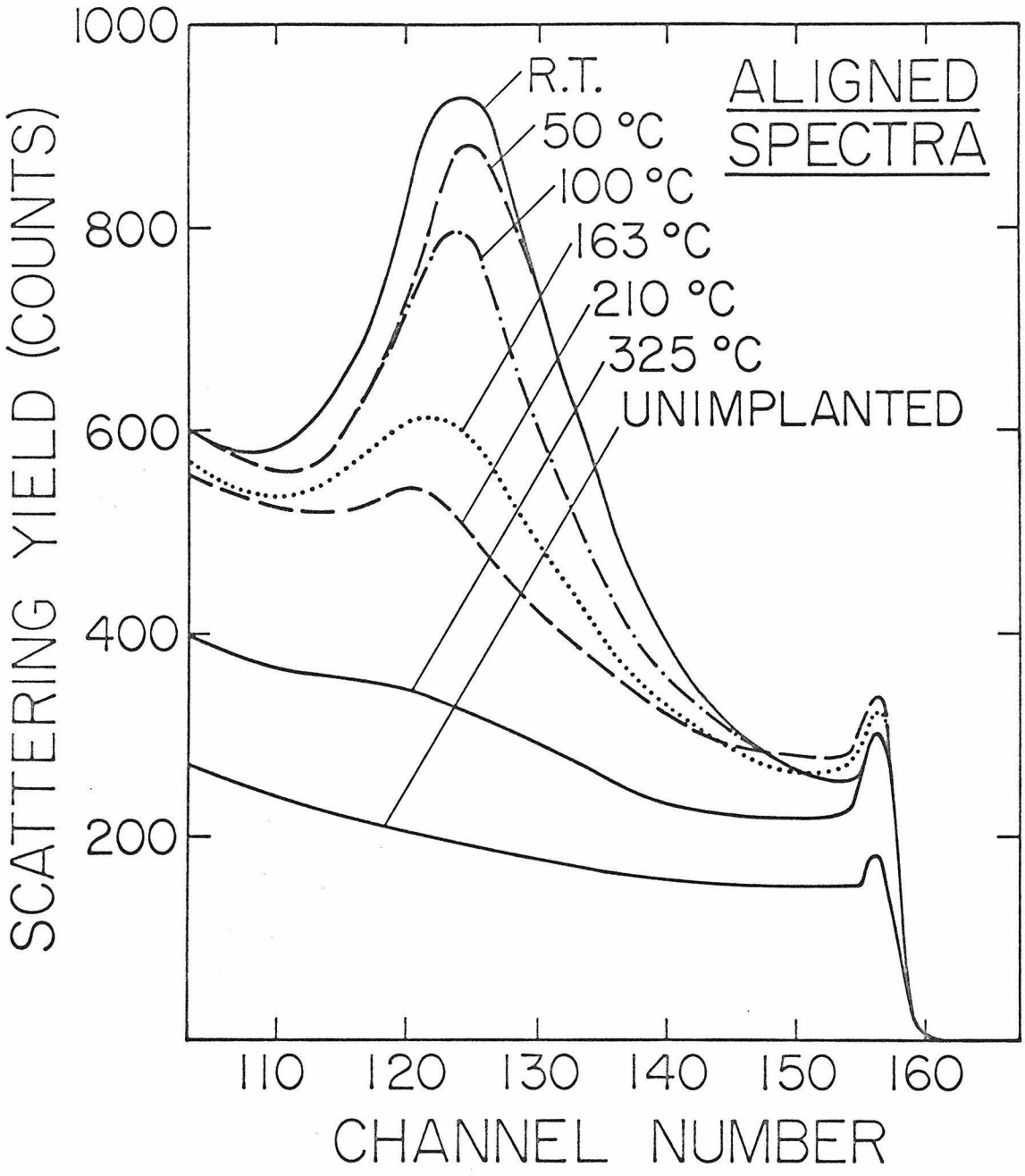


Fig. 18. Spectra from 1.8 MeV $^4He^+$ analyses representing results of ten minute isochronal anneal treatments performed on samples after implantation at -150°C with 2 x $10^{14}$ 200 keV boron ions/$cm^2$. Spectrum from unimplanted sample included for comparison.

still residual disorder present since the aligned spectrum after the 325°C anneal is still ~1.5 times the level of the unimplanted aligned spectrum. The initial curve of Fig. 18 has been designated RT because some anneal takes place between the implantation temperature and room temperature (RT).

Isochronal anneal sequences from -150°C to 300°C were obtained from analyses performed at the North American Rockwell Science Center and at Caltech. The reason for breaking the experiment into two stages is that the implantation apparatus at the North American Rockwell Science Center could use a 450 keV proton analyzing beam in situ from -150°C up to temperatures of 100°C. To continue the annealing sequence, it was then necessary to remove the sample and continue the process with the Caltech 3 MeV accelerator. The lower temperature anneal stages yield a sequence of curves analogous to Fig. 18. The data for the two portions of the anneal curve for 200 keV implants were fitted in the region from RT to 100°C and are presented in Fig. 19. Figure 19 also shows relative numbers for the amount of disorder produced as a function of the temperature of the silicon substrate during the boron implantation. For these measurements, the sample was implanted, then cooled to 10°C below the implantation temperature and analyzed in situ with the 450 keV proton analyzing beam. The shift of the boron disorder anneal curve to higher temperatures than the implantation curve shows the nonequivalence of dynamic anneal during implantation and anneal treatments after the disordered regions have been formed. The temperature dependence of the amount of disorder produced for 200 keV boron implantations into silicon

Fig. 19. Amount of disorder produced by implantation of $1 \times 10^{15}$ 200 keV boron ions/cm$^2$ from analyses with 450 keV protons (+). Results are given for anneal treatments performed on samples implanted with $2 \times 10^{14}$ 200 keV boron ions/cm$^2$ and analyzed with 1.8 MeV $^4He^+$ (x,o,□) or 450 keV protons (Δ). Annealing characteristics (dash-dot line) for divacancies (1.8μ absorption band) in samples at room temperature during 400 keV oxygen ion implantation are from Ref. 67. Growth (dotted line) of divacancies (1.8μ absorption band) in samples at -190°C during 400 keV boron ion implantation are from Ref. 69.

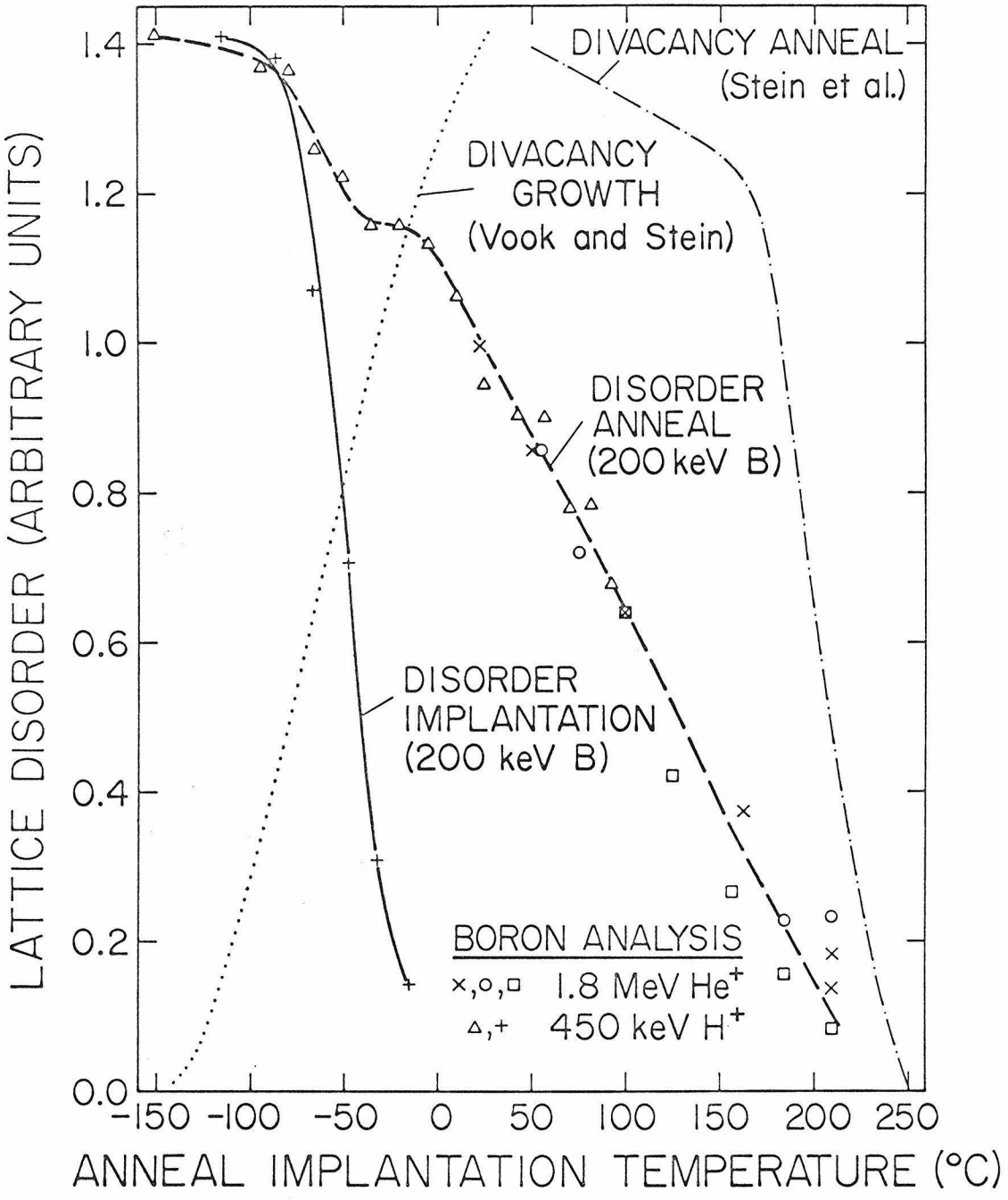
DIVACANCY ANNEAL
(Stein et al.)
DIVACANCY
GROWTH
(Vook and Stein)
DISORDER
ANNEAL
(200 keV B)
DISORDER
IMPLANTATION
(200 keV B)
BORON ANALYSIS
×,○,□ 1.8 MeV He+
△,+ 450 keV H+
LATTICE DISORDER (ARBITRARY UNITS)
ANNEAL IMPLANTATION TEMPERATURE (°C)
0.0
0.2
0.4
0.6
0.8
1.0
1.2
1.4
-150
-100
-50
0
50
100
150
200
250

Figure 19

is very strong. This amount changes by a factor of about twenty from -85°C to room temperature, with a midpoint of the decrease at about -50°C.

The large angle backscattering technique averages over the defect structures present in an increment of thickness. It does not distinguish between particular defects. For this reason, the studies of this part of the thesis are not appropriate to investigate the detailed mechanism responsible for the low temperature anneal behavior discovered in these boron implants. At best it is possible that comparison of uniaxial alignment analyses with single alignment investigations might show different backscattering yields or different dechanneling dependences for the same samples from which one might infer some measure of the overall strain or lattice distortion present. However, the use of other techniques such as anomalous x-ray transmission measurements[65] to study strain and electron spin resonance[66] and infrared absorption studies[67] to identify and follow specific defects are suggested should one wish to pursue the detailed mechanisms of the annealing of the disordered regions. Much work with these techniques has been and is being performed and no comprehensive survey is intended by the single references given. Only a single representative work is given in each case.

Stein et al. studied[67] the anneal of divacancies produced in silicon by implantation of 400 keV oxygen ions at silicon substrate temperatures of ~50°C. These data are included in Fig. 19. They noted that the anneal of the divacancies was similar to the lower temperature

(near 200°C) isochronal anneal stage of the disorder produced in silicon by low doses of 40 keV antimony ions and concluded[68] that the "low influence ion damage annealing is dominated by divacancy motion." However, as shown in Fig. 19, the drop in the amount of disorder produced during the 200 keV implantation itself and the reduction in the disorder peak produced by anneal treatments after implantation both occur at lower temperatures than the drop in the divacancy concentration in 400keV oxygen implants. The second set of divacancy data[69] was obtained after the boron anneal results presented in this thesis. It shows the growth of the divacancy concentration with anneal temperature for 400 keV boron implantations made into silicon substrates at -190°C. The measurements were also made at -190°C. Part of the growth of the divacancy concentration occurs in the same region in which the channeling effect analyses show a decrease in the amount of disorder. The work of this thesis in the area of temperature effects thus clarifies early suggestions that the channeling effect was detecting principally divacancies and the strained regions of the samples around divacancies. In the low temperature boron implantations in silicon these channeling effect measurements suggest that other defect structures than divacancies must also be present.

IV.C Effect of Analyzing Beam on Disorder Measurement

Bombardment of an implanted sample with the analyzing beam can influence the disorder measurement. A sample was implanted with $3 \times 10^{14}$ 200 keV boron ions/cm$^2$ with the substrate held at -150°C during the boron implantation, then warmed to room temperature and the 1 MeV $^4He^+$ analyzing beam aligned with the <110> crystal axis. The alignment required a dose of (3-5) $\times 10^{16}$ $He^+$ ions/cm$^2$ typical for the experimental geometry employed in the work of this thesis. The beam was then moved to an unbombarded spot on the implanted region of the sample. One analyzing run comprising a disorder measurement and requiring $6 \times 10^{15}$ $He^+$ ions/cm$^2$ was made and is the first curve shown in Fig. 20. The analyzing beam bombardment was continued, stopping periodically to make a disorder measurement requiring the standard $6 \times 10^{15}$ ions/cm$^2$, and the total dose to the sample was recorded. Figure 20 shows the sequence of spectra obtained in this manner with the backscattering yield dropping successively with increasing dose of the analyzing beam. Further, the level behind the disorder peak also drops successively showing that the amount of dechanneling in the disordered layer also decreases. This sequence of curves shows immediately the large effect that the dose of analyzing beam required for alignment alone can have on a disorder measurement. The analyzing beam spot had a typical area of 2mm$^2$. If, after a dose of $3 \times 10^{17}$ $He^+$ ions/cm$^2$, the analyzing beam is moved to an adjacent unbombarded region of the sample, the spectrum is identical to the original one from the bombarded spot recorded before large amounts of analyzing beam had struck that spot.

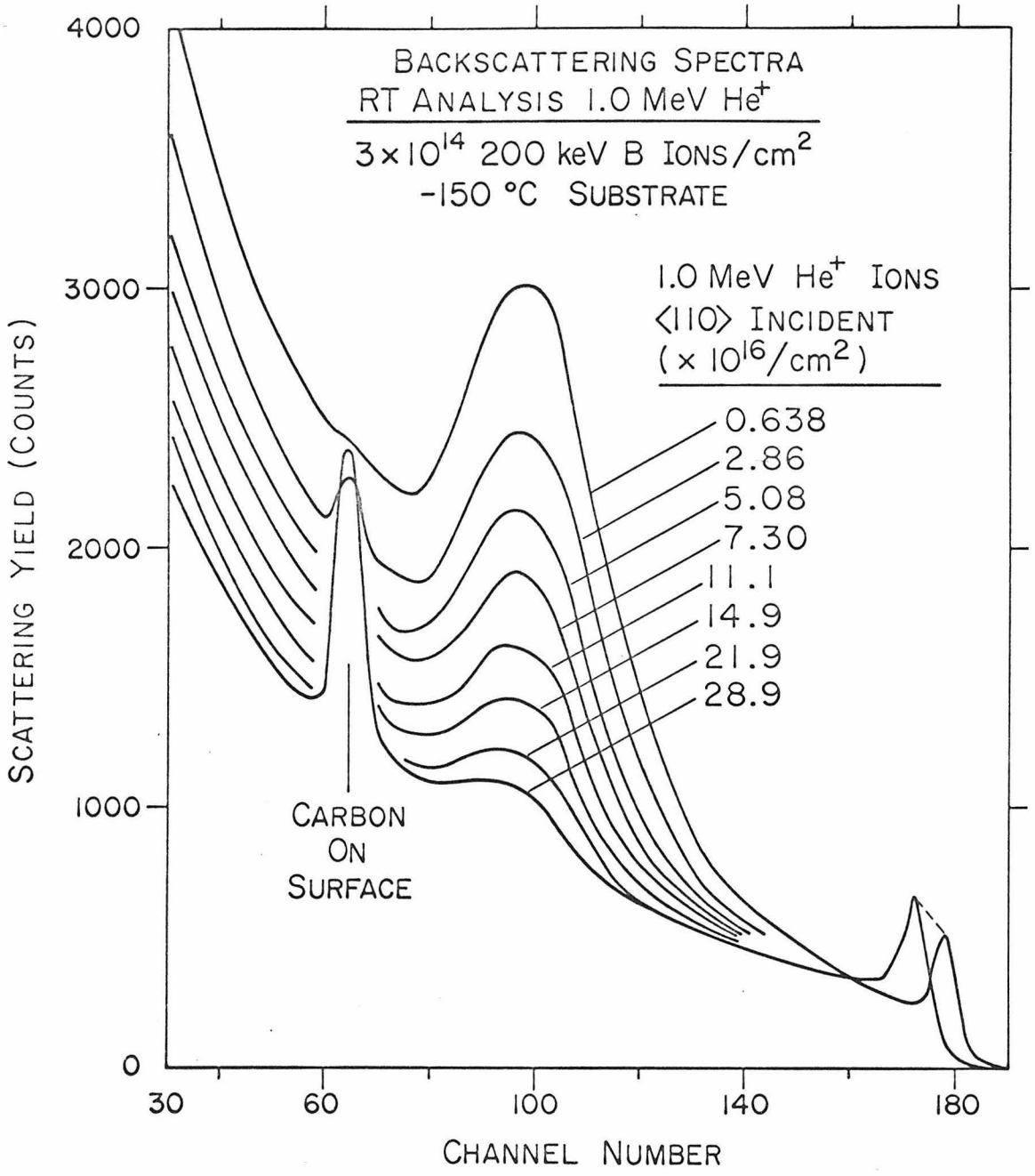


Fig. 20. Effects of 1.0 MeV $^4He^+$ analyzing beam on disorder measurement. Sample at room temperature during analyzing beam bombardment.

as would be expected
This indicates that the disorder reduction does not propagate any macroscopic distance laterally. So for each successive analyzing run on the same sample, for example, in a sequence of layer removals and analyzing runs, the analyzing beam was moved to a different spot to minimize this change in the disorder.

Each measurement is really an average over the disorder as it changes, but after the first run shown in Fig. 20, another spectrum, not shown, was recorded with the next dose of $6 \times 10^{15}$ ions/cm$^2$. This second analyzing run caused a change of only 6%. Although a dose of $6 \times 10^{15}$ ions/cm$^2$ was required to give adequate statistics, it was judged that the spectrum from this dose represented a measurement at most only 3% different from the disorder present in a sample prior to any bombardment. Such an error is acceptable, so all analyzing runs are taken as representative of the initial condition in a sample, and no attempt is made to correct for any such slight reduction.

The disorder reduction effect is observed in the 450 keV proton analyses as well as those employing helium beams in implants made at -150°C with boron doses $\leq 5 \times 10^{14}$ ions/cm$^2$. However, the disorder reduction effect of the helium or proton analyzing beam is not observed
comparable amounts
in measurements of of disorder in samples held at room temperature during the boron implantation.

A thermocouple was fixed to one of the samples so that the helium and the proton analyzing beams struck positions both adjacent to the thermocouple-sample junction and directly on top of this junction. No temperature rise greater than 2°C was observed for beam currents a

factor of five higher than that used to produce the effects shown in Fig. 20. This suggests that the measured reduction of disorder was not due to a rise in sample temperature during the analyzing beam bombardment.

The beam annealing effect may be another manifestation of the phenomena responsible for the different temperature dependence of disorder production during implantation and of anneal of disorder after implantation. The thermal annealing of low temperature implanted samples at temperatures slightly above room temperature has already been shown to produce a reduction in the amount of disorder. Therefore, it is possible that beam annealing is due to low nuclear energy transfers (much less than those required to produce lattice atom displacement) which may introduce enough energy into lattice atom motion to cause some annealing of disorder to occur at room temperature. Ionization effects in the form of hole-electron pairs generated by electronic energy loss may also be responsible. Charge state effects are known to exist.[70] For example, the neutral vacancy $V^{\circ}$ in silicon is not mobile below temperatures of the order of 150°K whereas the doubly negative charged vacancy $V^{=}$ is mobile at least down to temperatures of 80°K. The stability of divacancies in silicon has also been known[71] to be influenced by charge state effects.

Figure 20 shows a sharp peak at relatively low energy. This is the carbon building up on the sample surface. This carbon causes energy loss in the incident beam moving the front edge of the silicon spectra to lower energies.

# V. Depth Scale Determination and Applications.

## V. A General Description.

The disorder distribution calculation described in (II.E) requires a determination of the thickness of the sample equivalent to one channel in the backscattering spectra. This quantity was then used in (III.C) to determine the depth of the disorder peaks and the widths of the scattering center distributions. A layer removal technique by anodic oxidation and stripping will be presented first. This allows removal of a known amount of the sample. Large angle backscattering techniques were used to analyze the composition of these oxide layers. A general expression for the depth scale expression of the type already employed in this thesis in (II.D) and (II.E) will be derived and the approximations involved indicated. Then the results of the direct measurement of a depth scale for the single alignment spectra will be described. In conclusion, an application of the general depth scale expression to stopping power measurements with the two addition experiments used to measure the aligned and random stopping power for helium in silicon at one energy will be presented.

V.B Anodic Oxide Procedure and Results

Oxide layers were anodically grown on the sample of interest using a solution composed by weight of 97% N-methylacetamide, 2% water (distilled and deionized), and 1% potassium nitrate ($KNO_3$). The area of the anodic oxide layer was determined by the hole in a vinyl overlay placed on the sample to be anodized. By using the same piece of vinyl each time, it was only necessary to use the same increase in voltage $\Delta V$ and the same current I to accurately define layers of reproducible thickness. The anodic oxide layers were stripped off the sample with concentrated (48%) hydrofluoric acid (HF). Two standard oxide thicknesses were used. They will be referred to simply as $T_1$ and $T_2$. Oxide $T_1$ had a nominal thickness of 1550Å and an area of ~0.72 $cm^2$. This oxide was accurately defined by $\Delta V$ = 284 volts with the current I maintained at 6.55 mA. throughout the growth process. Oxide $T_2$ had a nominal thickness of 1000Å and an area of ~0.080 $cm^2$ and was accurately defined by $\Delta V$ = 188 volts and I = 0.74 mA. (The different size of oxide $T_2$ arose simply because of the smaller size of the implanted regions on the samples on which these oxide layers were to be grown.) The uniformity of the color of the oxide grown on the implanted portion of the sample showed that these anodic oxide layers were uniform.

The usual nondestructive film thickness measuring techniques such as ellipsometry[72,73] require a knowledge of the index of refraction of the substrate beneath the thin film. Since this index was not known for the implanted portion of the sample, control oxides were grown on unimplanted silicon at least after every two or three layers

were grown on the implanted region. The thickness of the layer removed could then be checked by a comparison of the color of the control oxides and the color of known standard oxides, and by measurement by ellipsometry of the thickness of the control oxides.* The average thickness for the oxide layer $T_1$ from ellipsometry was 1550Å. This was the average of the measurement of 21 films and the calculated standard deviation was 35Å. For oxide $T_2$ the average of the measurement of 3 layers was 1010Å with a standard deviation of 20Å. Optical measurement by the Tolansky multiple beam interference technique[74] of the step in the unimplanted material after stripping the control oxide gave for the layer $T_1$ the amount of silicon removed per strip $\Delta t$ = (665 ± 20Å). This value is the average of 69 fringes measured on 10 photographs, and the error quoted is again the calculated standard deviation. The value of 665Å is 6% less than the 705Å of silicon which would be removed in a stripping of a stoichiometric silicon dioxide layer of the thickness of 1550Å given by ellipsometry.**

The discrepancy between the ellipsometric and interferometric results was outside the errors of either of these processes. This suggested that the anodic oxide layers did not have the composition of stoichiometric silicon dioxide. There was another possible difficulty in that the oxides grown on the implanted regions of the samples might have different thicknesses from those grown under identical conditions

---

*The ellipsometry measurements were performed by T. Smith at the North American Rockwell Science Center.

**Stoichiometric silicon dioxide has a density of 2.27 g/cm$^3$.[75] Using a gram molecular weight for $SiO_2$ of 60.09 g., this is equivalent to 2.28 x $10^{14}$ silicon atoms/cm$^2$ per Å of oxide.

on unimplanted silicon. Two types of large angle backscattering measurements similar to those already described in the context of measuring disorder were performed to resolve these questions.

The first type of backscattering measurement was used to compare the oxides grown on the implanted and unimplanted silicon. This was to determine whether ellipsometric measurements of anodic oxides on unimplanted material could be used for the thicknesses of anodic oxides grown on the implanted region of the sample. A 1 MeV $^4He^+$ beam was allowed to impinge on the oxide layers in a "random" direction (far from any high symmetry direction of the underlying silicon crystal). Figure 21 shows the resulting energy spectrum of the backscattered particles (recorded in the single alignment geometry of Fig. 1) for one of the oxide layers $T_1$. The spectrum shows a step at the front edge because there are a smaller number of silicon atoms per unit stopping power for the helium analyzing beam in the anodic layer than in the silicon substrate beneath the layer. The mesa at lower energy riding on the silicon substrate spectrum is the yield from the oxygen atoms in the anodic layer. The helium particles scattered from the surface of the anodic layer have energies $E_{obs} = k^2_{Si} E_{In}$ and $E_{obs} = k^2_O E_{In}$ for the silicon and oxygen atoms respectively where $E_{In}$ is the incident energy, 1.0 MeV. Under the experimental conditions of the measurement, $\theta_L = 164°$ so the values of $k^2$, calculated from Eq. (10), are for helium scattered from silicon 0.569 and for helium scattered from oxygen 0.367. The midpoint of the Si front edge is in channel number 173.5 and the midpoint of the front edge of the oxygen mesa is

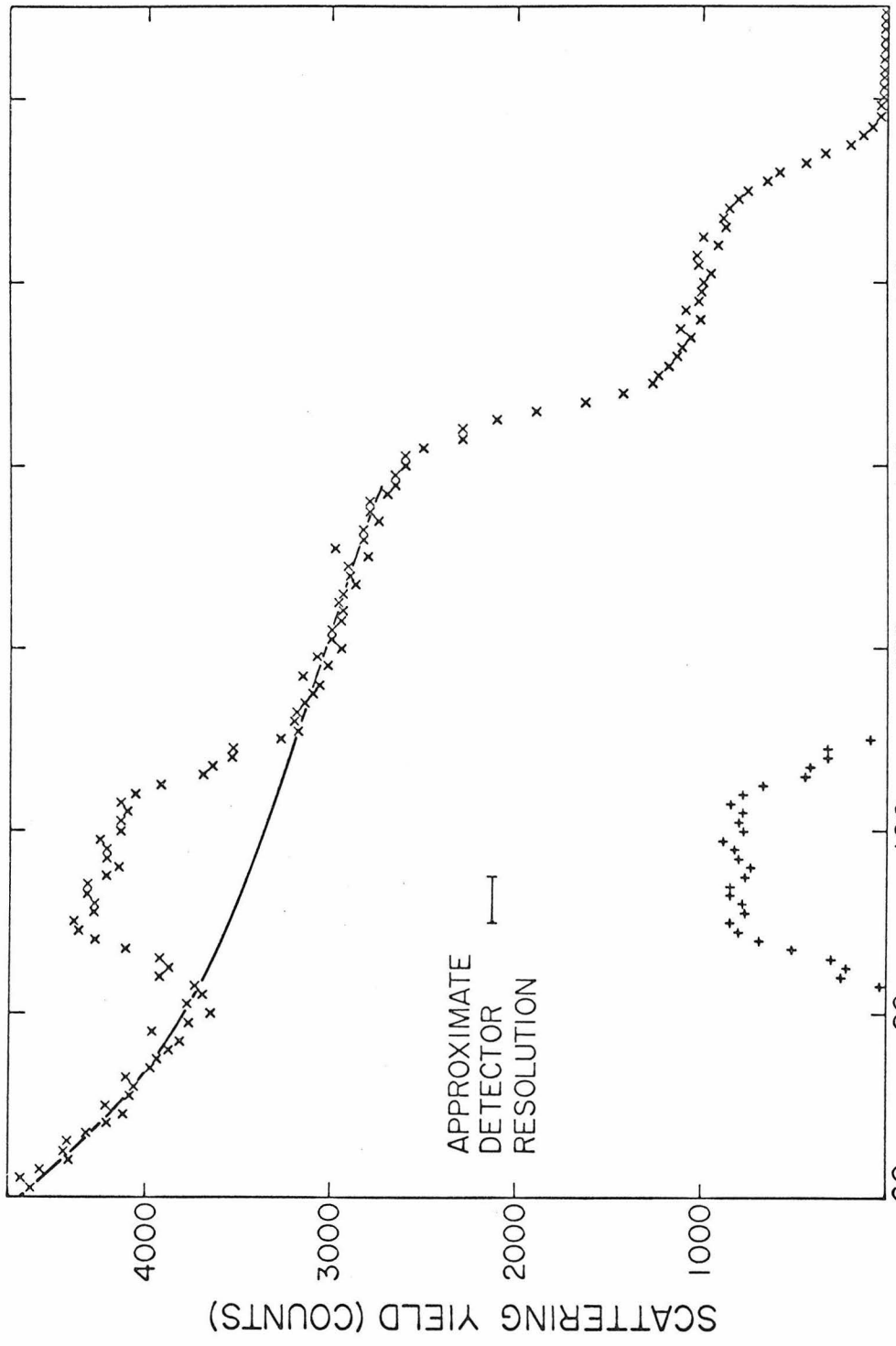


Fig. 21. Random spectrum from 1.0 MeV $^4He^+$ analysis of anodic oxide layer $T_1$ ( 1550Å thick, see text). Yield from oxygen in layer (+) is after substraction of yield from silicon substrate (solid line).

in channel number 107.3 giving an energy per channel of 3.05 keV.

In all cases the spectra from oxides on the implanted region coincided with the spectra from oxides on unimplanted material to within statistics ($\lesssim$5%) both in the yield in the region of the silicon step and in the position of the leading edge of the underlying silicon substrate yield. In some cases due to mild channeling effects, the substrate yield varied by as much as 10%. In the worst of these cases where direct comparison of the silicon step was somewhat difficult the oxygen peaks were also compared by subtracting the silicon background (solid line in Fig. 21) and they agreed again within statistics. This indicates that the anodic oxide layers on both implanted and unimplanted silicon were nearly identical.

To examine the possibility that the anodic oxide layers were not stoichiometric silicon dioxide, those grown on unimplanted silicon were evaluated in more detail. The 1 MeV $^4He^+$ analyzing beam was aligned with the <110> axis of the underlying silicon. This aligned spectrum with a background for the yield (solid line) from the silicon substrate and the resulting oxygen peak after the background subtraction are shown in Fig. 22. A random spectrum for this sample was also recorded. It is not presented here because it has the same features as Fig. 21. The aligned and random spectra are analyzed by the method described in detail by Mitchell et al.[31] to separate the contributions from the substrate and the oxide layer. Briefly, one assumes that the random spectrum (R) is composed of an amorphous target yield from the silicon substrate (B) and the yield from the silicon in the oxide (C)

Fig. 22. Aligned spectrum from 1.0 MeV $^4He^+$ analysis of anodic oxide layer $T_1$ (~1550Å, see text). Yield from oxygen in layer ( o and shaded) is after substraction of yield from silicon substrate (solid line). Yield from silicon in layer ( □ and shaded) is after correction for yield from silicon substrate.

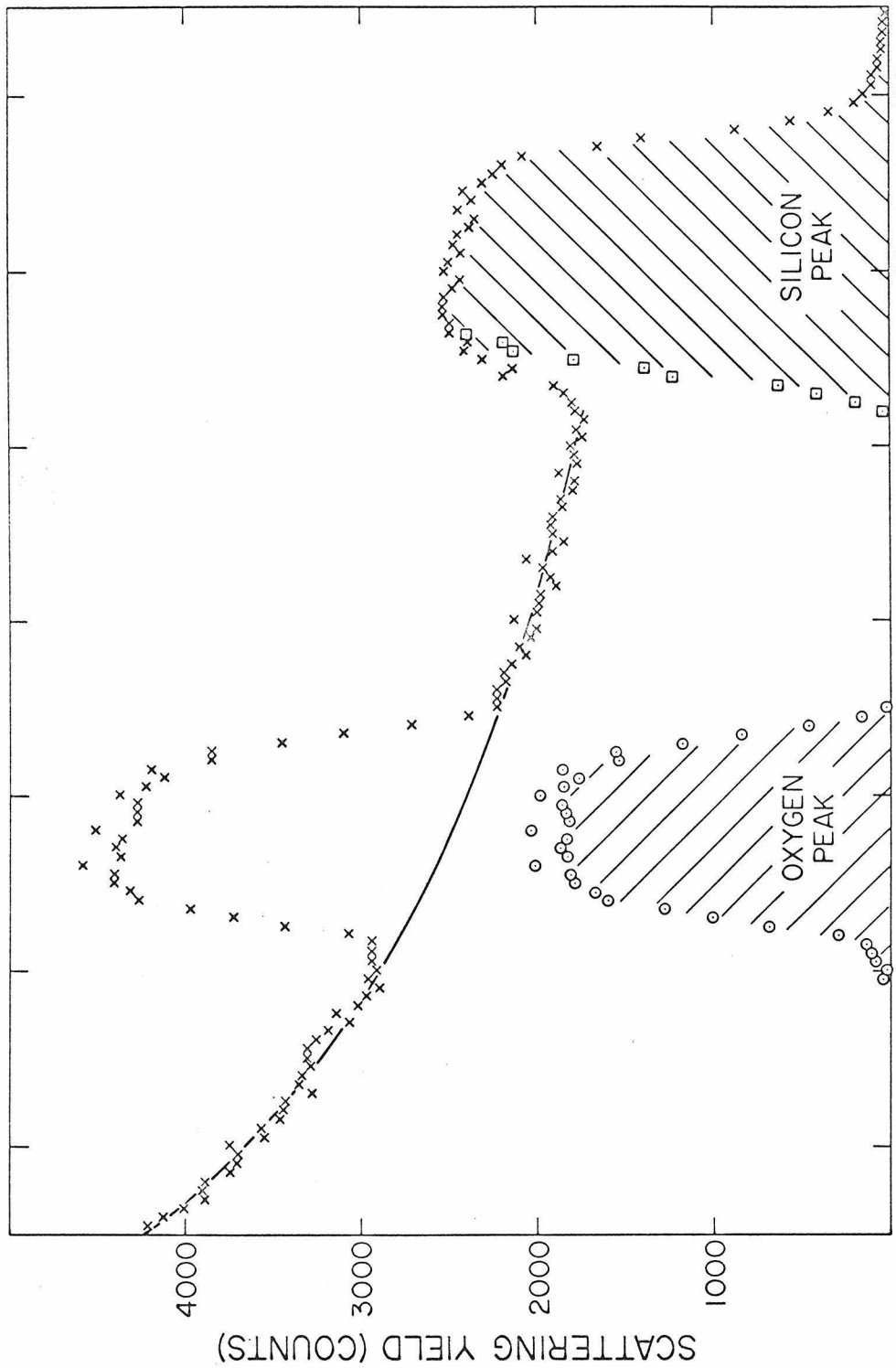
SCATTERING YIELD (COUNTS)
4000
3000
2000
1000
60
80
100
120
140
160
180
CHANNEL NUMBER
OXYGEN PEAK
SILICON PEAK

Figure 22

as follows:

$$R = B + C \tag{42}$$

Equation (42) is applied to the spectra from about 15 channels 46 (keV) below the oxide substrate interface, that is, for example, for energies above about channel number 130 in Fig. 22. Then one assumes that the aligned spectrum (A) is composed of the yield from the silicon in the oxide (C) and the amorphous target yield from the silicon substrate properly scaled as follows:

$$A = fB + C \tag{43}$$

Equation (43) is similarly assumed to hold for energies above about channel number 130 in Fig. 22. The scale factor f is the ratio of the minimum yield determined as the average over ten channels in the aligned spectrum behind the silicon in the oxide layer, i.e., about 1830 in channel 146 in Fig. 22, to the value of the random spectrum (not shown in Fig. 22) in the same energy region. The value of f for Fig. 22 was 0.303, a typical value for oxides of this thickness. One then solves Eqs. (42) and (43) for C for each channel. This constructed spectrum coincides with both the aligned and the random spectrum away from the overlap, that is, above approximately channel 145 in Fig. 22. The open squares are the constructed values in the region of the overlap. (The aligned spectrum with its lower substrate background and hence greater sensitivity was not used in the comparison of oxide layers on the implanted and unimplanted samples because in the implanted sample it would have been very difficult to separate the effects of the disorder

from those of the anodic layer itself in order to make the desired comparison).

The following equation gives the ratio of the total amount of oxygen in the layer to the total amount of silicon:

$$\frac{N_O}{N_{Si}} = \frac{R_O}{R_{Si}} \cdot \frac{\sigma_{Si}}{\sigma_O} \tag{44}$$

where $R_O$ is the total number of counts in the oxygen peak (shaded in Fig. 22), $R_{Si}$ is the total number of counts in the constructed yield of the silicon in the oxide layer only (shaded in Fig. 22), and

$$\frac{\sigma_{Si}}{\sigma_O} = \frac{\left(\frac{d\sigma}{d\Omega_{cm}}\right)_{Si} \left(\frac{d\Omega cm}{d\Omega_L}\right)_{Si} \Delta\Omega_{L,Si}}{\left(\frac{d\sigma}{d\Omega_{cm}}\right)_{O} \left(\frac{d\Omega cm}{d\Omega_L}\right)_{O} \Delta\Omega_{L,O}} \tag{45}$$

$\Delta\Omega_{L,X}$ is the laboratory solid angle for element X, $d\sigma/d\Omega_{cm}$ is given in Eq. (27), and, from, for example, Leighton,[46]

$$\frac{d\Omega_{cm}}{d\Omega_L} = \frac{\left[(M_1/M_2)^2 + 2(M_1/M_2)\cos\theta_{cm} + 1\right]^{3/2}}{(M_1/M_2)\cos\theta_{cm} + 1} \tag{46}$$

where $M_1$ is the projectile, $M_2$, the target atoms, and $\theta_{cm}$ is the scattering angle in the center-of-mass system, related to $\theta_L$ the scattering angle in the lab system by Eq. (30). Since $\Delta\Omega_{Si,L} = \Delta\Omega_{O,L}$ and under these experimental conditions again $\theta_L = 164°$, then $\sigma_{Si}/\sigma_O = 3.33$.

Two anodic oxide samples $T_1$ were measured giving values of $N_O/N_{Si}$ of 2.14 and 2.13. After heating these anodic layers for 1.5 hours at 500°C in a dry nitrogen atmosphere, the measurements were repeated

giving values of, respectively, 1.91 and 1.95. For comparison a thermally grown oxide gave a value of 1.94 for $N_O/N_{Si}$. The error in a given measurement of $N_O/N_{Si}$ is estimated to be $\pm 5\%$. A direct comparison of the spectra can be made, and the level of the yield from the silicon in the thermal oxide agrees with that from the silicon in the two anodic oxides only after the heat treatment. Before heat treatment the levels were lower than that of the thermal oxide. Further, ellipsometric measurements on three heat treated anodic oxide layers gave an average thickness of 1485Å with a standard deviation of 30Å. Assuming that the layers are now stoichiometric silicon dioxide, the silicon removal would be 675Å with a standard deviation of 15Å. This result now agrees with the interferometric measurement of the value of the silicon removal.

Although the absolute errors in a given determination of $N_O/N_{Si}$ may be about 5%, the relative changes in this quantity can be found to greater accuracy by a direct comparison of the spectra from two different samples. Heat treatment reduces the value of $N_O/N_{Si}$ for an anodic oxide layer to that for a thermal oxide. This indicates that the anodic films are taking on the composition of a thermally grown oxide after the heat treatment, apparently by losing water of hydration. A similar change is found in the ellipsometrically measured values of thickness.

Based on the above analysis an anodic oxide $T_1$ contains $(3.33 \pm 0.10) \times 10^{17}$ silicon atoms/cm$^2$ or is equivalent to a thickness of crystalline silicon of $(665 \pm 20)$Å. The chemical composition of

the anodic oxide layers $T_1$ is assumed to be the same as that of the anodic oxide layers $T_2$. The value of $2.29 \times 10^{17}$ silicon atoms/cm$^2$ indicated by the thickness value of (1010 $\pm$ 20)Å determined by ellipsometry is then scaled by the ratio of the interferometric to ellipsometric values for the anodic oxide $T_1$. This procedure indicates that an anodic oxide $T_2$ contains $2.16 \times 10^{17}$ silicon atoms/cm$^2$ or is equivalent to a thickness of crystalline silicon of 430Å.

In conclusion, this section illustrates the applicability of the backscattering technique to other than disorder distributions and suggests its use in the evaluation of many thin layer systems.

V.C Depth Scale Measurement.

The general depth scale expression will now be derived and the application of the layer removal technique to direct depth scale measurement will be presented.

The detected energy $E_{obs}$ of a particle incident with energy $E_{In}$ and backscattered from a depth t in a sample (see schematic in Fig. 23) is the following:

$$E_{obs} = k^2 \left[E_{In} - \int_{o}^{t/\cos\theta_1} S_{In}(E)\cdot d\ell_1\right] - \int_{t/\cos\theta_2}^{o} S_{Out}(E)\cdot d\ell_2 \quad (47)$$

where $k^2$ has been defined in Eq. (10) and the first and second integrals are the energy losses along the incoming and outgoing trajectories, $\ell_1$ and $\ell_2$. The angle of the beam with respect to the surface normal is $\theta_1$, the angle of the detected backscattered particle with the surface normal is $\theta_2$, and the scattering angle is $\theta_L$. $S_{In}(E)$ and $S_{Out}(E)$ are the stopping powers for the entering and outgoing beam respectively in units of energy/length. If t = 0, $E_{obs} = k^2 E_{In}$. A depth scale is the change in $E_{obs}$ for a given change in t.

If the incident beam is aligned, $\theta_1 \lesssim 1°$. If the incident beam is random, $\theta_1 \simeq 6°$ because random orientations are obtained by increasing $\phi_1$ (see Fig. 1) to 6°, then gradually changing $\phi_2$ while monitoring the backscattering yield until a place far from any high symmetry plane of the crystal is found. In either case $\cos\theta_1 \simeq 1$. For all of the work presented in this thesis the energy loss along $\ell_1$

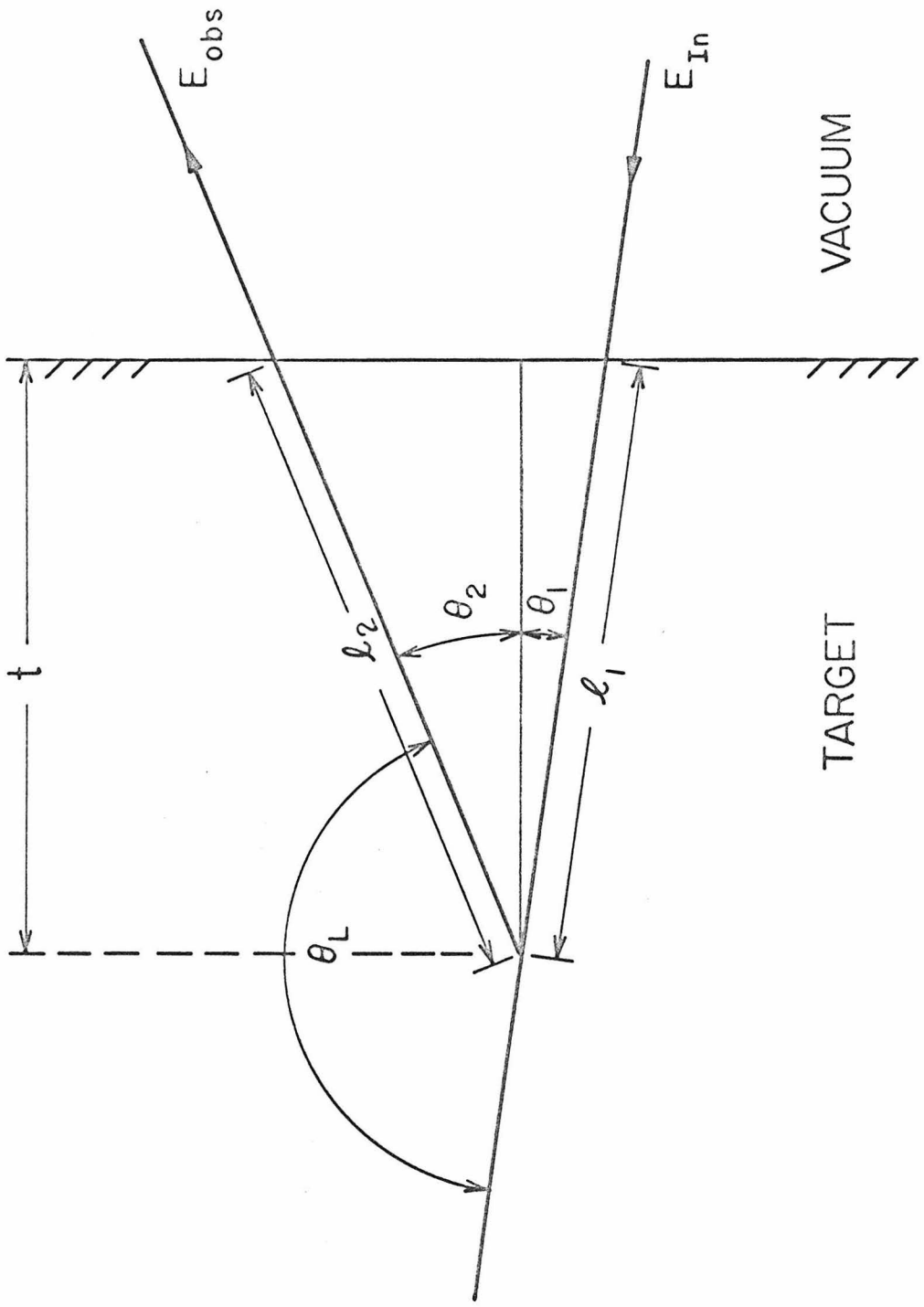


Fig. 23. Schematic of path of backscattered particle in sample.

or $\ell_2$ is small compared to the energy of the particle on that trajectory* and the stopping power changes sufficiently slowly with energy that Eq. (47) can be written to a good approximation as follows:

$$E_{obs} = k^2 [E_{In} - tS_{In}(E_{In})] - \frac{t\, S_{Out}(k^2 E_{In})}{\cos \theta_2} \tag{48}$$

Integrated depth scales are desired, so the change in $E_{obs}$ of interest is $\Delta E$ as follows:

$$\Delta E = E_{obs}(t = 0) - E_{obs}(t = \Delta t) \tag{49}$$

Finally, since $\cos \theta_2 \simeq - \cos \theta_L$, and then using $E_2 = k^2 E_{In}$, the depth scale expression becomes the following:

$$(\Delta E/\Delta t) = k^2 S_{In}(E_{In}) - \sec \theta_L \, S_{Out}(E_2) \tag{50}$$

The special case of the depth scale expression Eq. (50) to be discussed now is that for the single alignment type of spectra with 1.8 MeV $^4He^+$. The helium atoms lose a large amount of energy when they are backscattered from the silicon atoms of the sample and have a higher energy on their path entering the sample from their energy on their path exiting from the sample. Further the depth scale for single alignment (SA) spectra involves the aligned stopping power for helium in silicon

*The worst case occurs for the 300 keV implants where the energy lost by the particle on $\ell_2$ is $\approx$20% of the energy of the particle. The energy of the particle on $\ell_2$ changes from ~940 keV to ~740 keV. The calculated values[76] of the stopping power for helium in silicon only change $\lesssim$4% for this range of energies.

at one energy and random stopping power at another energy as follows:

$$(\Delta E/\Delta t)_{SA} = k_{Si}^2 \; S_A(E_1) - \sec \theta_L \; S_R(E_2) \qquad (51)$$

where $k_{Si}^2 = 0.569$, $S_A(E_1)$ is the aligned stopping power for the incident energy $E_1 = 1.8$ MeV, $\theta_L = 164°$, and $S_R(E_2)$ is the random stopping power at the energy after backscattering $E_2 = 1$ MeV. The value of the aligned stopping power for helium in silicon at 1.8 MeV, $S_A(E_1)$ in Eq. (51), was not known, and more accurate results were desired than would be permitted by the estimated $\pm$ 10% errors[14] in the measured values of the random stopping powers. So it was undertaken to measure $(\Delta E/\Delta t)_{SA}$ directly.

The anodic oxidation layer removal technique described in (V.B) was the tool used to determine a depth scale for the 1.8 MeV $^4He^+$ aligned spectra. The silicon single crystal samples were implanted with $5 \times 10^{14}$ boron ions/cm$^2$ at energies of 200 and 300 keV. The substrate was held at -150°C during the boron implantation. Under these conditions the disorder spectrum has a sharp peak. Anodic oxide layers were grown on and then stripped off the sample as has already been described. After each strip or set of strips the 1.8 MeV $^4He^+$ beam was aligned with the <110> axis incident on the implanted and stripped region of the sample, and a spectrum was recorded. Figure 24 shows a sequence of such aligned spectra after successive layer removals performed on a 200 keV implant. The energy shift $\Delta E$ of the peak of the disorder was measured from data similar to those shown in Fig. 24. Table IV gives the values obtained for five measurements. The average value is 30.0 keV per removal of an anodic oxide $T_1$ with a standard deviation of 1.24

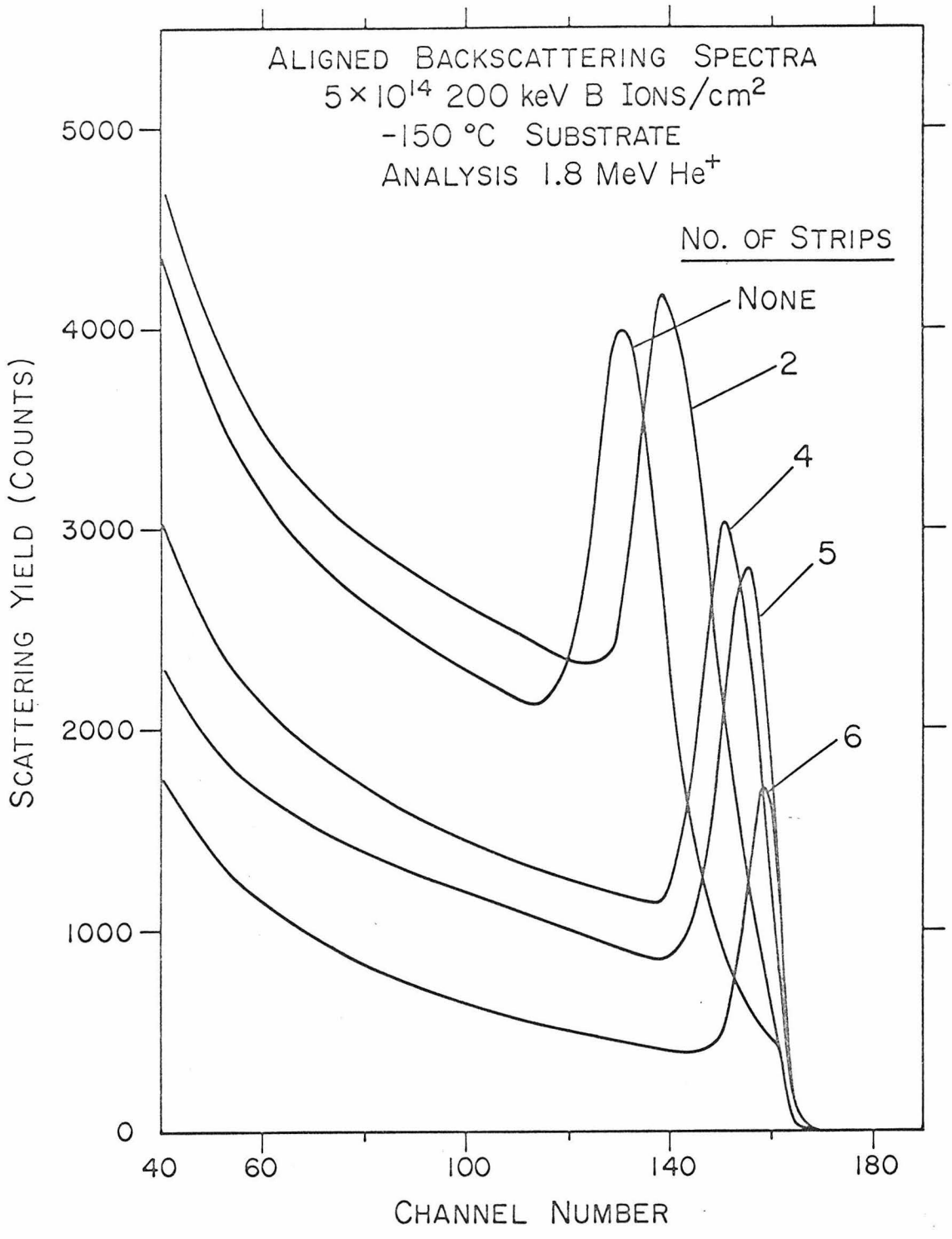


Fig. 24. Aligned spectra from 1.8 MeV $^{4}He^{+}$ analyses showing movement of disorder peak to sample surface with measurements after successive layer removal.

TABLE IV

Depth Scale Results

| Number of $T_1$ Oxide Layer* Removals | Total Silicon Removed (Å) | Peak Shift ΔE (keV) |
|---|---|---|
| 2 | 1330 | 57.4 |
| 3 | 1995 | 95.1 |
| 2 | 1330 | 57.0 |
| 3 | 1995 | 90.9 |
| 3 | 1995 | 92.7 |

*See text for definition of $T_1$ oxide layer.

keV. Combining the fractional deviation in $\Delta E$ in the usual sum of the squares approach to uncorrelated errors with the fractional deviation for the thickness of the silicon removal $\Delta t$ from (V.B) gives a value for $(\Delta E/\Delta t)_{SA}$ of 45 eV/Å with a fractional deviation of 0.05 or 2 eV/Å. This value is for the 1.8 MeV helium aligned spectra in our experimental geometry. The error of approximately $\pm$5% is a significant improvement over anything that might be estimated from existing values of stopping powers.

The depth scale just presented is for aligned spectra from lightly damaged samples because the aligned yield from the region of the crystal removed by stripping is ~10% of the random yield. The error involved in using this depth scale throughout the whole spectrum, even in the region of the disorder peak, is, however, small. As the amount of disorder in some region of a sample increases, the stopping power of that portion of the sample for the aligned beam increases from the aligned value $S_A(E_1)$ toward the random value $S_R(E_1)$. For example, for the sample of Fig. 4a, using the previously reported value[14] of 26 eV/Å for the random stopping power of 1.8 MeV helium in silicon the depth scale changes only ~4% from 45 eV/Å at the surface to 47 eV/Å at the peak of the disorder. Allowing for this depth dependence of the depth scale only changes the calculated peak depth of this 200 keV implant from 4220Å to 4160Å. In fact, the depth scale for 1.8 MeV helium analyses for the experimental geometry employed here would change only ~9%, its maximum amount, to 49 eV/Å in regions of a sample in which the aligned beam experienced the random stopping power, that

is, where $S_A(E_1)$ in Eq. (51) would be replaced by $S_R(E_1)$.

In conclusion, an energy to depth conversion of (45 $\pm$ 2) eV/Å was found for the single alignment spectra using 1.8 MeV helium. This depth scale should be applicable to disorder distributions similar to that shown in Fig. 4a.

V.D Application of Depth Scales to Stopping Power Determination

In addition to the obvious application to determining the depth in a sample represented by a given point in the backscattering spectra, the general depth expression (Eq. (50)) can be applied to two additional experiments to obtain the random and aligned stopping powers for helium in silicon at one energy.

The first additional experiment required was a uniaxial analysis, whose scattering geometry was described in Fig. 3. Figure 25 shows a spectrum collected in single alignment and one collected in uniaxial alignment from the same spot on a sample which was implanted at -150°C with $5 \times 10^{14}$ 300 keV boron ions/cm$^2$. A significant reduction of the disorder peak is apparent in the uniaxial spectrum. This change has taken place because of the relatively large size of the total dose of analyzing beam (~$2 \times 10^{17}$ 1.8 MeV $He^+$ ions/cm$^2$) required to complete the uniaxial spectrum. This is the same disorder reduction effect which was discussed in (IV.C). Recalling that section, one can compare in Fig. 20 the effect of this dose of 1.0 MeV $He^+$ ions/cm$^2$ on a similar disorder peak. Despite the reduction of the amount of disorder, as Fig. 20 shows, the location of the disorder peak has not changed. So the disorder peak is a fixed marker at a known depth (from the SA analysis and SA depth scale) inside the sample. The peak shift $\Delta$ of 44 keV between the two spectra in Fig. 25 then makes it immediately clear that different stopping powers are involved in uniaxial alignment as compared to single alignment. The peak depth in energy $\Delta E$ (Fig. 25) in the uniaxial case then gives a depth scale for uniaxial alignment

Fig. 25. Spectra from 1.8 MeV $^{4}He^{+}$ single (SA) and uniaxial (UA) alignment analyses of the same sample. The random spectra (not shown) have a ratio (SA to UA) of 79 in channel 161 and 70 in channel 100. Normalized to the respective random values, the ratio of the peak heights is 140 and the ratio of the minimum values of the aligned spectra behind the respective peaks is 110.

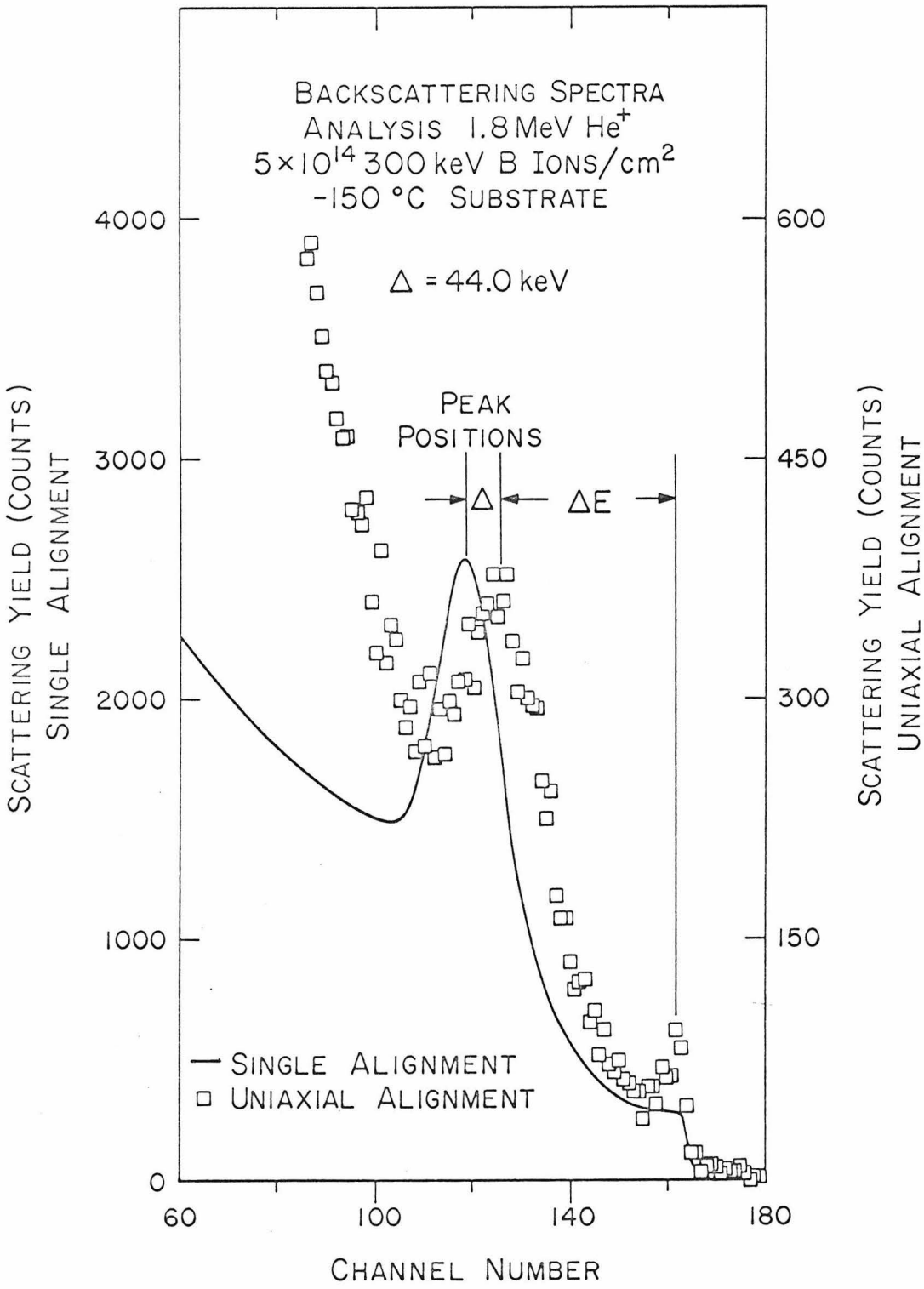
BACKSCATTERING SPECTRA
ANALYSIS 1.8 MeV He+
5×10^14 300 keV B IONS/cm^2
-150 °C SUBSTRATE
Δ = 44.0 keV
PEAK POSITIONS
Δ
ΔE
SINGLE ALIGNMENT
UNIAXIAL ALIGNMENT
SCATTERING YIELD (COUNTS) SINGLE ALIGNMENT
SCATTERING YIELD (COUNTS) UNIAXIAL ALIGNMENT
CHANNEL NUMBER
4000
3000
2000
1000
0
600
450
300
150
60
100
140
180

Figure 25

(UA). This depth scale involves stopping powers for helium in silicon, aligned but at two different energies, as follows:

$$(\Delta E/\Delta t)_{UA} = k_{Si}^2 \, S_A(E_1) - \sec \theta_L \, S_A(E_2) \qquad (52)$$

where $S_A(E_1)$ is the aligned stopping power for the incident energy $E_1 = 1.8$ MeV, $S_A(E_2)$ is the aligned stopping power at the energy after backscattering $E_2 = 1$ MeV, $\theta = 179.8°$, and $k_{Si} = 0.563$. For this sample $\Delta t = 6100$Å from the single alignment analysis, so $(\Delta E/\Delta t)_{UA} = 38$ eV/Å. From Eqs. (51) and (52) one has for the <110> axis the following:

$$(\Delta E/\Delta t)_{SA} - (\Delta E/\Delta t)_{UA} = 7 \text{ eV/Å} = (1.04 \, S_R(E_2) - S_A(E_2)) \qquad (53)$$

Using previously reported values of $S_R(E_2)$ of 29 eV/Å[14] in Eq. (53) gives $S_A/S_R \simeq 0.8$ for helium in silicon at 1.0 MeV.

The random stopping power for helium in silicon at 1 MeV $S_R(E_2)$ can be determined directly. For this measurement a silicon single crystal was implanted* with $8 \times 10^{14}$ 400 keV antimony ions, then annealed for 1.5 hours at 700°C in a dry nitrogen atmosphere. The annealing was necessary to reorder the lattice of the sample sufficiently to be able to grow reproducible anodic oxides on it. A 1.08 MeV $^4He^+$ analyzing beam was allowed to impinge in a random orientation on the sample in the single alignment geometry. The spectrum was recorded with the

*E. Bøgh of the Institute of Physics, University of Aarhus, Aarhus, Denmark, kindly supplied the 400 keV antimony implant.

electronic gain adjusted to give an energy per channel of 3.3 keV and is shown as the open squares in Fig. 26. This spectrum of a heavy mass impurity is a fixed marker $\approx 1500\text{Å}$[8] deep in the sample. The midpoint of the rear edge of the antimony was chosen as the point to observe since it is the most accurately defined feature. Two successive anodic oxides $T_2$ were grown on and stripped off of the sample by the layer removal technique already described with a spectrum recorded after each layer was removed as shown in Fig. 26. The experiment was repeated on another section of the same sample for another two layer removals. The four values of the energy shift in keV of the midpoint of the rear edge of the antimony peak per strip were 28.2, 25.5, 31.2, and 25.5. The average value was 27.5 keV with a calculated standard deviation of 2.3 keV. The energy loss of the helium atoms when they are backscattered from antimony (Sb) is small since for $\theta_L = 164°$, $k^2_{Sb} = 0.879$. The helium atom entering and exit energies are close to the same value. The depth scale for this experiment involves only the random stopping power for helium in silicon at essentially one energy as follows:

$$(\Delta E/\Delta t)_{SbR} = k^2_{Sb}\, S_R(E_1) - \sec\theta_L\, S_R(E_2) \qquad (54)$$

where $k^2_{Sb} = 0.879$, $\theta_L = 164°$, and the assumption is $E_1 = E_2 = 1$ MeV. This experiment gives for helium in silicon at 1 MeV, a random stopping power $S_R(E_2)$ of 33 eV/Å, a value 14% higher than the 29 eV/Å previously reported.[14] This value has been confirmed recently by measurements at another laboratory.[35]

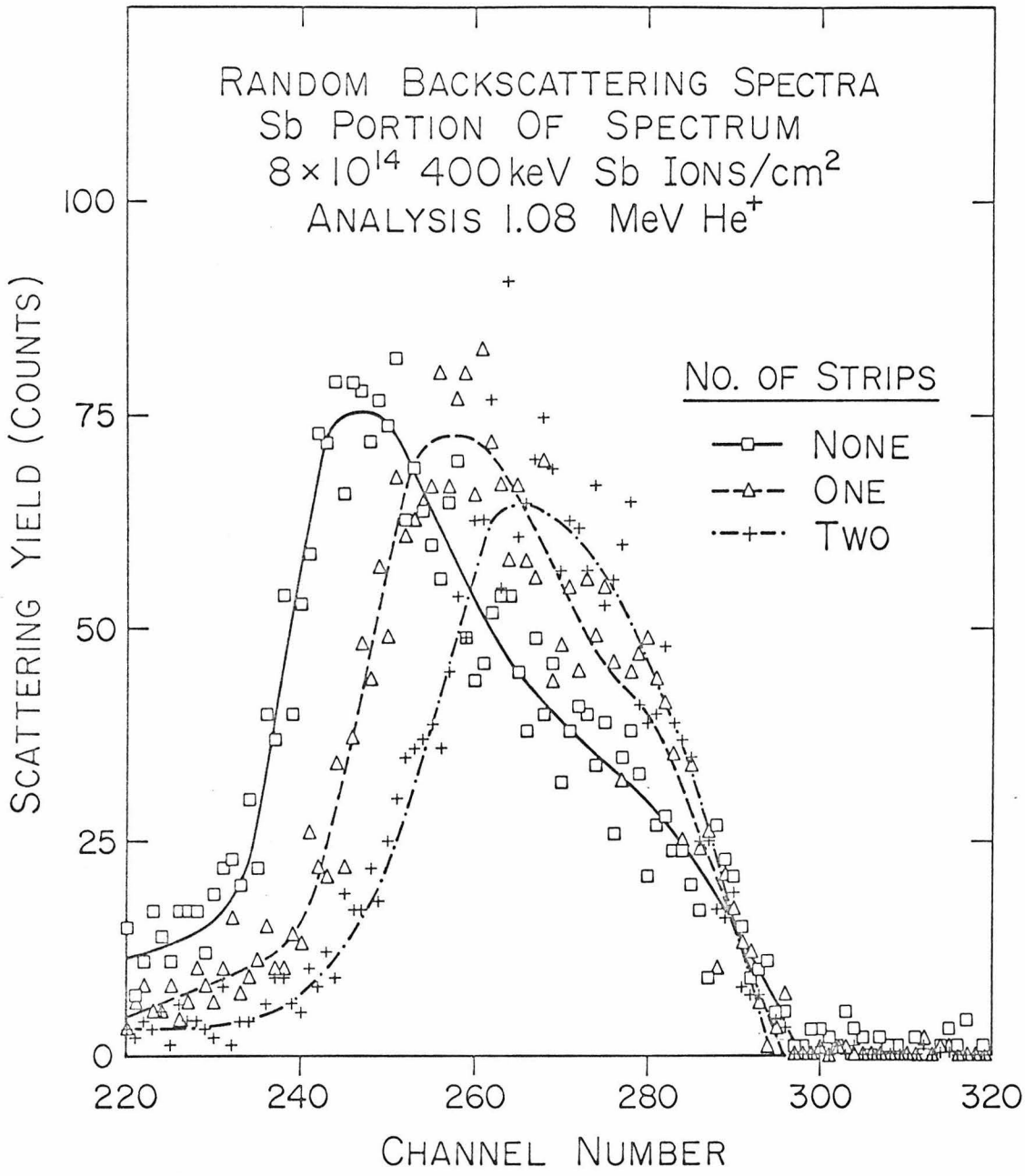


Fig. 26. Antimony portion of random spectrum (3.3 keV/channel) from 1.08 MeV $^4He^+$ analysis of sample implanted with 8 x $10^{14}$ 400 keV antimony ions/cm$^2$ and annealed for 1.5 hr. at 700°C. Spectra are presented for original sample and same sample after removal of 430Å and 870Å from surface.

Inserting $S_R(E_2)$ in Eq. (51) gives for helium in silicon at 1.8 MeV, an aligned stopping power $S_A(E_1)$ of 19 eV/Å. Inserting $S_A(E_1)$ in Eq. (52) gives for helium in silicon at 1 MeV, an aligned stopping power $S_A(E_2)$ of 27 eV/Å.

The significant result of the stopping power measurements is that for 1 MeV helium in silicon the aligned (<110>) stopping power is about 80% of the random stopping power. This stopping power ratio as seen by backscattering measurements appears to differ considerably from early proton transmission results[77] which showed that the channeled energy loss peak had suffered only about 40% of the energy loss of the random energy loss peak. This is perhaps not surprising since the channeled energy loss peak represents just the particles which have been almost perfectly channeled as they penetrated the sample. However, the backscattering will always average over some particles which have not been so well channeled and so have undergone somewhat higher energy losses. It is also possible that the ratio of aligned to random stopping power only tends to values of 0.4 to 0.5 as the energy increases, in particular, above 2 MeV for helium in silicon. This would be an interesting aspect of the stopping power question to resolve. Some investigations of this problem are underway at another laboratory.[35]

## VI. Summary

This thesis used channeling effect analyses to investigate disorder distributions and temperature effects on the disorder produced in silicon by boron ion implantation. A self-consistent method for the extraction of disorder distributions in regions from 300Å to 10,000Å from the surface of a crystalline sample was described, and for illustration, distributions were obtained for the disorder in 200 keV and 300 keV boron implanted silicon crystals. The channeling effect technique utilizing both 1.8 MeV helium and 450 keV proton analyzing beams was employed to obtain aligned and random backscattering spectra. The behavior of the analyzing beam was first investigated by studies of the minimum yield from single crystal substrates underlying surface amorphous layers from 2900Å to 6500Å thick. The insight into the scattering processes gained from the amorphous layer results was applied to an iterative analysis of the backscattering spectra from discrete disorder peaks.

The model employed was a simple description of the interactions of the analyzing beam in partially disordered samples to see whether physically meaningful, self-consistent results could be obtained. The description chosen consisted of an aligned component interacting only with the disordered lattice atoms and a random component interacting with all lattice atoms. The dechanneling of the analyzing beam from the aligned component into the random component for the case of interest was assumed to be due to small angle forward scattering in the plural scattering regime from the same disordered atoms that produce the

backscattering of the aligned component. Particles scattered outside the critical angle for channeling were treated as being in the random component. No attempt was made to account for possible different scattering probabilities due to the association of defects into clusters or more complicated structures because such a refinement would imply a knowledge of the disordered regions that did not exist. This approach was acceptable for obtaining the disorder peak depth and shape when applied to both helium and proton backscattering spectra obtained from samples held at temperatures below -45°C during the boron implantations, provided that the boron doses were greater than $\approx 2 \times 10^{14}$ ions/cm$^2$ and less than $\approx 8 \times 10^{14}$ ions/cm$^2$. Although for the amounts of disorder easily detectable by the backscattering technique and amenable to the approach of this thesis the dechanneling in cold implants was shown to be predominantly in the plural scattering regime, single scattering was studied and found to agree with plural scattering in the regions of lower disorder density near the surface of the implanted sample.

A multiple scattering treatment was also given for dechanneling in the disordered regions created in silicon samples held at room temperature during boron implantation. Although the treatment was essentially phenomenological, it gave an adequate description of the desired disorder distributions.

Data were presented showing that in the disordered regions produced in samples held at room temperature during the boron ion implantation there was a faster rate of dechanneling for the amount of

disorder present than was observed in the low temperature implants. Hence, the mechanism governing the dechanneling depended on the detailed structure of the disordered layer. For this reason it was suggested that an all-inclusive treatment of backscattering spectra to extract arbitrary disorder distributions was not feasible at the present time.

The measured results for the disorder peak depths and the widths of the disorder distributions were compared with the values for these quantities calculated by D.K. Brice. The depths agreed quite well, but the measured widths were 60% to 70% less than the calculated values. This effect was attributed to annealing of the disorder, or possibly to the same nonlinear processes seen for antimony in silicon. The measured disorder peak depths were 80% to 85% less than the calculated boron projected range and the measured widths were comparable to the calculated widths of the boron projected range distributions.

The disorder was then discussed with respect to its having been created by boron ion implantations into silicon. Temperature effects were described with special attention given to the drastic dependence of the amount of disorder produced on the temperature of the silicon substrate during the boron ion implantation. The amount of disorder seen in samples implanted at room temperature was about a factor of twenty less than that seen in samples implanted at -150°C with the same dose of boron ions. The anneal of a -150°C implant was measured and shown to suggest that the nature of the annealing process was governed to a considerable extent by different mechanisms than

those responsible for the anneal behavior of the disorder produced by light doses of heavy ions such as antimony implanted into silicon at room temperature. The observed temperature dependence of the disorder production process during implantation was different from the temperature dependence of the effects of subsequent anneal treatments performed on the samples after the disordered regions had been produced. This showed the nonequivalence of dynamic anneal processes at a given temperature and thermal instabilities of disorder produced at lower temperatures and then warmed to the given temperature.

It was shown that the low temperature implantation-produced disorder was unstable with respect to analyzing beam bombardment, while the room temperature implantation-produced disorder was not, and that this instability was not a temperature effect.

A process utilizing successive layer removals by anodic oxidation and stripping for measuring directly the depth scale of backscattering spectra was described. The backscattering analysis was applied to measure the composition of the anodic oxide layers employed in the layer removal because there were differences in the ellipsometric and interferometric indications of the amount of silicon removed per anodic oxide layer stripped off. The anodic oxide layers were found to contain an oxygen excess suggested to be in the form of hydrated water, but they attained the composition of thermal oxide layers after heat treatment. Finally an application of the depth scale expressions to stopping power measurements was given. A value of 33 eV/Å for the random stopping power for helium in silicon at 1.0 MeV was obtained. This value was 14% higher than the results of previous

measurements. Then it was shown that the aligned analyzing beam stopping power as measured by backscattering measurements was ≈80% of the random value at 1.0 MeV, an energy near the maximum of the random stopping power curve for helium in silicon. In contrast values as low as 40% had been seen by other workers for the channeled energy peak in early proton transmission work.

In conclusion this thesis described a method of obtaining consistent disorder distributions from helium and proton backscattering analyses of the disordered regions in boron implanted silicon. Measurements were given of temperature effects on the disorder in regions of low temperature where such effects were not anticipated. An application of the backscattering analysis technique to study the composition of thin layers was presented.

## REFERENCES


1. E. Bøgh, in Proceedings of Cairo Solid State Conference, American University in Cairo, 1966, Interaction of Radiation with Solids, edited by A. Bishay, Plenum Press, Inc., New York, 1967.
2. J.A. Davies, J. Denhartog, L. Eriksson, and J.W. Mayer, Can. J. Phys. 45, 4053 (1967).
3. J.W. Mayer, L. Eriksson, S.T. Picraux, and J.A. Davies, Can. J. Phys. 46, 663 (1968).
4. E. Bøgh, Can. J. Phys. 46, 653 (1968).
5. F. Brown, D.A. Marsden, and R.D. Werner, Phys. Rev. Letters 20, 1449 (1968).
6. L. Eriksson, J.A. Davies, N.G.E. Johansson, and J.W. Mayer, J. Appl. Phys. 40, 842 (1969).
7. S.T. Picraux, J.E. Westmoreland, J.W. Mayer, R.R. Hart, and O.J. Marsh, Appl. Phys. Letters 14, 7 (1969).
8. J.W. Mayer, L. Eriksson, and J.A. Davies, Ion Implantation in Semiconductors, Academic Press, New York, 1970.
9. E. Bøgh, Proc. Roy. Soc. A.311, 35 (1969).
10. W.M. Gibson, F.W. Martin, R. Stensgaard, F. Palmgren Jensen, N.I. Meyer, G. Galster, A. Johansen, and J.S. Olsen, Can. J. Phys. 46, 675 (1968).
11. K. Björkqvist and G. Flädda (private communication).
12. D.E. Davies, Appl. Phys. Letters 14, 227 (1969).
13. R.R. Hart and O.J. Marsh, Appl. Phys. Letters 15, 206 (1969).

14. W. Whaling, Handbuch der Physik 34, 204 (1958).

15. J. Lindhard, Mat. Fys. Medd. Dan. Vid. Selsk. 34, No. 14 (1965).

16. L.C. Feldman, Ph.D. Thesis, Rutgers University, December, 1966.

17. L.C. Feldman and C. Erginsoy, Bull. Am. Phys. Soc. 12, 391 (1967).

18. L.C. Feldman and J.U. Andersen (to be published).

19. J.U. Andersen, Mat. Fys. Medd. Dan. Vid. Selsk. 36, No. 7 (1967).

20. S.T. Picraux, J.A. Davies, L. Eriksson, N.G.E. Johansson, and J.W. Mayer, Phys. Rev. 180, 873 (1969).

21. S.T. Picraux and J.U. Andersen, Phys. Rev. 186, 267 (1969).

22. B. Domeij, Nucl. Inst. Meth. 38, 207 (1965).

23. D.S. Gemmell and R.E. Holland, Phys. Rev. Letters 14, 945 (1965).

24. A.F. Tulinov, V.S. Kulikauskas, and M.M. Malov, Phys. Letters 18, 304 (1965).

25. V.S. Kulikauskas, M.M. Malov, and A.F. Tulinov, Zh. Eksp. Teor. Fiz. 53, 487 (1967) (Soviet Physics JETP 26, 321 (1968)).

26. B.R. Appleton and L.C. Feldman, in Proceedings of International Conference on Atomic Collision Phenomena in Solids, University of Sussex, Brighton, England, 1969 (North-Holland Publishing Company, 1970).

27. S.T. Picraux, Ph.D. Thesis, California Institute of Technology, June, 1969.

28. L.C. Feldman, B.R. Appleton, and W.L. Brown, in Solid State Research with Accelerators, Brookhaven Natl. Lab., Rept. No. 50083 (1968).

29. G. Dearnaley, I.V. Mitchell, R.S. Nelson, B.W. Farmery, and M.W. Thompson, Phil. Mag. 18, 985 (1968).

30. S.T. Picraux (private communication).

31. I.V. Mitchell, M. Kamoshida, and J.W. Mayer, submitted to J. Appl. Phys.

32. F.H. Eisen, unpublished work.

33. G.W. Gobeli, Phys. Rev. 103, 275 (1956).

34. J.F. Janni, Technical Report No. AFWL-TR-65-150.

35. I. Bottiger and F.H. Eisen (private communication).

36. E. Keil, E. Zeitler, and W. Zinn, Z. fur Naturfosch. 15a, 1031 (1960).

37. G. Moliere, Z. fur Naturfosch. 3a, 78 (1948).

38. F.H. Eisen, B. Welch, J.E. Westmoreland, and J.W. Mayer, in Proceedings of International Conference on Atomic Collision Phenomena in Solids, University of Sussex, Brighton, England, 1969 (North Holland Publishing Company 1970).

39. G. Moliere, Z. Naturfosch. 2a, 133 (1947).

40. S. Leisegang, Z. Phys. 132, 183 (1952).

41. A.O. Hanson, L.H. Lanzl, E.M. Lyman, and M.B. Scott, Phys. Rev. 84, 634 (1951).

42. O. Knecht and J.W. Bothe, Z. Naturforschg. 8a, 805 (1953).

43. W.T. Scott, Revs. Mod. Phys. 35, 231 (1963).

44. H. Bichsel, Phys. Rev. 112, 182 (1958).

45. L.C. Feldman (private communication).

46. R.B. Leighton, Principles of Modern Physics, McGraw-Hill Book Co., Inc., New York, 1959, Ch. 14.

47. G. Carter and J.S. Colligon, Ion Bombardment of Solids, American Elseview, New York, 1968.

48. J. Lindhard, V. Nielsen, M. Scharff, and P.V. Thomsen, Mat. Fys. Medd. Dan. Vid. Selsk. 33, No. 10 (1963).

49. P. Sigmund and J.B. Sanders, in Proceedings of the International Conference on the Applications of Ion Beams to Semiconductor Technology, edited by P. Glotin, Centre d'etudes Nucleaire, Grenoble, 1967.

50. J.E. Westmoreland and P. Sigmund, in Proceedings of International Conference on Ion Implantation in Semiconductors (Thousand Oaks, California, 1970, Rad. Effects 6, 187 (1970).

51. D.K. Brice, Appl. Phys. Letters 16, 103 (1970).

52. D.K. Brice, in Proceedings of International Conference on Ion Implantation in Semiconductors, Thousand Oaks, California, 1970, Rad. Effects, to be published.

53. A.R. Sattler, Phys. Rev. 138, A1815 (1965).

54. C. Chasman, K.W. Jones, R.A. Ristinen, and J.T. Sample, Phys. Rev. 154, 239 (1967).

55. A.R. Sattler, F.L. Vook, and J.M. Palms, Phys. Rev. 143, 588 (1966).

56. P. Sigmund, M.T. Matthies, and D.L. Phillips (to be published).

57. P.V. Pavlov, D.I. Tetel'baum, E.I. Zorin, and V.I. Alekseer, Fiz. Tverd. Tela 8, 2679 (1966) (Sov. Phys. Solid State 8, 2141 (1967)).

58. A.R. Sattler and F.L. Vook, Phys. Rev. 155, 211 (1967).

59. A.R. Sattler and F.L. Vook, Phys. Rev. 173, 435 (1968).

60. A.R. Sattler, in Proceedings of the Santa Fe Conference on Radiation Effects in Semiconductors, 1967, Radiation Effects in Semiconductors edited by F.L. Vook, Plenum Press, New York, 1968.

61. H.J. Stein, F.L. Vook, and J.A. Borders, Appl. Phys. Letters 16, 106 (1970).

62. K.L. Brower, F.L. Vook, and J.A. Borders, Appl. Phys. Letters 16, 108 (1970).

63. J. Lindhard, M. Scharff, and H.E. Schiott, Mat. Fys. Medd. Dan. Vid. Selsk. 33, No. 14 (1963).

64. S.T. Picraux, W.H. Weisenberger, and F.L. Vook, in Proceedings of International Conference on Ion Implantation in Semiconductors, Thousand Oaks, California, 1970, Rad. Effects, to be published.

65. T.O. Baldwin and J.E. Thomas, J. Appl. Phys. 39, 4391 (1968).

66. G.D. Watkins, in Proceedings of the Santa Fe Conference on Radiation Effects in Semiconductors, 1967, Radiation Effects in Semiconductors, edited by F.L. Vook, Plenum Press, New York, 1968.

67. H.J. Stein, F.L. Vook, and J.A. Borders, Appl. Phys. Letters 14, 328 (1969).

68. F.L. Vook and H.J. Stein, Rad. Effects 2, 23 (1969).

69. F.L. Vook and H.J. Stein, in Proceedings of International Conference on Ion Implantation in Semiconductors, Thousand Oaks, California, 1970, Rad. Effects, to be published.

70. H.J. Stein, in Proceedings of Radiation Effects Conference, Albany, New York, August, 1970, Rad. Effects, to be published.

71. S.T. Picraux (private communication).

72. K.H. Zaininger and A.G. Revesz, RCA Review 25, No. 1 (1964).

73. F.L. McCrackin, J. of Research, U.S. Nat. Bur. of Standards 67A, 363 (1963).

74. S. Tolansky, Multiple Beam Interferometry of Surface Films, Oxford University Press, London, 1948.

75. A.S. Grove, Physics and Technology of Semiconductor Devices, John Wiley and Sons, Inc., New York, 1967, p. 102.

76. C. Williamson and J.P. Boujot, CEA-2189 (1962).

77. A.R. Sattler and G. Dearnaley, Phys. Rev. Letters 15, 59 (1965).